University of Alberta

STRESS CONCENTRATION IN BUILT-UP STEEL MEMBERS

by

CHRISTIAN WOKEM

A thesis submitted to the Faculty of Graduate Studies and Research

in partial fulfillment of the requirements for the degree of

Master of Science

in

Structural Engineering

Department of Civil and Environmental Engineering

FALL 2010

Edmonton, Alberta

Examining Committee

Gilbert Y. Grondin, Department of Civil & Environmental Engineering.

Samer Adeeb, Department of Civil & Environmental Engineering.

Chong Qing Ru, Department of Mechanical Engineering.

Abstract

In the past riveting was commonly used for connecting steel structures, such as bridges. These fasteners usually develop a low and unreliable level of pretension such that the joints are assumed to behave like bearing type connections. Under cyclic loading, and depending on the stress concentration around the fastener holes, fatigue failure can occur at nominal stresses significantly lower than in members with no stress concentration. The current design standards account for this by calculating the stress range on the net section and using fatigue category B and D to assess the fatigue life for bolted and riveted details respectively. The net area used for the calculation of the stress range is based on the procedure proposed by Cochrane (the $s^2/4g$ rule), which is adequate shear type failure. Tests have shown, however, that the Cochrane approach does not apply for fatigue failure since rupture does not take place in a ductile shear mode.

An investigation into the effect of connection size and hole pattern on the fatigue resistance of built-up I section to gusset plate connections was carried out. A design equation that considers the connection size and hole layout on the stress concentration factor is proposed. An appropriate fatigue category for these members is also recommended.

Acknowledgements

This research was funded by the National Sciences and Engineering Research Council of Canada. I appreciate the supervision, encouragement and financial support from my supervisor, Dr G. Y. Grondin. I also extend my gratitude to the Faculty of Graduate Studies and Research of the University of Alberta for the various forms of support given to me.

Table of Contents

Abstract iii

Acknowledgements iv

List of Tables vii

List of Figures ix

List of Symbols xi

1. Introduction

1.1 General 1

1.2 Background 1

1.3 Scope and Objectives 3

2. Literature Review

2.1 Introduction 4

2.2 Stress Concentration in Components with Circular Holes 5

2.3 SCF and Fatigue of Components with Staggered Holes. 6

2.4 Summary 8

3. Finite Element Model Development

3.1 Introduction 14

3.2 Finite Element Model Description 14

3.2.1 Model Geometry, Material Properties 14

3.2.2 Mesh Refinement Study, Mesh Type and Element Type 15

3.2.3 Boundary Conditions and Loads 16

3.3 Analysis 17

3.4 Model Validation 18

3.4.1 Flat Plate with Centered Hole 18

3.4.2 Thin Flat Plate Element with Staggered Circular Hole in Uniaxial Tension 19

4. Parametric Study

4.1 Introduction 29

4.2 Finite Flement Analysis Results 30

4.2.1 Effect of Fastener/Plate Stiffness 30

4.3 Effect of Hole Stagger, Gauge Distance and Edge Distance 31
4.4 Effect of Fastener Hole Diameter and Width of Angle Leg Connected to Gusset Plate 33
4.6 Effect of Angle Size (equal/unequal angle) and Angle Thickness 34
4.7 Fatigue S-N Curve for Bearing-Type Connections 34
4.7.1 Current Fatigue Practices 34
5. Development of Simplified Design Equation
5.1 Introduction 55
5.2 Regression Analysis for Built-Up I Sections 56
5.2.1 Effect of Hole Stagger 56
5.2.2 Effect of Gauge Distance 57
5.2.3 Effect of Edge Distance E_2 57
6. Summary, Conclusions and Recommendations
6.1 Summary 79
6.2 Conclusions 80
6.3 Recommendations 80
List of References 82
Appendix A. Regression Analysis of Finite Element Results 84

List of Tables

Table **Page**

2-1 Stress concentration factor for various hole layouts by Schulz (1941) 9
2-2 Results of fatigue test on flat plates by Graf (1951) 9
2-3 SCF for different gauge dimensions and hole staggers by Josi *et al* 10
2-4 SCF for different edge distances and hole staggers by Josi *et al* (1999)....10

3-1 MeshRefinement for different element types 20
4-1 Different cases investigated in the parametric study 40
4-2 Effect of fastener/plate stiffness on the stress concentration factor 43
4-3 Stress concentration factor for different hole staggers and gauge distances 43
4-4 Stress concentration factor for different hole staggers and edge distances 44
4-5 Stress concentration factor for different hole diameters and angle flange width connected to gusset plate 44

4-6 Stress concentration factor for different web thickness and web depth ... 45
4-7 Stress concentration factor for different angle sizes 45
4-8 Results of fatigue test on Flat plates by Josi *et al*. (2004) 46
4-9 Results of fatigue test on Flat plates by Graf (1951) 47
4-10 Results of fatigue test on built-up section by DiBattista *et al*. (1999) and SCF from finite element analysis 47

5-1 Effect of hole stagger on SCF (gauge = 38.1 mm) 65
5-2 Effect of gauge distance on the SCF (stagger = 38.1 mm) 65
5-3 Effect of edge distance on the SCF 66
5-4 Effect of web thickness 66
5-5 Effect of web depth 67
5-6 Effect of angle thickness (152x152 mm angle) 67
5-7 Results of regression analysis for general Equation for built-up I section 68
5-8 Results of regression analysis for reduced Equation for built-up I section (Equation (5.2)..... 69

5-9 Predicted SCF and SCF from finite element for the built-up I section 70
5-10 Finite Element analysis results for flat plates presented by Josi *et al* . (1999) 70

5-11 Results of regression analysis for Equation for flat plate 71
A-1 Effect of hole stagger on SCF (gauge = 38.1 mm) 86

A-2 Effect of hole stagger on SCF (gauge = 46.5 mm) 87
A-3 Effect of hole stagger on SCF (gauge = 50.8 mm) 88
A-4 Effect of hole stagger on SCF (gauge = 55.0 mm) 89
A-5 Effect of hole stagger on SCF (gauge = 60.4 mm) 90
A-6 Effect of gauge distance on SCF (stagger = 38.1 mm) 91
A-7 Effect of gauge distance on SCF (stagger = 46.5 mm) 92
A-8 Effect of gauge distance on SCF (stagger = 50.8 mm) 93
A-9 Effect of gauge distance on SCF (stagger = 55.0 mm) 94
A-10 Effect of gauge distance on SCF (stagger = 60.4 mm) 95
A-11 Effect of edge distance on SCF (stagger = 38.1 mm) 96
A-12 Effect of edge distance on SCF (stagger = 46.5 mm) 97
A-13 Effect of edge distance on SCF (stagger = 50.8 mm) 98
A-14 Effect of edge distance on SCF (stagger = 55.0 mm) 99
A-15 Effect of edge distance on SCF (stagger = 60.4 mm) 100
A-16 Effect of angle thickness on SCF (angle size = 152×152 mm) 101
A-17 Effect of angle thickness on SCF (angle size = 152×102 mm) 102
A-18 Effect of angle thickness on SCF (angle size = 152×89 mm) 103

List of Figures

Figure **Page**

2-1 Finite-width plate with centered circular hole in tension (Howland, 1930) 11

2-2 Thin element with staggered circular holes in uniaxial tension Schulz (1941) 11

2-3 Top chord detail investigated by DiBattista and Kulak (1995).....12

2-4 Example of shear splice detail investigated by Josi *et al*. (1999.....13

3-1 Typical section of riveted built-up tension member.....21

3-2 Finite element model of built-up I-section 21

3-3 Plot of SCF versus element size in the refined zone (mesh study) 23

3-4 Mesh study 23

3-5 Constaint used to tie the angle and web rivet holes 25

3-6 Flat plate with centered hole 26

3-7 Flat Plate with staggered holes 27

4-1 Built-up I section and critical hole location shown in Table 4-1(Locations of maximum principal stress) 48

4-2 Built-up I section 49

4-3 Effect of stagger on the stress concentration factor 50

4-4 Effect of gauge distance on the stress concentration factor 50

4-5 Effect of edge distance (for fixed stagger) on the stress concentration factor..... 51

4-6 Effect of web thickness on the stress concentration factor 51

4-7 Effect of web depth on the stress concentration factor 52

4-8 Effect of angle thickness on the stress concentration factor 52

4-9 Test results and fatigue curve from Josi *et al*. (2004) compared to fatigue category A In terms of peak stress 53

4-10 Mean fatigue curve for flat plates from two different sources 53

4-11 Comparison with fatigue curve for all test data with fatigue category A . 54

5-1 Effect of stagger on the SCF (gauge = 38.1 mm) 72

5-2 Effect of gauge distance on the SCF (stagger = 38.1 mm) 72

5-3 Effect of edge distance, E_2 on the SCF 73

5-4 Effect of angle thickness on the SCF 73

5-5 Effect of shear lag and area ratios on the SCF 74

5-6 Fatigue curve from the use of the SCF Equation for flat plates 77

5-7 Fatigue curve from the use of general SCF Equation for built-up I members.....77

5-8 Fatigue curve from the use of simplified SCF Equation for built-up I members 78

A-1 Effect of hole stagger on SCF (gauge = 38.1 mm) 86
A-2 Effect of hole stagger on SCF (gauge = 46.5 mm) 87
A-3 Effect of hole stagger on SCF (gauge = 50.8 mm) 88
A-4 Effect of hole stagger on SCF (gauge = 55.0 mm) 89
A-5 Effect of hole stagger on SCF (gauge = 60.4 mm) 90
A-6 Effect of gauge distance on SCF (stagger = 38.1 mm) 91
A-7 Effect of gauge distance on SCF (stagger = 46.5 mm) 92
A-8 Effect of gauge distance on SCF (stagger = 50.8 mm) 93
A-9 Effect of gauge distance on SCF (stagger = 55.0 mm) 94
A-10 Effect of gauge distance on SCF (stagger = 60.4 mm) 95
A-11 Effect of edge distance on SCF (stagger = 38.1 mm) 96
A-12 Effect of edge distance on SCF (stagger = 46.5 mm) 97
A-13 Effect of edge distance on SCF (stagger = 50.8 mm) 98
A-14 Effect of edge distance on SCF (stagger = 55.0 mm) 99
A-15 Effect of edge distance on SCF (stagger = 60.4 mm) 100
A-16 Effect of angle thickness on SCF (angle size = 152×152 mm) 101
A-17 Effect of angle thickness on SCF (angle size = 152×102 mm) 102
A-18 Effect of angle thickness on SCF (angle size = 152×89 mm) 103

List of Symbols

A_{fg} = Gross section area of the leg of the angle in contact with the gusset plate.

A_T = Total gross sectional area of the connection.

E = Edge distance.

E_1 = Edge distance away from the web.

E_2 = Edge distance close to the web.

F_{sc} = Stress correction factor.

G = Gauge distance.

L = Length of connection.

L_t = Angle thickness.

N = Fatigue life.

S = Stagger.

SCF = Stress concentration factor.

S_r = Stress range obtained using peak stress approach.

W_d = Web depth.

W_t = Web thickness.

X = Distance from the shear plane to the centroid of the portion of the cross-section connected to the shear plane.

$\Delta\sigma_g$ = Gross section stress range.

$\Delta\sigma_{sc}$ = Stress range obtained using the stress correction factor approach.

σ_{app} = Gross section applied stress.

σ_{max} = Peak normal stress.

θ = Angle

CHAPTER 1

INTRODUCTION

1.1 GENERAL

Many existing steel structures that have been fabricated prior to the early 1960's, before high strength bolts became widely accepted, have been assembled using riveted connections. Rivets were installed after preheating and part of the installation process consisted of forging the button head at one end of the rivet. As a result of the cooling process, rivets contracted and exerted a clamping force on the joint, but this clamping force is well known to be widely variable and relatively low (Kulak *et al*., 1987). Consequently, these connections are treated as bearing type connections. Typically in recent times, bolted connections used for applications where loads are cyclic are designed as slip-critical, i.e. the service loads are transferred by friction rather than by bearing of the bolts against the assembled plates. When bearing type connections are subjected to repeated cycles of loading stress concentration at the net section can lead to fatigue failure at nominal stresses significantly lower than details with no stress concentration. So it is expected that two different details having the same gross section applied stress, but with different stress concentration, should have stress ranges proportional to their stress concentration factor (SCF). In this report, SCF is defined as the ratio of the maximum principal stress to a nominal stress (that is applied stress).

1.2 BACKGROUND

Due to aging infrastructures, the need to establish the remaining fatigue life of many structural systems, such as bridges, has become increasingly necessary. To assess the remaining fatigue life of old structures, we need good knowledge of the fatigue behaviour of riveted connections. Earlier research has shown that the following factors influence the fatigue life of a structure:

1. The stress range at the location of the detail;
2. The number of load cycles applied to the structure;
3. The type of detail under consideration.

In the above, the stress range is a function of the SCF at the location of the detail. Since most existing bridges have connections that are assumed to be in bearing, the need to evaluate the SCF created by the presence of these fastener holes and the bearing pressure that the fasteners exert on the plate becomes very important, since a larger SCF means that the details may be more susceptible to shorter fatigue life.

Current design standards account for this by calculating the stress range on the net section and using the appropriate fatigue category for assessment of the fatigue life, that is, accounting for the stress concentration in an implicit manner in the derivation of the fatigue categories. The net stress calculation used is based on the Cochrane ($s^2/4g$) rule which was originally derived for shear type rupture. Tests have shown however, that the Cochrane's approach does not apply for fatigue failure since the rupture does not take place in a ductile shear mode.

DiBattista and Kulak (1995) carried out fatigue tests on riveted built-up tension members connected to gusset plates, and observed that the fatigue crack in joints with staggered rivet holes propagated on a plane perpendicular to the axis of the member, thus invalidating a stress calculation based on the Cochrane's rule. These researchers also suggested that an investigation be carried out to study the effect of staggered hole pattern, since it was suspected that the close proximity of the bolt holes to the plane of fracture for test specimens with staggered holes may increase the effective stress on the failure plane.

Josi *et al* (1999) investigated the effect of fastener hole stagger on the fatigue resistance of shear splices with flat plates, and proposed a method for calculating the stress range for flat plates, which involves multiplying the gross section stress by a stress correction factor (obtained by normalizing the SCF for any geometry by the SCF for a flat plate geometry with no stagger). It was then observed that

the use of the commonly used fatigue constant (inverse of the slope on a log-log scale) of 3 for the fatigue design curve of bearing type bolted or riveted joints is not accurate; a slope of 7 was recommended. The method proposed by Josi *et al.* for calculating an effective stress range cannot be easily implemented for built-up members since it is not clear how the stress concentration factor for a detail with no hole stagger could be calculated within the confines of the geometry that we usually have with built-up members, Therefore, the applicability of their findings for built-up tension members needs to be investigated.

1.3 SCOPE AND OBJECTIVES

This study is carried out to provide answers to the following issues raised by earlier researchers into the behaviour of bearing type connections;

1. The effect of hole pattern, i.e. stagger, gauge, edge distance, hole diameter and connection size on the SCF of a built-up member in tension, and hence its overall effect on the fatigue resistance.
2. Obtaining a simple unifying equation for calculating the stress concentration for built-up members, and hence the fatigue resistance of a built-up member.
3. Review the finding of various researchers on the validity of existing stress range calculations, using a net area computed using the $s^2/4g$ rule.
4. Establish a relationship between fatigue stress range and the SCF for bearing type details.
5. The fatigue design curves propose for use, and what slope is recommended?

This study of the SCF in built-up members will be conducted entirely numerically, so comparison with available test results from various researchers will be conducted.

CHAPTER 2

LITERATURE REVIEW

2.1 INTRODUCTION

One of the main factors affecting the fatigue resistance of steel structures is the presence of stress concentration. Stress concentration can arise as a result of the geometry of the structural component or from unintentional surface or sub-surface flaws. In bolted or riveted connections, the presence of the fastener holes is an obvious source of stress concentration. In the design of new structures, bolted joints subjected to cyclic loading are designed as slip-critical joints to avoid fracture on the net section, away from the stress concentrations present at the fastener holes. However, when old riveted structures are evaluated, the joints must be evaluated as bearing-type and the effect of factors such as rivet hole size, spacing and edge distance on the governing stresses must be taken into account. This chapter presents a review of the literature on factors that affect the fatigue resistance of bearing type bolted or riveted connections. For a general review of literature on fatigue behaviour of mechanically fastened members the reader is referred to Josi *et al.* (1999). Fatigue behaviour of a bolted or riveted joint is dependent on factors such as hole preparation, fastener type, and installation method. However, this work focuses only on stress concentration in joints with multiple fastener holes and the interaction between the holes. Section 2.2 presents a review of existing knowledge on stress concentration in flat plates with circular holes. A review of the stress concentration factor (SCF) and fatigue behaviour of details with staggered hole is the focus of section 2.3. Section 2.4 summarizes the recommendations and research needs identified as a result of this literature review.

2.2 STRESS CONCENTRATION IN COMPONENTS WITH CIRCULAR HOLES

Although this research focuses on the determination of stress concentration factor (SCF) in built-up members, fatigue life prediction of a riveted detail requires that we understand and accurately predict the stress concentration around the critical fastener holes. In order to quantify the peak stress around a hole or other discontinuity, the nominal stress calculated using basic strength of materials principles is multiplied by a stress concentration factor.

Stress concentration in mechanically fastened connections results from the presence of fastener holes and the resulting disruption of the stress flow around the hole and bearing of the fastener against the hole of the connected elements. The peak stress can be obtained from a finite element analysis of the member with holes. The SCF is based on a reference stress, such as the gross cross sectional stress at some distance from the location of the maximum stress, and is taken as the ratio of the maximum stress, $\sigma_{\max}$,which is the major principal stress, to the applied reference stress, σ_{app} ,

$$SCF = \frac{\sigma_{\max}}{\sigma_{app}} \tag{2-1}$$

Howland (1930) demonstrated the simple case of SCF based on the net and gross section areas of a finite width thin plate with a centered circular hole loaded in tension as shown in Figure 2-1. An illustration of the variation of the SCF with the hole diameter to plate width ratio is shown in Peterson's stress concentration factors (Pilkey, 1997). From the work of Howland (1930) it is evident that for an infinitely wide flat plate of small thickness with a circular hole and loaded in uniaxial tension, the maximum stress is three times the stress calculated on the gross section. The stress concentration factor based on the gross section stress increases with increase in hole diameter to plate width ratio.

2.3 SCF AND FATIGUE OF COMPONENTS WITH STAGGERED HOLES

In many connections where the width of the connected element is limited, fastener holes are staggered in order to minimize the required length of the connections. Schulz (1941) derived a chart for gross section based SCF for a double row of staggered circular holes in a thin rectangular plate under uniaxial tension as illustrated in Figure 2-2. Schulz observed that as the transverse distance L increases, the SCF based on gross section stress reduces. If θ = 0°, the net area is small because all the holes are aligned in one plane perpendicular to the applied tensile stress, which leads to the highest SCF. Table 2-1 presents the values of SCF for some of the cases derived by Schulz.

Graf (1951) tested double lap shear splices consisting of 13 mm thick main plates, and 10 mm thick splice plates, all 97 mm wide and with a single line of bolts,. Two of Graf's test specimens consisted of loosely tightened bolts and four test specimens were prepared with bolts that had some pretension. Table 2-2 presents the results from Graf's test program, which include the gross section stress range, $\Delta\sigma_g$, the SCF obtained by Josi *et al.* (1999) using finite element analysis, and the fatigue life of each of the specimens.

DiBattista and Kulak (1995) conducted fatigue tests on riveted built-up tension members obtained from a Canadian National Railway bridge built in 1911 and dismantled in 1991. Figure 2-3 shows a diagram of a typical connection detail at the diagonal member to the top chord connection. The connection of the same member to the bottom chord had a similar riveted joint detail to the one at the top chord, except that the rows of fasteners parallel to the axis of the member were interchanged and the rivet spacing in the first few holes was larger than in the other holes in the same connection. They observed that fracture propagated on a plane perpendicular to the axis of the member despite the fact that the minimum area calculated using Cochrane's $s^2/4g$ rule was not on a plane perpendicular to the line of action of the force. The top chord detail (the so-called TD series)

exhibited a lower strength than the bottom chord detail (the BD series) and two possible factors were identified, namely, 1) the web angle rivet holes were close to the critical hole in the top chord specimen and, 2) the magnitude of clamping force exerted by the rivets in the bottom chord connection was suspected to be higher than for the rivets in the top chord connection. It was also suggested that the close proximity of holes to the fatigue fracture surface for members with staggered holes may increase the effective stress on the failure plane.

Josi *et al*. (1999) investigated the fatigue resistance of flat steel plates with staggered bolt holes in double lap joints with snug tight bolts (pretension adjusted to about 10 percent of the tensile strength of the bolts). The snug tight bolts were intended to simulate rivets in riveted joints. The effect of various parameters such as hole stagger, gauge distance, and edge distance on the value of the SCF was investigated using finite element models. A diagram showing one of the joint geometries investigated by Josi *et al.* (1999) is shown in Figure 2-4. Table 2-3 shows the SCF obtained for different gauge dimensions and hole staggers whereas, Table 2-4 shows the values of SCF obtained for different values of edge distance and hole stagger. Josi *et al*. observed that for a given gauge distance and edge distance, an increase in stagger from 25 mm to 75 mm had negligible effect on the SCF and, hence, its fatigue resistance. A comparison of joints with hole stagger with joints with no stagger indicated that plates with staggered holes had higher SCF and a reduced fatigue resistance. Changes in the geometry such as a change in gauge and edge distances did not significantly affect the fatigue resistance of such details. Also they observed that the use of Cochrane's $s^2/4g$ rule, or any other method to calculate the cross-sectional area, provided poor correlation between the calculated area and test results. Hence, an alternative method was proposed to calculate the stress range for bearing type connections. This involves computing a corrected stress range, obtained by multiplying the gross section stress range by a stress correction factor obtained by dividing the SCF(obtained from a finite element analysis) for a particular geometry with staggered holes by a SCF for a geometry without any stagger. A fatigue S-N curve was plotted from which a slope of 7 was obtained, and hence they recommended

the use of a slope of 7 rather than the commonly used slope of 3 for fatigue of bearing type bolted lap splices. These researchers indicated that the use of the stress range correction factors developed for flat plates may not be applicable for other cross-sections.

2.4 SUMMARY

Although extensive research has been conducted to assess the effect of circular holes on the SCF in flat plates, only limited fatigue tests have been conducted to assess the effect of hole stagger on the fatigue resistance of bearing-type joints. From the research on bearing shear splices presented by Josi *et al*. (1999), it is evident that the validity of the stress correction method for calculating the stress range for other shapes, such as built-up I sections, needs to be investigated. The approach proposed by Josi *et al*. (1999) to calculate the stress range is based on a stress concentration factor for a similar plate without hole stagger. This approach is not easily applicable to built-up sections. Therefore, a different method, based on the actual peak stress in the member, needs to be investigated. This is consistent with the recommendation of DiBattista and Kulak (1995) who suggested that the effect of stagger in built-up members in tension be investigated, because, from their test results, the close proximity of holes seemed to increase the stress in the fatigue failure plane. A parametric study into the effect of hole pattern and detail size for built-up I section on the SCF will be carried out.

Table 2-1: Stress concentration factor for various hole layouts by Schulz (1941)

L / d	**Angle (θ)**			
	0°	45°	60°	90°
3	3.95	3.52	3.36	3.06
4	3.26	3.20	3.12	3.02
5	3.12	*	*	3.02

* The chart presented by Schulz (1941) did not give the values of SCF for these layouts

Table 2-2: Results of fatigue test on flat plates by Graf (1951)

Specimen number	**Fatigue Life**	$\Delta\sigma_g$	**SCF**
4	372 000	125	4.21
14	1 384 000	101	4.21
7	78 000	195	4.21
9	249 000	156	4.21
12	517 000	140	4.21
11	1 005 000	125	4.21

Table 2-3: SCF for different gauge dimensions and hole staggers by Josi *et al.* (1999)

Gauge distance (mm)	**Stagger (mm)**		
	25.4	50.8	76.2
44.5	3.21	3.26	3.26
52.5	3.26	3.35	3.35
60.4	3.32	3.42	3.45

Table 2-4: SCF for different edge distances and hole staggers by Josi *et al*. (1999)

Edge distance (mm)	**Stagger (mm)**					
	25.4		50.8		76.2	
	inside	outside	inside	outside	inside	outside
25.4	3.04	3.21	2.95	3.26	2.91	3.26
38.1	3.33	3.26	3.19	3.31	3.13	3.30
50.8	3.78	3.57	3.48	3.53	3.40	3.53

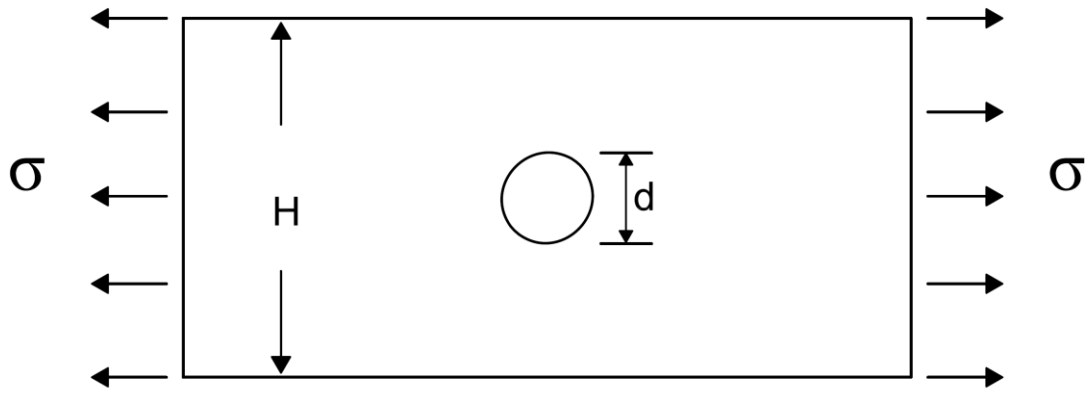

Figure 2-1: Finite-width plate with centered circular hole in tension (Howland, 1930)

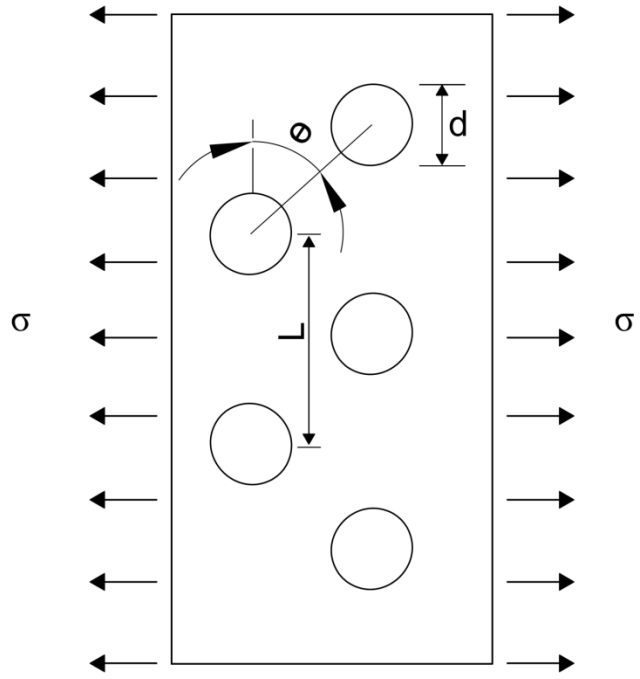

Figure 2-2: Thin element with staggered circular holes in uniaxial tension (Schulz 1941)

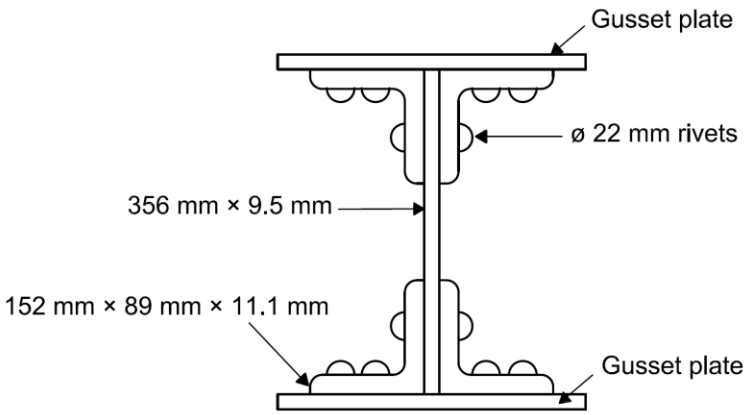

(a) Typical section

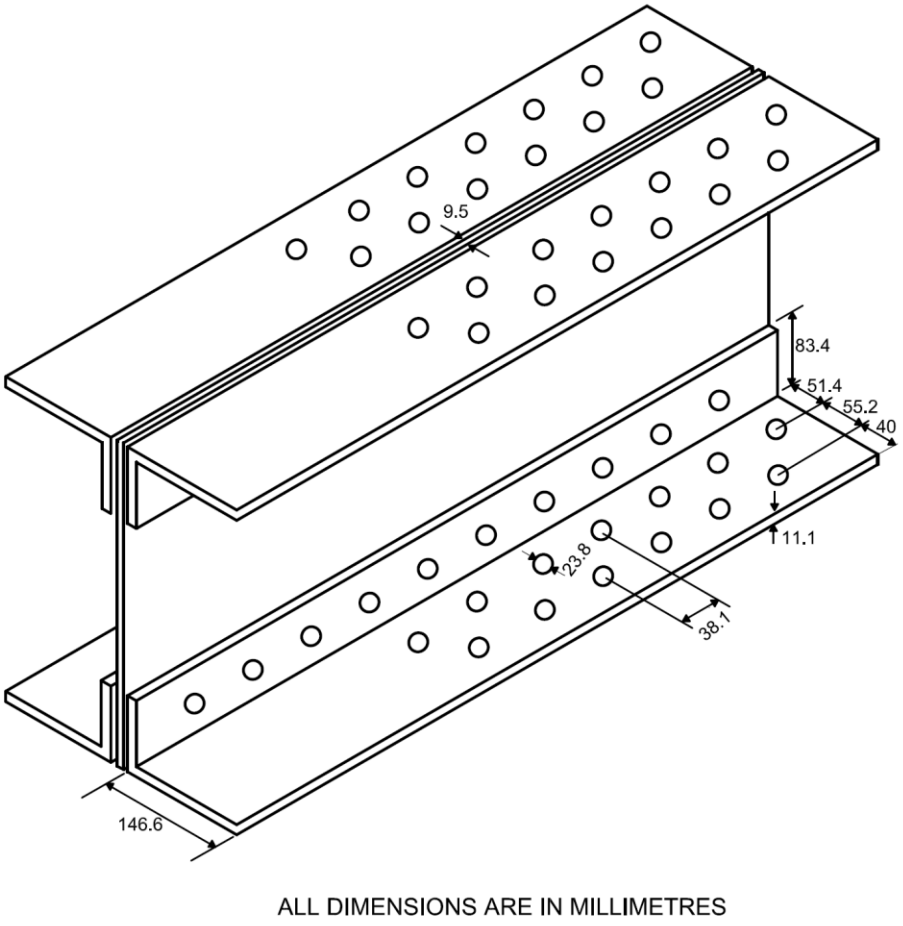

(b) One quarter of the top chord detail

Figure 2-3: Top chord detail investigated by DiBattista and Kulak (1995)

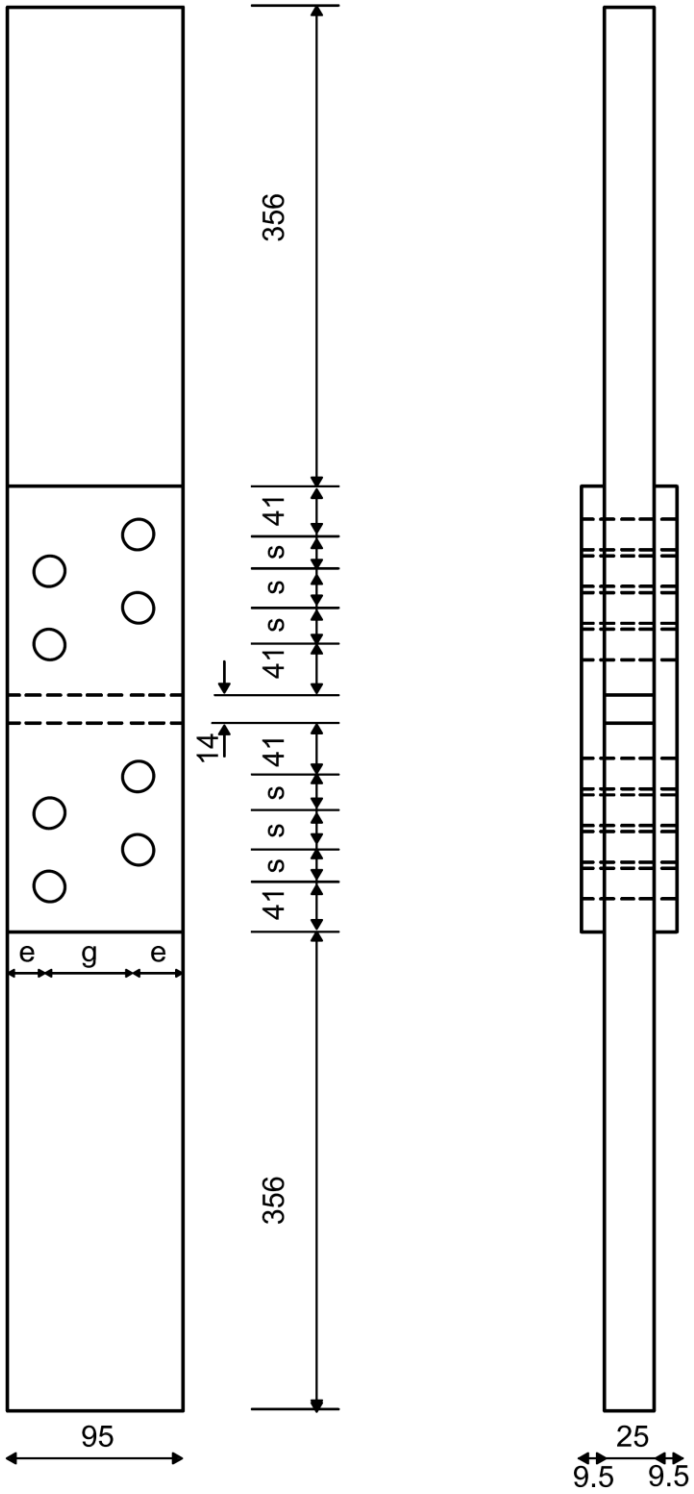

Figure 2-4: Example of shear splice detail investigated by Josi *et al*. (1999)

CHAPTER 3

FINITE ELEMENT MODEL DEVELOPMENT

3.1 INTRODUCTION

This chapter describes the finite element model developed to investigate the effect of fastener hole pattern on the stress concentration factor (SCF) for built-up I shape tension members riveted to gusset plates. A detailed description of the model geometry, material properties, element type, mesh type, mesh refinement, boundary conditions and loads is presented.

Two models of a plate with a circular hole were developed for a preliminary investigation of the behaviour observed in the built-up sections and to validate the element type and size used for this study. The first model used for the validation of the procedure consisted of a plate with a central hole loaded in tension. The second model consisted of a plate with staggered circular holes. This detail was used for the validation process because the results of analyses on flat plate with staggered holes can be compared with the behaviour observed in built-up sections with staggered holes presented in the next chapter. The same material properties, but different restraint conditions, are used for all the models.

3.2 FINITE ELEMENT MODEL DESCRIPTION

3.2.1 MODEL GEOMETRY, MATERIAL PROPERTIES

The effect of fastener hole layout and connection size for tension members is investigated using a typical diagonal tension member to gusset plate connection of the top chord of a bridge truss investigated experimentally by DiBattista and Kulak (1995). The model consists of a diagonal member with built-up I section comprising four 152×89×11.1 mm angles riveted to a 356×9.5 mm web plate. The rivet hole spacing in the built-up tension members tested by DiBattista and Kulak

(1995) was variable, decreasing from 76 mm at the loaded end of the gusset plate to 38.1 mm at the unloaded end of the tension member. A cross-section of the built-up I section is shown in Figure 3-1. Since the built-up I section is doubly symmetric, only one quarter of the connection is modelled in the finite element analysis as shown in Figure 3-2 (a). One quarter of the connection consists of one quarter of the web plate and one angle. The connection was modeled with 22.0 mm diameter fasteners, intended to simulate rivets or snug-tight bolts of size commonly used in the field. The 3D deformable shell element from ABAQUS with an elastic material defined by Young's modulus of 200 000 MPa and Poisson's ratio of 0.3 is used for the model. Since the analyses were conducted to determine the stress concentration factor for application in fatigue life calculations, the stresses in existing structures with these members are expected to be well below the yield strength of the material. Therefore, only linear elastic analyses were conducted. Figures 3-2 (b) and (c) show the model in ABAQUS/CAE.

3.2.2 Mesh refinement study, mesh type and Element type

The model was partitioned into various zones to generate the mesh. A rectangular region of refined mesh was formed around three fastener holes where the critical hole, the one with the peak principal stress, was expected to be located. The remaining portion of the model made use of a coarser mesh with an average element size of 20 mm. The refined mesh zone was located around the first three loaded holes to capture properly the interaction between the critical hole and the adjacent holes. An overall view of the finite element mesh is shown in Figure 3-2 (c).The mesh in each partition was generated using the free meshing technique of ABAQUS/CAE. To choose an appropriate element size and element type, a mesh refinement study was carried out using shell elements S4R, S4 and S8R. S4 is a linear, fully integrated quadrilateral four node shell element and the S4R element is a linear reduced-integration quadrilateral four node shell element, both of which are general purpose shell elements. S8R is a reduced-integration eight

node shell element. Only shell elements were investigated because out-of-plane behaviour was expected. The mesh size within the refined mesh partition was decreased gradually from 6.35 mm to 2.54 mm to ensure that convergence was reached. Element S8R with an element size of 2.54 mm was selected because, as shown in Table 3-1 and Figure 3-3, the peak stress with element S8R had converged, and although an element size of 6.4 mm or 5.08 mm may have been adequate. It was found that there was no significant difference computational time between using the different element sizes. Figure 3-4 shows a closer view of the mesh around the refined mesh area for shell element S8R and different element sizes. Quadrilateral shaped elements dominated the model.

3.2.3 Boundary conditions and loads

The boundaries of the model were defined and all loads and boundary conditions were applied before the mesh was generated. One quarter of the perimeter of the holes in the angle leg connected to the gusset plate had all translational and rotational degrees of freedom fixed, except for the translation in the load direction, that is, the 3-direction (refer to Figure 3-2 (a) for the axis and directions used). The degree of freedom in the loading direction was restrained with springs. The combined stiffness of all the springs restraining one hole was taken as 70 kN/mm, which corresponds to the stiffness of a single fastener and gusset plate in shear. This stiffness was obtained from the results of bolt shear tests on 22 mm high strength bolts presented by Moore *et al.* (2008). The quarter hole in the refined mesh region contained eight elements. Therefore, the fastener stiffness value was divided equally between the nine nodes defining the corners of these elements. Springs were added only to the corner nodes of the S8R elements, leaving intermediate nodes without any spring.

In addition to the boundary restraints at the fastener holes, symmetry boundary conditions were imposed to the nodes along the two planes of symmetry. The top of the web (1-3 plane) had vertical translational degrees of freedom (the 2-direction) and the rotational degrees of freedom about an axis perpendicular to the

axis of the member (the 1-axis) restrained. Also the entire web surface on the 2-3 plane of symmetry had the translation in the 1-direction restrained. It also had rotation about the 3-axis, parallel to the member axis, restrained.

To model the interaction between the web, the fasteners and the angle, constraint equations were used. Ties in the load direction (3-direction) were used to connect the nodes, A6, A7, and A8 in the angle in contact with the fasteners to corresponding nodes in the web plate, W4, W3, and W2 in contact with the same fasteners (see Figure 3-5 (a)). Constraint equations were also used to tie the portion of the hole in the angle, A8, A1 and A2 in contact with a rivet to the portion of the rivet hole in the web plate, W6, W5, and W4 in contact with the same rivet in the direction transverse to the applied load (the 2-direction) to account for the interference of the fasteners with the connected material (see Figure 3-5 (b)). Finally, constraint equations were used to tie the degree of freedom in the thickness direction (the 1-direction) of the hole in the angle (A1 to A8) in contact with the rivets to the same degree of freedom at a portion of the hole in the web (i.e. W4) in contact with the same rivet.

The free end of the angle was loaded with an edge load of 7.65 kN/mm, and the web was loaded with an edge load of 3.28 kN/mm. Since the angle and the web have thickness of 11.1 mm and 9.5 mm, the model then had a uniform tensile stress of 0.69 kN/mm^2 in the 3-direction.

3.3 ANALYSIS

A linear elastic analysis was conducted although, as noted in Josi *et al*. (1999), when loading a plate with holes, high stress concentration around the holes can cause localized plastic zones. Josi *et al*.(1999) also performed an inelastic analysis of flat plates with holes and concluded that the stress range around a hole becomes elastic after the first load cycle, hence this study considered only linear elastic analysis. The SCF is computed as the ratio of the maximum stress, $\sigma_{\max}$, to the applied gross section stress, σ_{app} , as described by Equation (2-1).The

maximum stress is the major principal stress in the 3-direction, since at the boundary of the rivet holes the shear stress is zero.

3.4 MODEL VALIDATION

The model developed in this research had to be validated so that it can be used to investigate the effect of hole pattern and connection size on the SCF in built-up sections. The first step in the validation process consisted of testing the adequacy of the mesh described in the previous section for the built-up section by using the same mesh type and size for a flat plate for which the solution is well known, as discussed in chapter 2. A flat plate with a centre hole, fixed at one end and loaded at the other end, was used for this phase of the analysis.

Further validation was carried out using the flat plate with staggered holes investigated by Schulz (1941), and discussed in Chapter 2. Since the solution has been established, the effect of parameters such as hole layout on the variation in SCF can be compared to the response of built-up I sections with similar variation in bolt layout.

3.4.1 FLAT PLATE WITH CENTERED HOLE

A flat plate model 102 mm×50.8 mm×6.4 mm with a 19 mm centre hole was modeled with S8R elements and the material properties described in section 3.2.1. Figure 3-6 (a) shows a diagram of the flat plate, and Figure 3-6 (b) shows the meshed model. The average element size near the hole is approximately 2.5 mm. One end of the model is restrained from rotation and translation in all directions and the other end has uniformly distributed load of 26.2 kN/mm, creating a gross section stress of 4.1 MPa. As reported in Kim and Sankar (2009), the maximum von Mises stress for this condition is 13.8 MPa. The mesh around the hole was further refined to an element size of 0.76 mm as shown in Figure 3-6 (c). Figure 3-6 (d) shows the contour plot for the von Mises stress for the flat plate modeled in ABAQUS. The maximum von Mises stress for an element size of 0.76 mm is about 2.2% less than with an element size of 2.54 mm, which has a

von Mises stress value of 13.8 MPa (2040 psi). Although the stress of interest in this study is not the von Mises stress, the reference from which the comparison was made with the finite element analysis results reported only the von Mises stress. Since the mesh and element type give good correlation with the theoretical value, the coarser mesh, element type and material properties for the built-up member are expected to yield reliable results.

3.4.2 THIN FLAT PLATE ELEMENT WITH STAGGERED CIRCULAR HOLE IN UNIAXIAL TENSION

A thin flat plate with staggered circular holes in uniaxial tension was used to validate further the finite element procedure proposed for built-up members. The plate model is 305 mm × 152 mm × 11.1 mm and has the same material properties, mesh type and element type as described in the previous section. This model was investigated by Schulz (1941) and the behaviour of this detail was reviewed in chapter 2. Figure 3-7 (a) shows the geometry of the plate investigated. The SCF obtained from the finite element analysis of this model is 3.46, which is about 8% higher than the SCF obtained from the chart presented by Schulz (1941). Figure 3-7 (b) shows the contour plot of the normal stresses parallel to the axis of the member. From the validation models it is observed that the S8R element with an element size of 2.54 mm gives good predictions of the maximum stress in flat plates with a single or multiple holes. Also, since we have used the same mesh type to predict the stresses for the staggered plate investigated by Schulz (1941), although the finite element analysis revealed that the SCF should have been 8% higher, we can confidently conclude that the mesh size and element type used for the flat plates is adequate for the built-up member.

Table 3-1: Mesh Refinement for different element types

Element type	**Average element size in the refined mesh zone (mm)**		
	6.4	5.1	2.5
S4R	2.85	3.01	3.58
S4	3.73	3.87	4.24
S8R	4.29	4.29	4.29

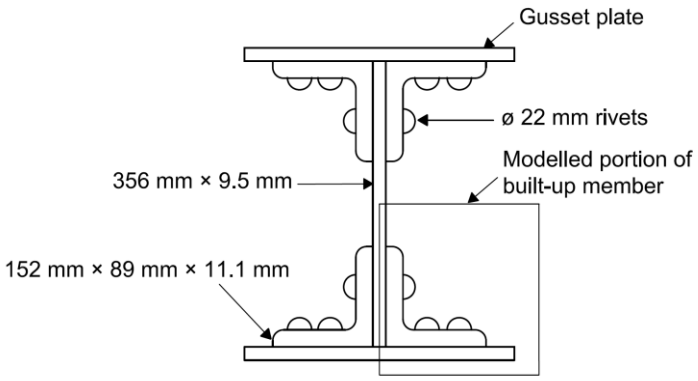

Figure 3-1: Typical section of riveted built-up tension member

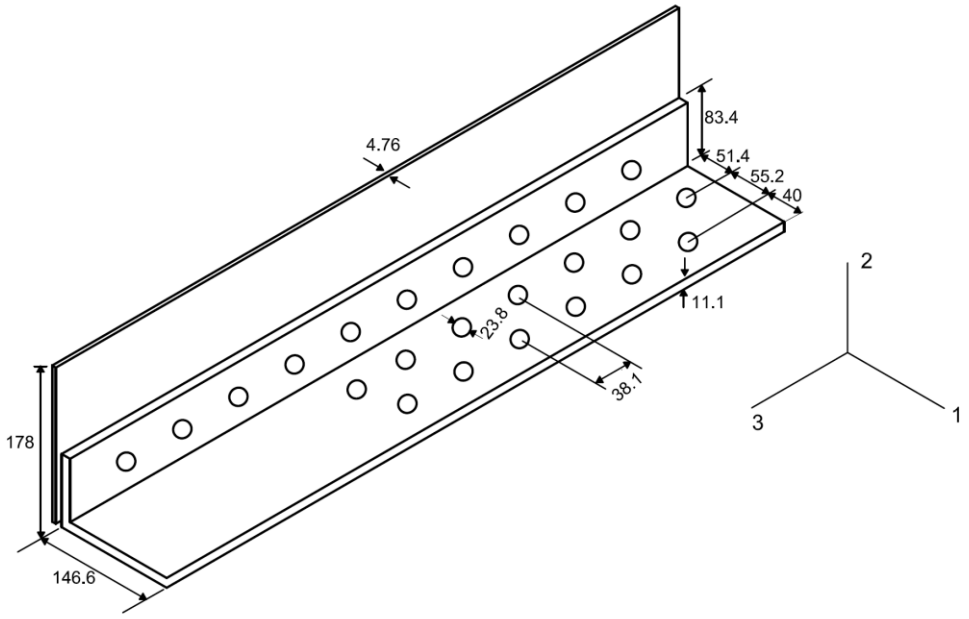

ALL DIMENSIONS ARE IN MILLIMETRES

(a) One quarter of the built-up member

Figure 3.2: Finite element model of built-up I-section

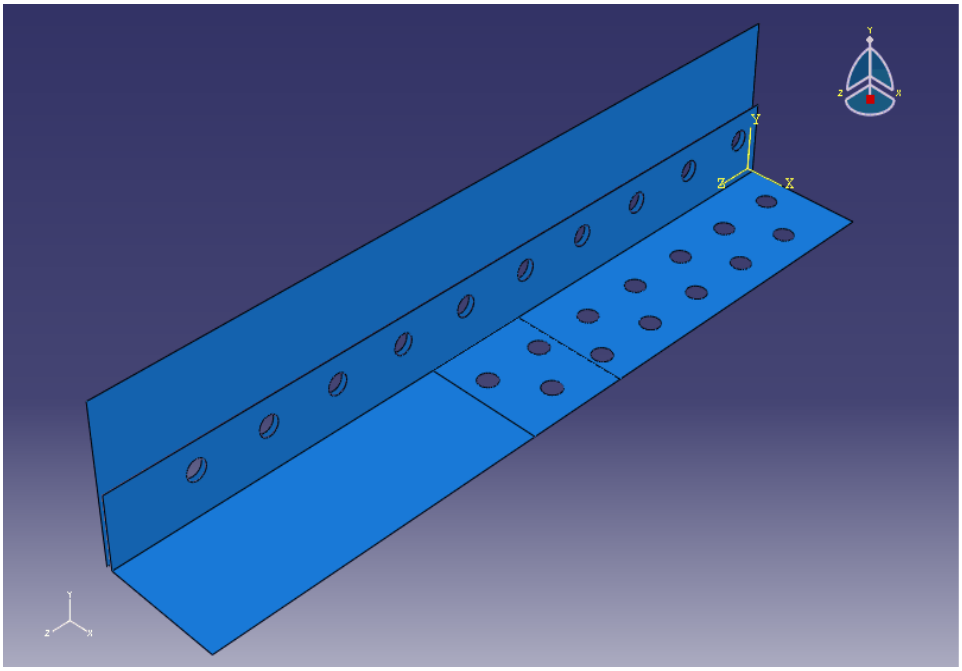

(b) ABAQUS/CAE Instance showing one quarter of the connection detail

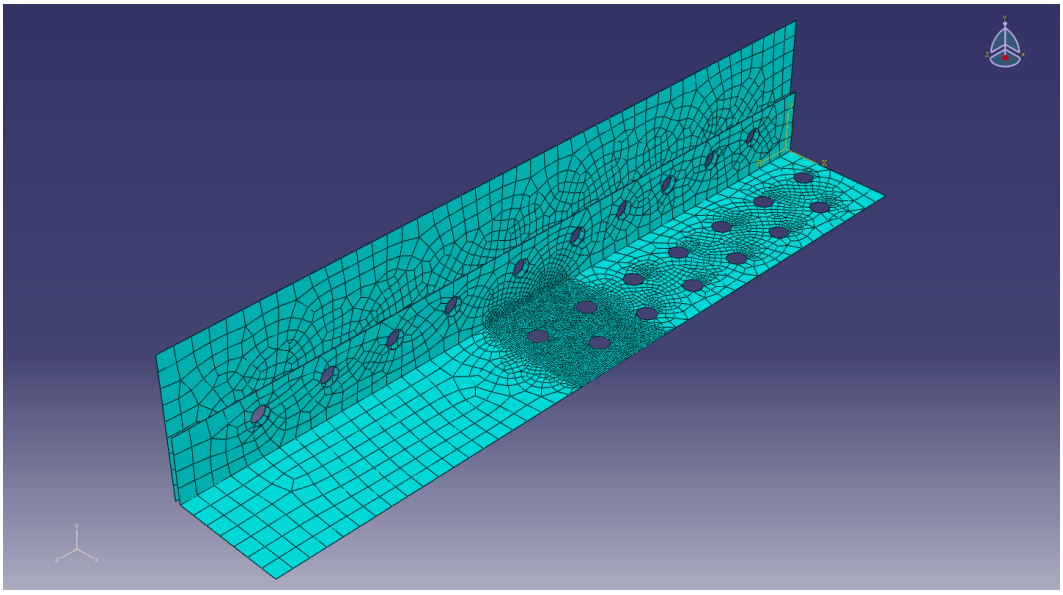

(c) Overall view of meshed connection

Figure 3.2: Finite element model of built-up I-section (Cont'd)

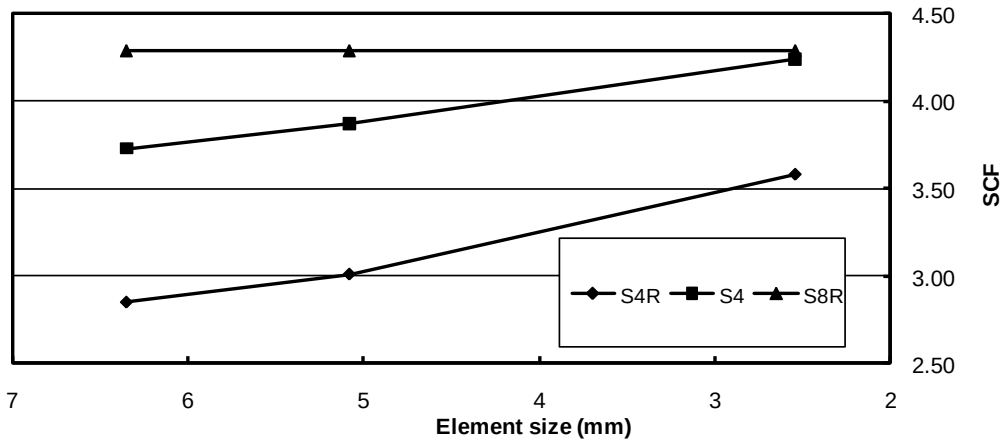

Figure 3-3: Plot of SCF versus element size in the refined zone (mesh study)

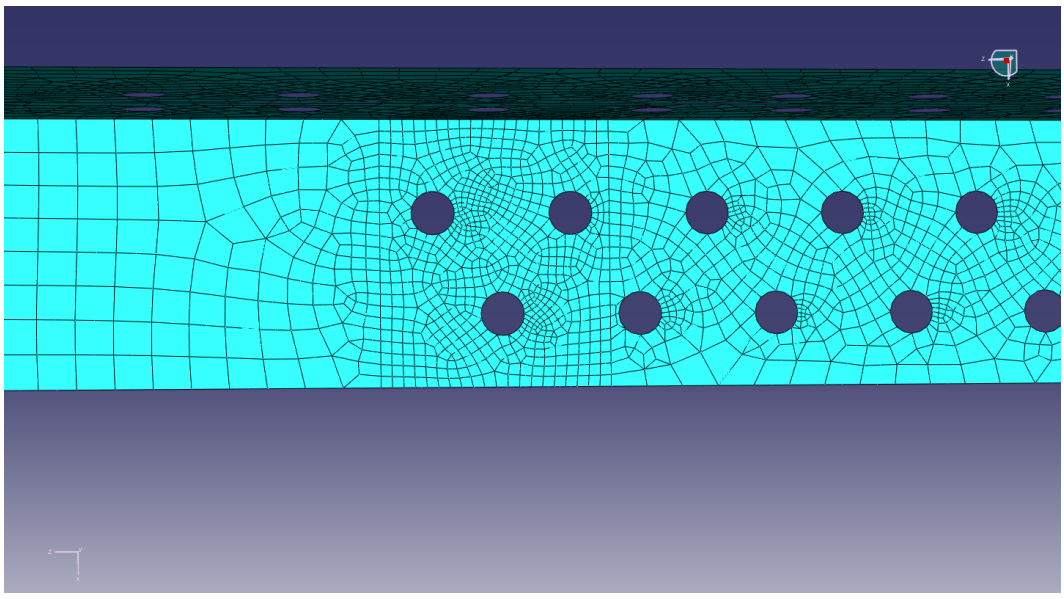

(a) Refined mesh for element size of 6.35 mm

Figure 3-4: Mesh study

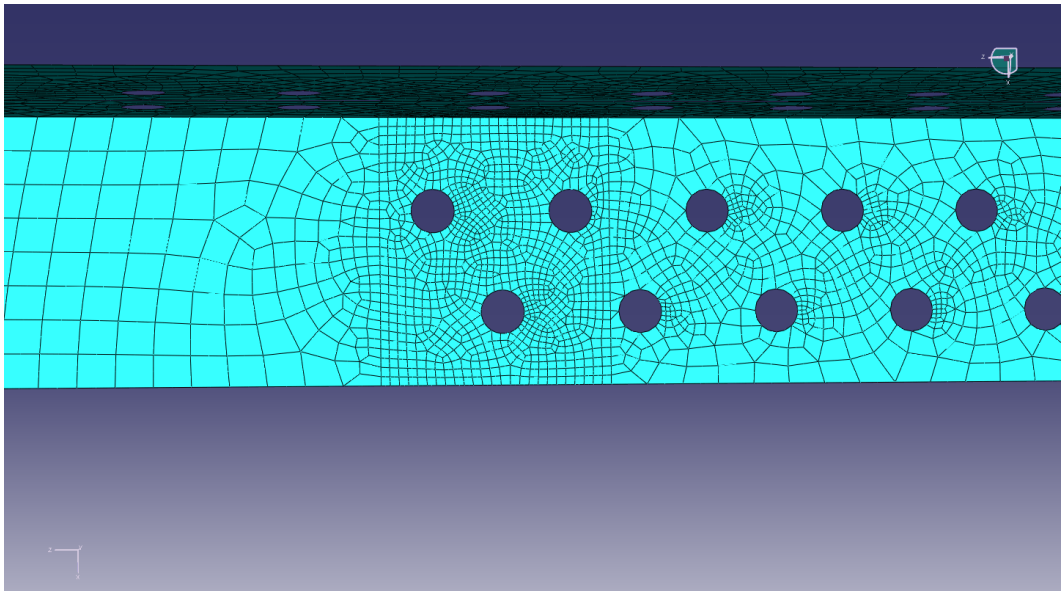

(b) Refined mesh for element size of 5.08 mm

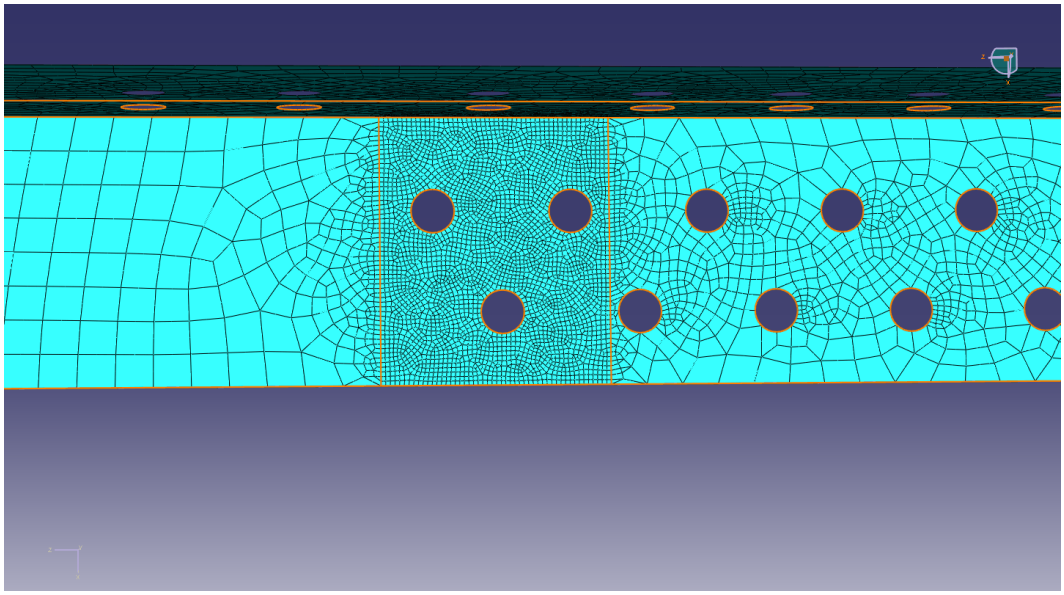

(c): Refined mesh for element size of 2.54 mm

Figure 3-4: Mesh study (Cont'd)

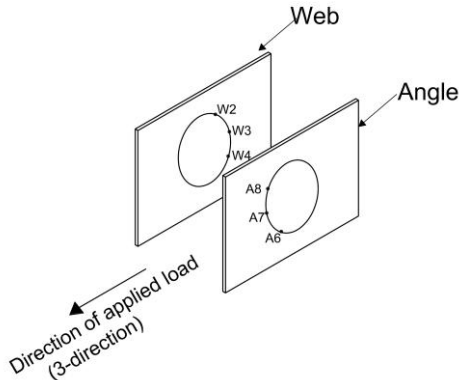

(a) Constraints in the load direction

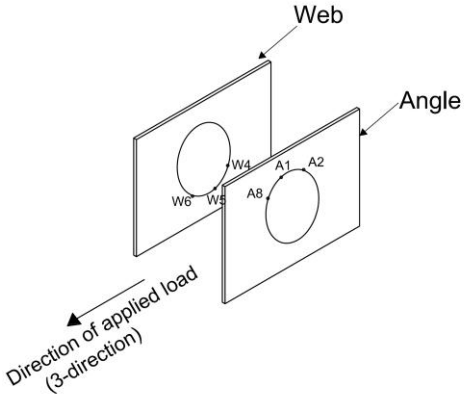

(b) Constraints in the 2- direction

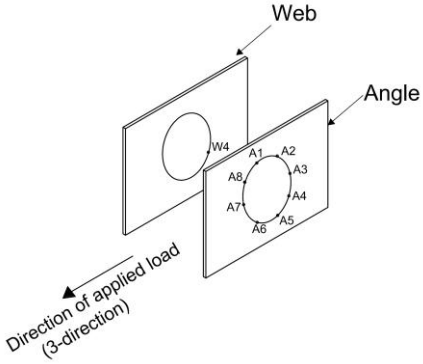

(c) Constraints in the 1- direction

Figure 3-5: Constaint used to tie the angle and web rivet holes

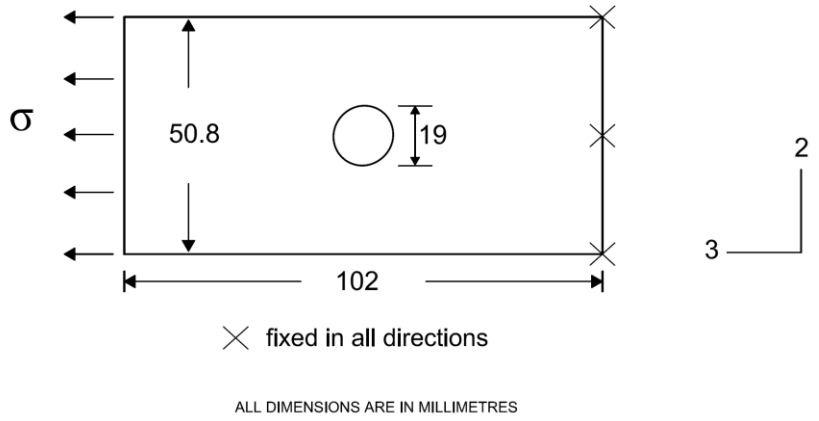

(a) Flat plate with centred circular hole restrained at one end

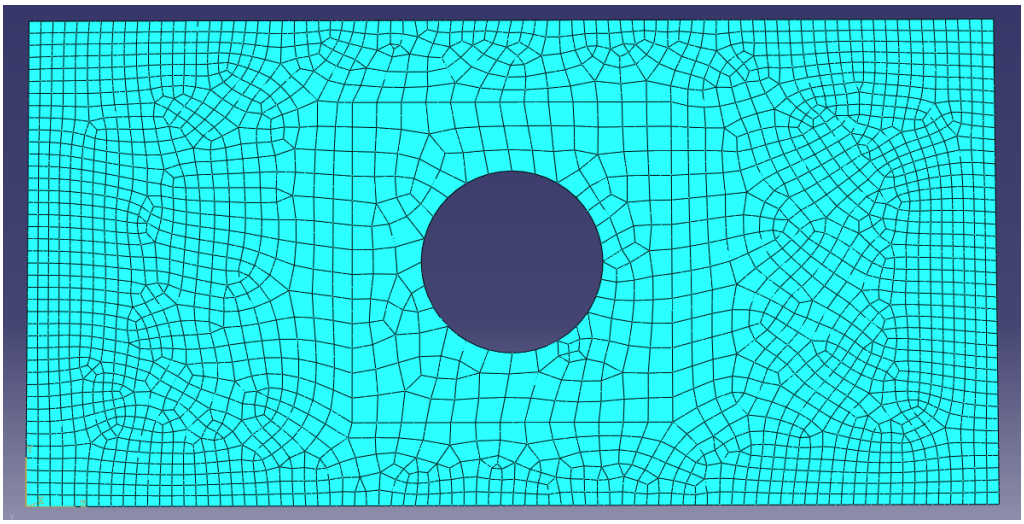

(b)Element size around hole of 2.54 mm

Figure 3-6: Flat plate with centered hole

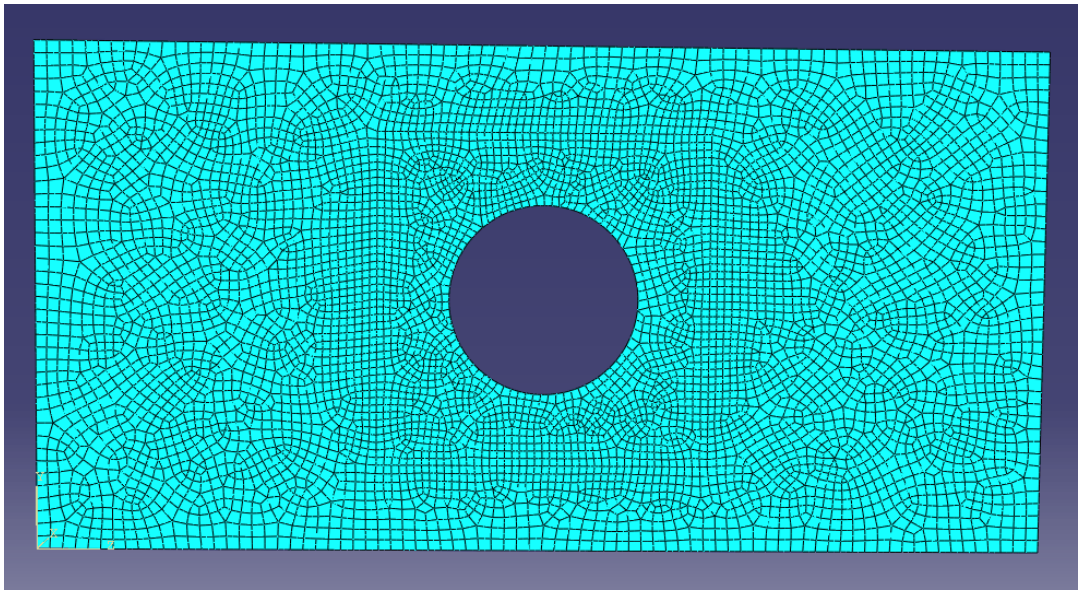

(c) Element size around hole of 0.76 mm

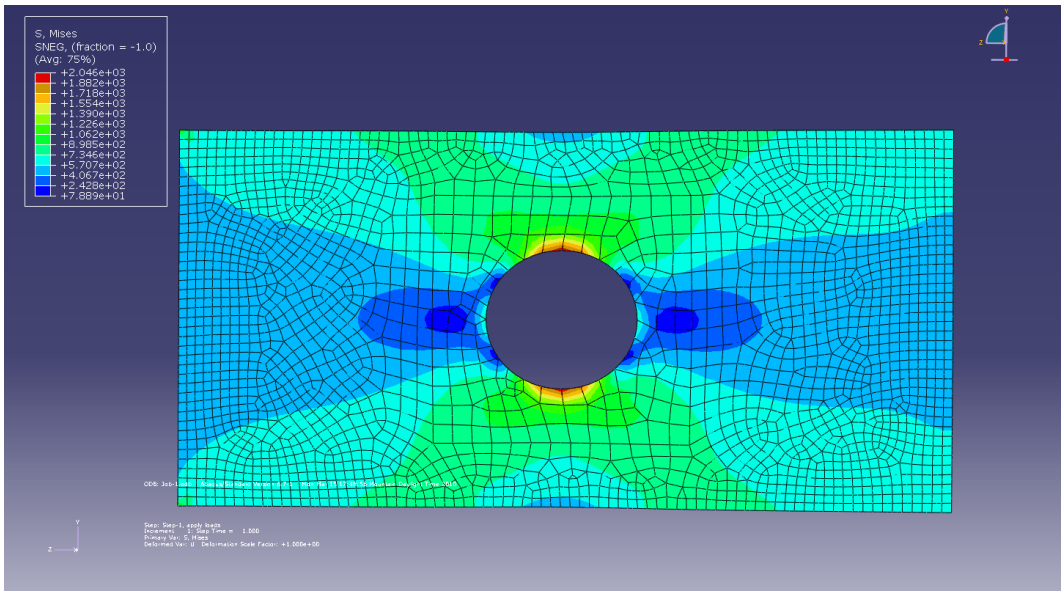

(d) Contour plot for maximum principal stress for a flat plate with a central hole (D = 19 mm)

Figure 3-6: Flat plate with centered hole (Cont'd)

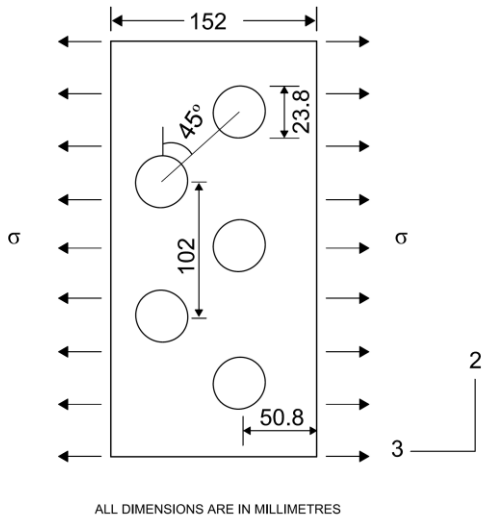

(a) Flat plate with staggered circular hole in uniaxial tension

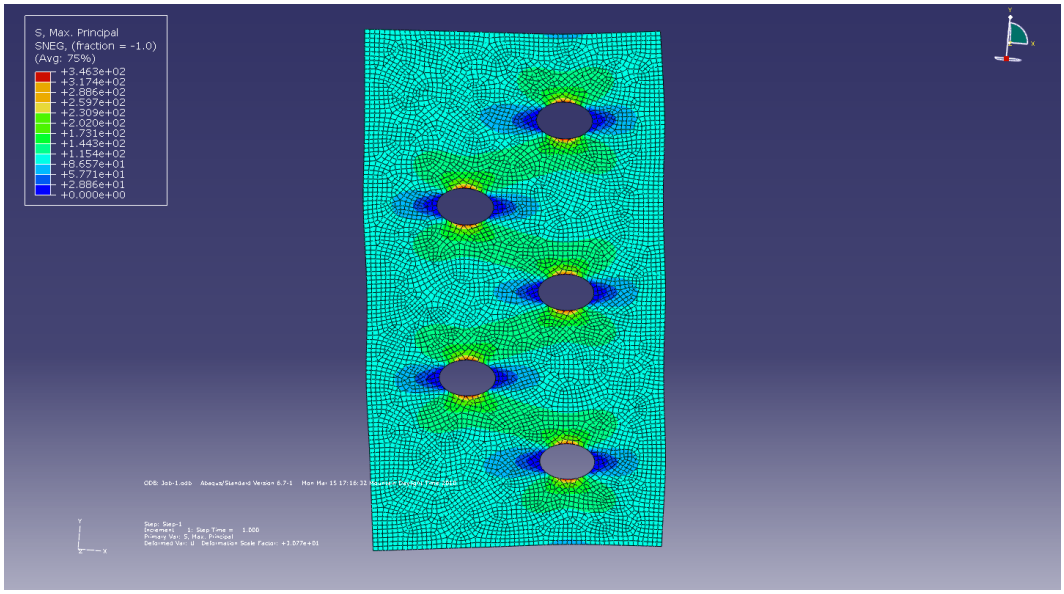

(b) Normal stress, σ_x, distribution

Figure 3-7: Flat Plate with staggered holes

CHAPTER 4

PARAMETRIC STUDY

4.1 INTRODUCTION

The effect on the stress concentration factor (SCF) of fastener hole pattern and size in built-up tension members was investigated using a built-up I-section connected to gusset plates. This model was developed using the finite element method described and validated in Chapter 3. The parameters investigated consist of: fastener hole stagger; gauge distance; edge distance; angle size and web size. Because the angle size was limited to standard sizes available from rolling mills, it was often not possible to vary only one parameter at a time.

A summary of the various connection geometries investigated is presented in Table 4-1. The hole stagger was varied from 38.1 to 60.4 mm for gauge distance varying from 38.1 to 60.4 mm, and keeping the edge distance close to the web constant. The effect of edge distance was investigated by varying the edge distance from 28.0 mm to 60.4 mm for hole staggers ranging from 38.1 to 60.4 mm, while the gauge distance was kept constant. The minimum hole spacing of 2.7 times the fastener diameter and the minimum edge distance specified in CSA-S16-09 was adhered to when choosing limiting values of stagger, gauge and edge distances. The effect of hole diameter was investigated by varying the hole diameter from 20.0 to 26.0 mm. The width of the angle leg connected to gusset plate was varied from 152.0 mm to 178.0 mm. The effect of web depth and web thickness was also examined in this study. A change in web size changes the ratio of the web area to the flange area (area of the angle leg connected to the gusset plates), which may be a parameter of interest that has a close relationship with the SCF since this is a factor that is known to affect the shear lag effect in a tension member (Munse and Chesson, 1963). The effect of angle size was investigated with equal and unequal leg angles of various sizes. Changing the angle size

invariably changes the area ratio, which will be discussed in details in the following chapter. The SCF is calculated in terms of the gross section stress (that is, the applied force divided by the gross section area). Figure 4-1 shows the portion of a built-up I section that was used in the finite element analysis and the geometric parameters that were investigated. The 1, 2, and 3 directions represent orthogonal reference axes, and the planes of symmetry are at the web mid height (the 1-3 plane) and at the mid-plane of the web (the 2-3 plane). Figure 4-1 also shows the locations of the maximum principal stress (MSL), identified as points a and b.

4.2 FINITE ELEMENT ANALYSIS RESULTS

4.2.1 EFFECT OF FASTENER/PLATE STIFFNESS

The geometry of the built-up I section tested by DiBattista and Kulak (1995) was used to investigate the effect of fastener/plate stiffness on the SCF. The dimensions of the built-up I section used in this section are presented as case 2 in Table 4-1. The member was built up from four 152×89×11.1 mm steel angles riveted to a 356×9.5 mm web plate. The rivet holes connecting the long leg of the angle to the gusset plate had a stagger of 38.1 mm and a gauge distance of 55.2 mm. The fasteners that were modeled were 22 mm (7/8 in.) rivets in 23.8 mm rivet holes and the connection length was 937 mm. Because the built-up member is doubly symmetric, only one quarter of the section was modelled, as can be seen in Figure 4-2(a). The rivets and the gusset plate were not incorporated to the model. Instead, the interaction between the member, the rivets and gusset plate was modeled with springs, as was explained in Chapter 3.

The first part of the investigation considered the effect of the stiffness of the member to gusset plate connection on the SCF. As shown in Table 4-2, different values of SCF are obtained with different stiffness. The stiffness for a 22 mm (7/8 in.) bolt/plate assembly in single shear is approximately 70 kN/mm, as obtained from the fastener/plate load deformation tests carried out by Moore *et al.* (2008).

Two other stiffness values, one of a 25.4 mm fastener/plate assembly and one for a 38.1 mm fastener/plate assembly were selected. The remaining six stiffness values were selected arbitrarily up to infinity as presented in Table 4-2. From Table 4-2 it can be seen that the SCF increases with increasing stiffness and reaches a limiting value of 9.69 at infinite stiffness. Figure 4-2(b) shows a stress contour plot for the connection with a fastener/plate stiffness of 70 kN/mm. Although the SCF increases significantly as the fastener stiffness increases, the variation for stiffness values corresponding to a large range of fastener diameter is relatively small. Therefore, the remaining investigation in this chapter will be conducted using a stiffness of 70 kN/mm. This is representative of the stiffness for the connections tested by DiBattista and Kulak (1995).

4.3 EFFECT OF HOLE STAGGER, GAUGE DISTANCE AND EDGE DISTANCE

Hole staggers of 38.1 mm, 46.5 mm, 50.8 mm, 55.0 mm and 60.4 mm are investigated for gauge distances of 38.1 mm, 46.5 mm, 50.8 mm, 55.0 mm and 60.4 mm. For all the cases investigated, the fastener spacing was at least 2.7D, which corresponds to the minimum spacing allowed in design standards (CSA 2001). It should be noted that, as the gauge distance is varied, the edge distance away from the web (that is, E_1 shown in Figure 4-1) also changes and so is the hole spacing. Table 4-3 shows the SCF for different values of stagger and gauge distance. The effect of stagger and gauge distance on the SCF is illustrated in Figure 4-3 for different values of gauge distance varying from 38.1 mm to 60.4 mm. The figure shows a decrease in SCF as the stagger increases. For the smallest stagger the SCF has a value of 4.30. This observation is consistent with the observation of DiBattista and Kulak (1995) who suggested that the close proximity of adjacent holes to the fatigue failure surface for members with staggered holes may increase the effective stress on the failure plane. It is also consistent with the observation by Schulz (1941), reviewed in section 2.3, which implied that an increase in stagger decreases the SCF. However, Josi *et al*. (2004)

observed that for a double lap shear splice with a stagger varying from 25.4 mm to 76.2 mm, the effect of stagger on the SCF was insignificant. Figure 4-4 shows plots of SCF versus gauge distance where it can be seen that the SCF decreases by less than 1.5% as the gauge distance increases from 38.1 mm to 60.4 mm, but for combinations of stagger and gauge distances that resulted in a spacing less than 2.7 times the fastener diameter, the analysis was not carried out. It is therefore evident that the gauge distance has a negligible effect on the SCF.

The effect of the edge distance close to the web, E_2, on the SCF was investigated for values of 28.0 mm, 38.1 mm, 45.0 mm, 51.4 mm and 58.4 mm. Hole staggers of 38.1 mm, 46.5 mm, 50.8 mm, 55.0 mm and 60.4 mm were also used with these edge distances. The gauge distance was kept constant at 55.2 mm for all combinations of edge distance and stagger. Table 4-4 shows the combination of stagger and edge distances used for this investigation. To illustrate the effect of edge distance, plots of SCF versus edge distance are shown in Figure 4-5. From the plot we can observe that, for a given stagger, as the edge distance increases the SCF decreases, but this trend changes depending on factors such as the proximity of the critical fastener hole to the hole in the angle flange connected to the web, the proximity of adjacent holes in the angle leg in contact with the gusset plate to the critical fastener hole, and finally, the edge distance E_1. For an edge distance of 28.0 mm, it was observed that the SCF was 4.36 for a stagger of 50.8 mm, and reduced to 4.16 for a stagger of 55.0 mm, and then increased again to 4.31 at a stagger of 60.4 mm. Apart from the fact that these holes are close to the web, for cases with stagger of 50.8 mm and 60.4 mm, a cross-section through the critical hole also intersects a hole in the angle leg connected to the web, hence the net section stresses would be higher for these particular cases. This is likely the cause for the increased SCF. Also, for an edge distance of 58.4 mm, and for staggers of 38.1 mm and 46.5 mm, the holes are getting close to the free edge of the angle (i.e. E_1 decreases), which tends to slightly increase the SCF, and the critical hole shifts to the second rivet hole, with the largest SCF at point b shown in Figure 4-1.

4.4 EFFECT OF FASTENER HOLE DIAMETER AND WIDTH OF ANGLE LEG CONNECTED TO GUSSET PLATE

Fastener hole diameters of 20.0 mm, 22.0 mm, 23.8 mm, and 26.0 mm were investigated although the hole diameter in most bridges would be typically 7/8 in (22.2 mm) plus 1/16 in (1.6 mm) or 23.8 mm. The effect of fastener hole diameter was investigated for two different sizes of angle leg connected to the gusset plate, namely, 152 mm and 178 mm. The stagger and gauge distance used were 38.1 mm and 55.2 mm, respectively, and the other dimensions were as shown for cases 72 to 79 of Table 4-1. Table 4-5 presents the values of the SCF for different hole diameters and two different widths of the angle leg connected to gusset plate. For the two angle sizes investigated, the SCF decreases by about 2.5%, as the hole diameter increases from 20.0 mm to 22.0 mm, and it then remains constant for increasing hole diameters up to 26.0 mm. The finite element models for all the hole diameters used the same element size around the fastener holes. However, it can be concluded that the influence of hole diameter is very small. The SCF is higher for a flange width of 178 mm than for a narrower flange width, possibly due to increased edge distance. This is consistent with the trend seen for the variation of SCF and edge distance for a stagger of 38.1 mm from Figure 4-5.

4.5 EFFECT OF WEB THICKNESS AND WEB DEPTH

Three web thicknesses were investigated, namely, 9.5 mm, 13.0 mm and 19.0 mm and three web depths were also investigated, namely, 254 mm, 356 mm and 508 mm. Table 4-6 shows the SCF for the various combinations of web thickness and web depth. Figure 4-6 shows the effect of web thickness on the SCF. From the plots it can be seen that for a constant web depth of 508 mm, the SCF versus the web thickness increasing at rate of about 0.077 per mm. At a web depth of 356 mm, it increases at a rate of 0.05 per mm, and for the smallest web depth of 254 mm the SCF increases with increase in web thickness at a rate of 0.032 per mm. Figure 4-7 shows a plot of SCF versus web depth. The SCF is found to

increase almost linearly with an increase in web depth. For web thicknesses of 9.50 mm, 13.0 mm and 19.0 mm, the slope of the plot between the SCF and the web depth increases at a rate of 0.00145, 0.00211, and 0.00311per mm, respectively.

4.6 EFFECT OF ANGLE SIZE (EQUAL/UNEQUAL ANGLE) AND ANGLE THICKNESS

The effect of change in angle size and angle thickness on the SCF was investigated and the results are presented in Table 4-7. All angles used for this investigation had a 152 mm leg connected to the gusset plate and a leg size connected to the web that varied from 89 mm to 152 mm. Although some of the angle thicknesses used in this study are not standard, the variety of thicknesses selected for this study should cover most thicknesses encountered in older bridges. Figure 4-8 illustrates an inverse non-linear relationship between the SCF and the angle thickness for all angle sizes. The SCF is also found to decrease as the size of the leg connected to the web of the member decreases. This is consistent with the earlier observation that shear lag effects decrease as the area of the web section (web plate and angle leg connected to the web, which are unconnected portions of the cross-section) decreases.

4.7 FATIGUE S-N CURVE FOR BEARING-TYPE CONNECTIONS

4.7.1 CURRENT FATIGUE PRACTICES

Current design standards, account for fatigue failure by calculating the stress range on the net section (obtained using Cochrane's $s^2/4g$ rule for staggered hole patterns) and assigning an appropriate fatigue category. The fatigue category used for bolted connection is category B and category D for riveted connections. This method accounts for the SCF in an implicit manner, namely, by selecting a fatigue category for different details. It has been observed that fatigue cracks propagate on a plane perpendicular to the axis of the member (DiBattista and Kulak, 1995; Josi *et al*., 2004) rather than on the plane of minimum net area calculated

according to Cochrane's rule. It was shown in earlier sections that the stagger, edge distance and the size of the connection do have an influence on the SCF for built-up I tension members in bearing, and these are not currently accounted for in the reference stress calculation. A net section calculated using the method proposed by Cochrane's $s^2/4g$ rule is not justified; hence a method that accounts for the SCF in the calculation of the stress range would be preferable.

Josi *et al.* (2004) proposed a method that takes into account the SCF in calculating the stress range for bearing type shear splices. Their proposed method is based on a calculated corrected stress range, obtained as follows. A stress concentration factor, taken as the ratio of the maximum stress, $\sigma_{\max}$, to the applied gross section stress, σ_{app}, is obtained as follows:

$$SCF_i = \frac{\sigma_{\max}}{\sigma_{app}} \tag{4-1}$$

A stress correction factor, F_{sc}, taken as the ratio of the stress concentration factor for the joint with hole stagger, SCF_i, to the stress concentration factor for the joint geometry without hole stagger, SCF_{so}, was proposed to obtain the design stress range, $\Delta\sigma_{sc}$, from the calculated gross-section stress range, $\Delta\sigma_g$, as shown in Equations (4.2) and (4.3).

$$F_{sc} = \frac{SCF_i}{SCF_{so}} \tag{4-2}$$

$$\Delta\sigma_{sc} = F_{sc}\Delta\sigma_g \tag{4-3}$$

Josi *et al.* (1999) tested 31 bearing-type shear splices at different stress ranges and the results are presented in Table 4-8. Using finite element analysis, they obtained the stress correction factor, F_{sc}, used to correct the gross section stress range for

fatigue life prediction. Based on the transformed stress ranges and the corresponding fatigue life obtained from the test program, the mean fatigue curve was obtained as follows,

$$LogN = 20.0 - 6.95Log\Delta\sigma_{sc} \quad (4\text{-}4)$$

From these findings, it was suggested that the slope of 3, used in the current fatigue design curves is inadequate for these details and a slope of 7 was proposed. It was also observed that limited evidence was available to assess the applicability of the stress range correction factor, F_{sc}, approach developed for flat plates to built-up sections. The main hindrance for the application of the stress calculation using the method proposed by Josi *et al*. is the calculation of the reference stress concentration factor for a member without hole stagger. A different approach is therefore proposed.

From the previous sections it can be seen that the behaviour of flat plates differs from that of built-up I sections. Therefore, using the flat plate geometry as reference geometry for calculating the stress correction factor for built-up I section is not be justified. A method based on the peak stress range is proposed where the design peak stress range is obtained as follows:

$$S_r = SCF\Delta\sigma_g \quad (4\text{-}5)$$

Since the calculated stress range incorporates the effect of stress concentration, the fatigue curve used for design should be the fatigue category A curve. Figure 4-9 shows corrected test data from the Josi *et al.* (2004) test program where the stress range was calculated using Equation (4-5). The mean fatigue equation obtained from a regression analysis is as follows:

$$LogN = 24.2 - 6.96LogS_r \quad (4\text{-}6)$$

Equation (4-6) indicates that the slope remains essentially the same as that reported by Josi *et al*. (2004) but the intercept is increased to 24.2. The shallower

slope of approximately 7 proposed by Josi *et al*. seems to be justified considering that these details must have a significant crack initiation life compared to welded members for which the fatigue curves with a slope of 3 were derived. A theoretical derivation of the fatigue curve for this type of connection indicated that the fatigue life initiation stage accounted for a large portion of the total fatigue life (Chen *et al.* 2005). Figure 4-9 also compares the fatigue data with fatigue category A and the mean minus 2.0 standard deviations curve for the test data. It is clear from the figure that fatigue category A is a poor representation of the fatigue behaviour of flat plates with staggered bolt holes.

Fatigue category A curve was developed from the work of Fisher *et al*. (1970), where 374 steel beams were tested. The test specimens included 86 plain rolled and plain welded beams, 204 beams fabricated with cover plates, and 84 beams fabricated with shear splices tested to determine the fatigue strength. They observed that fatigue cracks in the rolled beams started from the rolled surface of the tension flange. The flaws from which fatigue cracks initiated can be grouped into four crack initiation patterns: 1) cracks starting from the contact plane between the loading actuator used in the tests and the tension flange of the beam; 2) cracks originating from the inner surface of the flange, theses flaws were observed to be similar to the one above, except that they initiated from stress raiser caused by wooden stiffeners used in the tests; 3) cracks starting from the rolled surface at the extreme fibre of the tension flange; and 4) cracks initiated at the tension flange tip. These researchers stated that the surface notches or stress raisers from the loading apparatus may have caused the early failure of the rolled beam subjected to reversed loading. A slope of 3, which was obtained from a regression analysis of the test results, was recommended for the design S-N curve. To minimise some of these sources of cracks, Fisher *et al*. (1974) improved the test setup and also used lateral bracing in the shear span instead of wooden stiffeners, but observed that some local influences could not be eliminated, and most of these flaws or discontinuities must have been created in the rolling operation. From the work of these researchers it is evident that we cannot have an "ideal" fatigue category A, which should be a detail with no stress raisers, since

either the rolled beams used for testing must have had some flaws due to the rolling operation, transportation to the lab for testing, and even the test set-up could introduce stress raisers. But surely fatigue category A should not have the same slope as the slope for welded details, since we expect a significant crack initiation life from rolled shapes with no stress raisers.

Figure 4-10 shows a plot of the mean regression fatigue curve and its equation, for a combination of Josi *et al*. (2004) and Graf (1951) test data plotted in terms of the peak stress range in the plates. From the figure we observe that the mean regression line has a shallower slope than fatigue category A curve. However, the fatigue curve shown in Figure 4-10 is steeper than that shown in Figure 4-9. The data from Graf (1951), obtained at relatively high stress ranges, showed a longer fatigue life than the fatigue lives observed in the Josi *et al*. test program, possibly because of the higher pretension in the bolts used in Graf's test specimens. This has the effect of changing the slope of the mean regression line from 6.97 to 4.58. The coefficient of determination, R^2, for the regression line is 0.67.

A combination of the test data from Josi *et al*.(2004), Graf (1951) for flat plates, and the results from DiBattista and Kulak (1995) on built-up riveted members are plotted in Figure 4-11. Table 4-10 shows the specimen type, the applied stress calculated on the gross section area and the SCF. The finite element analysis presented in Chapter 4 indicated that the top chord detail has a SCF of 4.16, and the bottom chord detail has a SCF of 4.12. SCF of 4.29, and 4.24 were obtained by conservatively taking the hole stagger as 38.1 mm for the top and bottom chord respectively, and the latter was used for the S-N curve presented in Figure 4-11. The bottom chord connection has the same geometry as the top chord except that the line of rivets close to the web had six rivets and the other line had seven rivets and critical holes was closer to the hole in the web. The top chord connection had seven rivets in the line close to the web and six rivets in the other line. To determine how the SCF in the bottom chord differs from the SCF of the top chord, two combinations of gauge and stagger that gives the highest and the lowest SCF for the top chord were used to investigate the SCF of the bottom chord connection

under tensile stresses. This was done by using the geometry that had the maximum SCF in the top chord (case 1), and interchanging the transverse lines of rivet for the bottom chord analysis, a SCF of 4.27 is obtained for the bottom chord, and using geometry with the least SCF for the top chord detail (case 22) and interchanging the lines of fasteners parallel to the axis of the member, a SCF of 3.97 is obtained.

The smaller SCF for the bottom chord member explains why DiBattista and Kulak (1995) observed that the bottom chord detail had a longer fatigue life than the top chord. Compared to the test results from the other two test programs, the fatigue life for the specimens tested by DiBattista and Kulak were tested at a low stress range and showed a significantly shorter fatigue life than expected from the fatigue test results from the other test programs. Therefore, the equation of the mean regression curve for the test specimens from all three sources showed a steeper slope, approaching the slope expected for a welded detail. It is suspected, that the detail investigated by DiBattista and Kulak (1995) might have suffered from fatigue damage or corrosion related damage prior to testing since the bridge had been in service for 80 years before the test specimens were extracted from the bridge.

Although the combination of test results from three sources indicate that the slope of the mean S-N curve is close to 3.0, it seems that the test data from Graf (1951) and DiBattista and Kulak (1995) do not belong to the same population as those from Josi et al. (2004) and might inadvertently bias the fatigue curve slope. A slope of 7, based on the tests from a single source, seems more appropriate for a fatigue design curve for bolted or riveted joints.

Table 4-1: Different cases investigated in the parametric study

CASE	W_d	W_t	S_d	L_w	L_t	D	S	G	E_2	E_1	S_p	MSL[1]
1								50.8		44.4	63.5	b
2							38.1	55.2		40.0	67.1	b
3								60.4		34.8	71.4	a
4								46.5		48.7	65.8	a
5								50.8		44.4	68.9	a
6							46.5	55.2		40.0	72.2	a
7								60.4		34.8	76.2	b
8								38.1		57.1	63.5	a
9								46.5		48.7	68.9	a
10							50.8	50.8		44.4	71.8	a
11								55.2	51.4	40.0	75.0	a
12								60.4		34.8	78.9	a
13								38.1		57.1	66.9	a
14	356	9.50	89.0	146	11.1	23.8		46.5		48.7	72.0	a
15							55.0	50.8		44.4	74.9	a
16								55.2		40.0	77.9	a
17								60.4		34.8	81.7	a
18								38.1		57.1	71.4	a
19								46.5		48.7	76.2	a
20							60.4	50.8		44.4	78.9	a
21								55.2		40.0	81.8	a
22								60.4		34.8	85.4	a
23									28.0	63.4		a
24									38.1	53.3		a
25							38.1	55.2	45.0	46.4	67.1	a
26									51.4	40.0		b
27									58.4	33.0		b
28				127			46.5		28.0	63.4	72.2	a

***** Refer to Figure 4-1 for diagram showing all the parameters in Table 4-1

[1] MSL refers to the location of the maximum principal stress (that is, either a or b in Figure 4-1)

Table 4-1: Different cases investigated in the parametric study (Cont'd)

CASE	W_d	W_t	S_d	L_w	L_t	D	S	G	E_2	E_1	S_p	MSL
29									38.1	53.3		a
30							46.5		45.0	46.4	72.2	b
31									51.4	40.0		a
32									58.4	33.0		b
33									28.0	63.4		a
34									38.1	53.3		a
35							50.8		45.0	46.4	75.0	a
36									51.4	40.0		a
37	356								58.4	33.0		b
38		9.50							28.0	63.4		a
39									38.1	53.3		a
40							55.0		45.0	46.4	77.9	a
41									51.4	40.0		a
42			89.0	146	11.1	23.8		55.2	58.4	33.0		a
43									28.0	63.4		a
44									38.1	53.3		a
45							60.4		45.0	46.4	81.8	a
46									51.4	40.0		a
47									58.4	33.0		a
48												b
49	254	13.0										b
50		19.0										b
51		9.50										b
52	356	13.0					38.1		51.4	40.0	67.1	b
53		19.0										b
54		9.50										a
55	508	13.0										b
56		19.0										b

Table 4-1: Different cases investigated in the parametric study (Cont'd)

CASE	W_d	W_t	S_d	L_w	L_t	D	S	G	E_2	E_1	S_p	MSL
57				148	7.90							a
58				147	9.50							a
59			152	145	13.0							a
60				144	16.0							b
61				142	19.0							b
62				148	7.90							a
63				147	9.50	23.8						a
64			102	145	13.0							b
65				144	16.0							b
66				142	19.0							b
67				148	7.90							a
68	356	9.5		147	9.50		38.1	55.2	51.4	40.0	67.1	a
69				145	13.0							b
70				144	16.0							b
71				142	19.0							b
72						20.0						b
73			89.0	146		22.0						a
74						23.8						b
75					11.1	26.0						b
76						20.0						b
77				172		22.0						b
78						23.8						b
79						26.0						b

Table 4-2: Effect of fastener/plate stiffness on the stress concentration factor

Case Number*	Stiffness (kN/mm)	SCF
1 (22 mm bolt)	70	4.29
(25.4 mm bolt)	96.2	4.33
(38.1 mm bolt)	179	4.59
2	700	5.51
3	1750	6.41
4	123 000	9.51
5	1 230 000	9.67
6	2 450 000	9.68
7	∞	9.69

* The case number refers to the cases described in Table 4-1.

Table 4-3: Stress concentration factor for different hole staggers and gauge distances

Gauge width (mm)	Stagger (mm)				
	38.1	46.5	50.8	55.0	60.4
38.1	< 2.7D*	< 2.7D	4.12 [8]	4.08 [13]	4.06 [18]
46.5	< 2.7D	4.14 [4]**	4.11 [9]	4.07 [14]	4.06 [19]
50.8	4.30 [1]	4.13 [5]	4.10 [10]	4.07 [15]	4.00 [20]
55.2	4.29 [2]	4.12 [6]	4.10 [11]	4.06 [16]	3.99 [21]
60.4	4.24 [3]	4.12 [7]	4.08 [12]	4.05 [17]	3.98 [22]

* < 2.7D refers to the cases with hole spacing less than 2.7 times the diameter. These models were not investigated and no value of SCF is reported.

** The number in brackets refers to the case number described in Table 4-1.

Table 4-4: Stress concentration factor for different hole staggers and edge distances

Edge distance, E_2 (mm)	**Stagger (mm)**				
	38.1	46.5	50.8	55.0	60.4
28.0	4.44 [23]*	4.41 [28]	4.36 [33]	4.16 [38]	4.31 [43]
38.1	4.31 [24]	4.20 [29]	4.19 [34]	4.08 [39]	4.14 [44]
45.0	4.23 [25]	4.08 [30]	4.17 [35]	4.10 [40]	4.09 [45]
51.4	4.29 [26]	4.12 [31]	4.10 [36]	4.06 [41]	3.99 [46]
58.4	4.35 [27]	4.16 [32]	4.08 [37]	4.04 [42]	4.07 [47]

* The number in brackets refers to the case number described in Table 4-1.

Table 4-5: Stress concentration factor for different hole diameters and angle flange width connected to gusset plate

Flange width (mm)	**Hole diameter (mm)**			
	20.0	22.0	23.8	26.0
152	4.40 [72]*	4.29 [73]	4.29 [74]	4.29 [75]
178	4.49 [76]	4.38 [77]	4.38 [78]	4.38 [79]

* The number in brackets refers to the case number described in Table 4-1

Table 4-6: Stress concentration factor for different web thickness and web depth

Web depth (mm)	**Web thickness (mm)**		
	9.5	13.0	19.0
254	4.17 [48]*	4.27 [49]	4.47 [50]
356	4.29 [51]	4.46 [52]	4.77 [53]
508	4.54 [54]	4.81 [55]	5.27 [56]

* The number in brackets refers to the case number described in Table 4-1

Table 4-7: Stress concentration factor for different angle sizes

Angle size (mm)	**Angle thickness (mm)**				
	7.9	9.5	13.0	16.0	19.0
152×152	4.98 [57]*	4.84 [58]	4.61 [59]	4.52 [60]	4.47 [61]
152×102	4.60 [62]	4.45 [63]	4.24 [64]	4.20 [65]	4.14 [66]
152×89	4.52 [67]	4.37 [68]	4.17 [69]	4.13 [70]	4.07 [71]

* The number in brackets refers to the case number described in Table 4-1.

Table 4-8: Results of fatigue test on Flat plates by Josi *et al*. (2004)

Specimen type	**Fatigue Life**	$\Delta\sigma_g$	**SCF**	F_{sc}
P	569 000	113	3.95	0.96
S0	2 167 000	90	"	1.00
S0b1	5 800 000	90	"	"
S0b2	767 000	90	"	"
S0c1	355 000	113	"	"
S0c2	620 000	113	"	"
S0d	581 000	113	"	"
S1a1	255 000	110	4.11	1.04
S1a2	303 000	110	"	"
S1b	1 558 000	110	"	"
S1c1	2 827 000	88	"	"
S1c2	2 900 000	88	"	"
S1d	8 520 000	88	"	"
S2a2	307 000	110	4.17	1.06
S2b	649 000	110	"	"
S2c1	3 816 000	88	"	"
S2c2	1 518 000	88	"	"
S2d	2 662 000	88	"	"
S3a1	685 000	110	"	1.06
S3a2	695 000	110	"	"
S3b	515 000	110	"	"
S3c1	3 562 000	72	"	"
S3d	16 000 000	72	"	"
Ga1	518 000	113	4.09	1.03
Ga2	295 000	113	"	"
Gb	318 000	113	"	"
Gc1	1 915 000	90	"	"
Gc2	2 894 000	90	4.09	"
Gd	1 000 000	90	4.09	"

Table 4-9: Results of fatigue test on Flat plates by Graf (1951)

Specimen type	Fatigue Life	$\Delta\sigma_g$	SCF
4	372 000	125	4.21
14	1 384 000	101	4.21
7	78 000	195	4.21
9	249 000	156	4.21
12	517 000	140	4.21
11	1 005 000	125	4.21

Table 4-10: Results of fatigue test on built-up section by DiBattista *et al*. (1999) and SCF from finite element analysis

Specimen type	Fatigue Life	$\Delta\sigma_g$	SCF
BD1	2 401 580	59.2	4.24
BD2	3 958 270	55.9	4.24
BD3	2 849 000	59.2	4.24
BD4	5 250 610	53.5	4.24
TD1	1 944 670	59.0	4.29
TD2	2 415 840	57.1	4.29
TD3	2 415 140	53.4	4.29

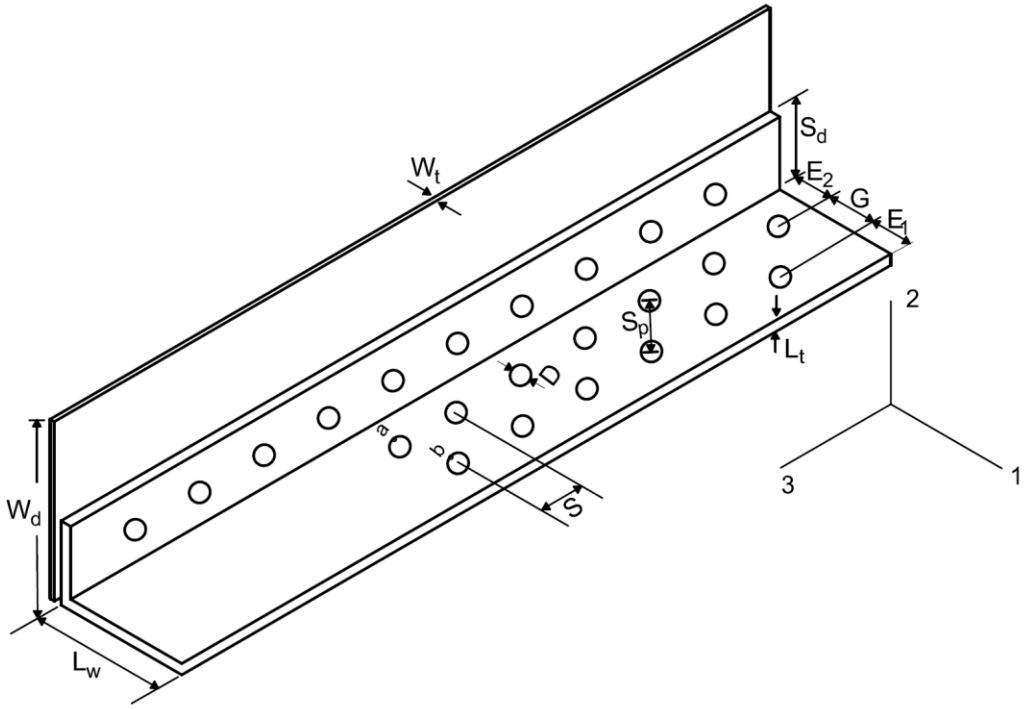

Figure 4-1: Built-up I section and critical hole location shown in Table 4-1(Locations of maximum principal stress)

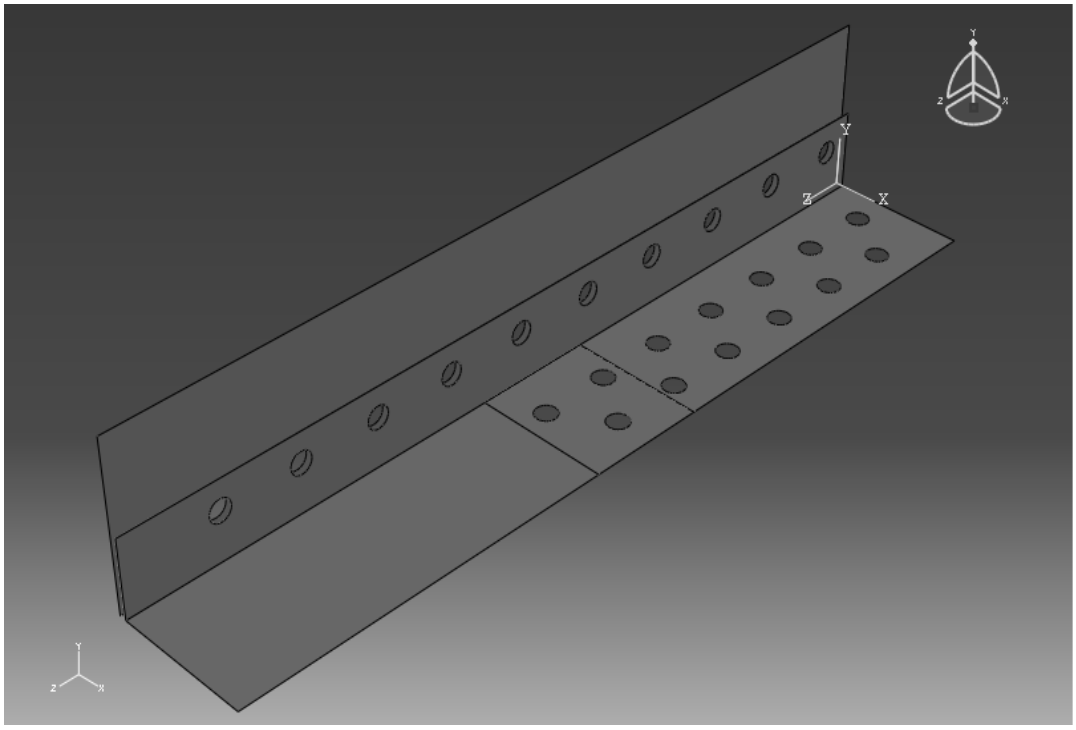

(a) One quarter of the built-up I section

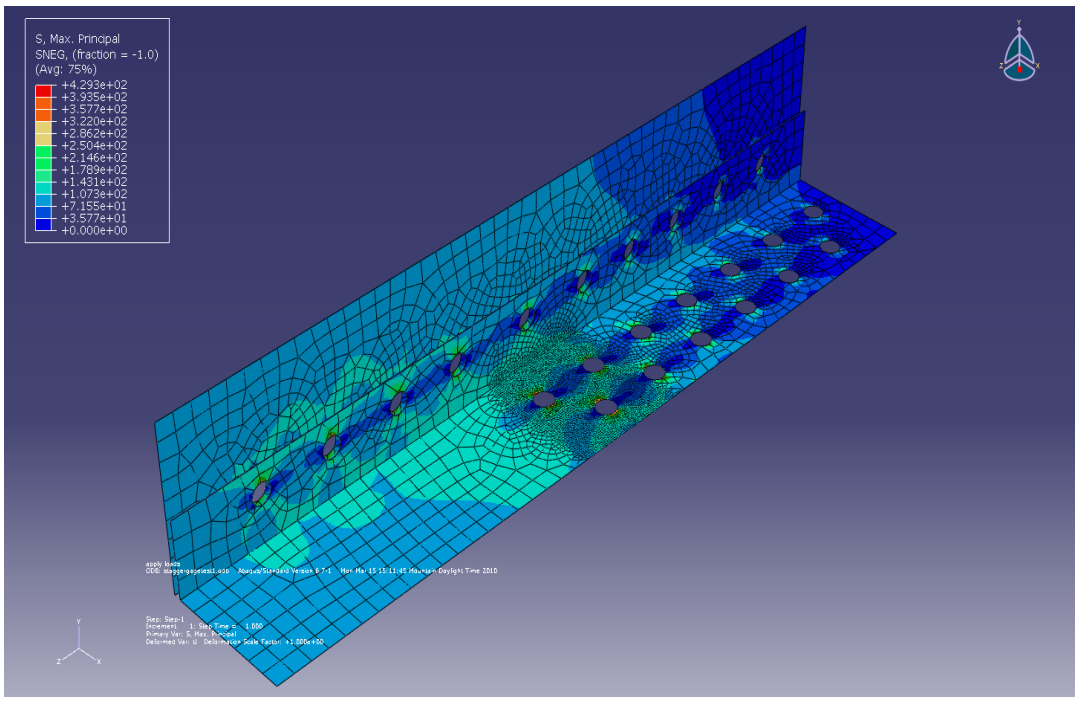

(b) Contour plot of maximum principal stresses with spring stiffness of 70.0 kN/mm

Figure 4-2: Built-up I section

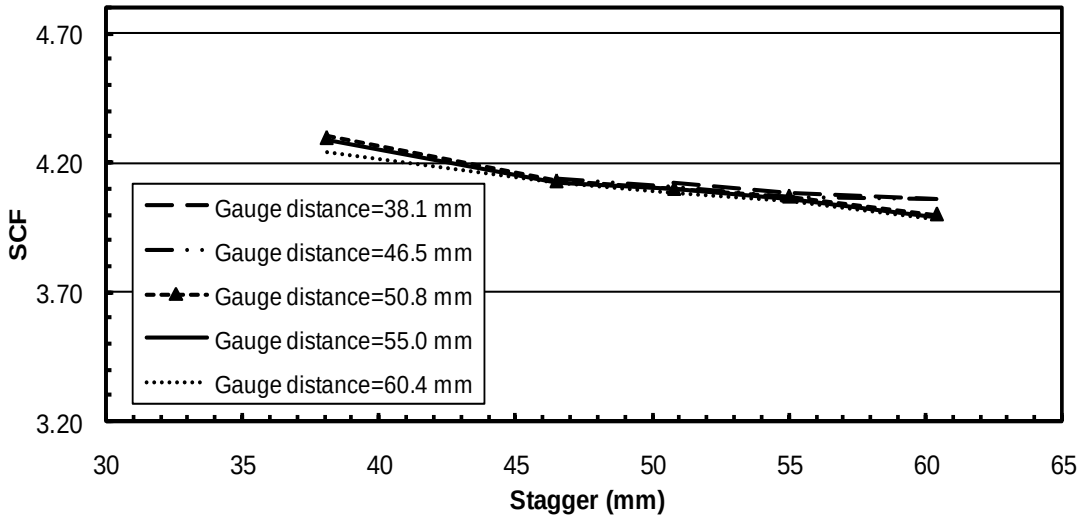

Figure 4-3: Effect of stagger on the stress concentration factor

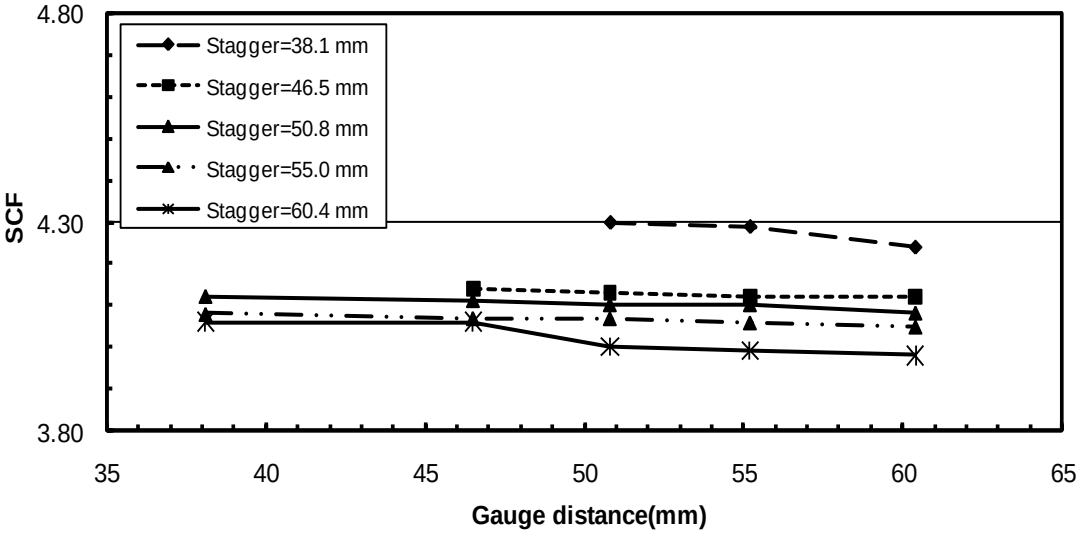

Figure 4-4: Effect of gauge distance on the stress concentration factor

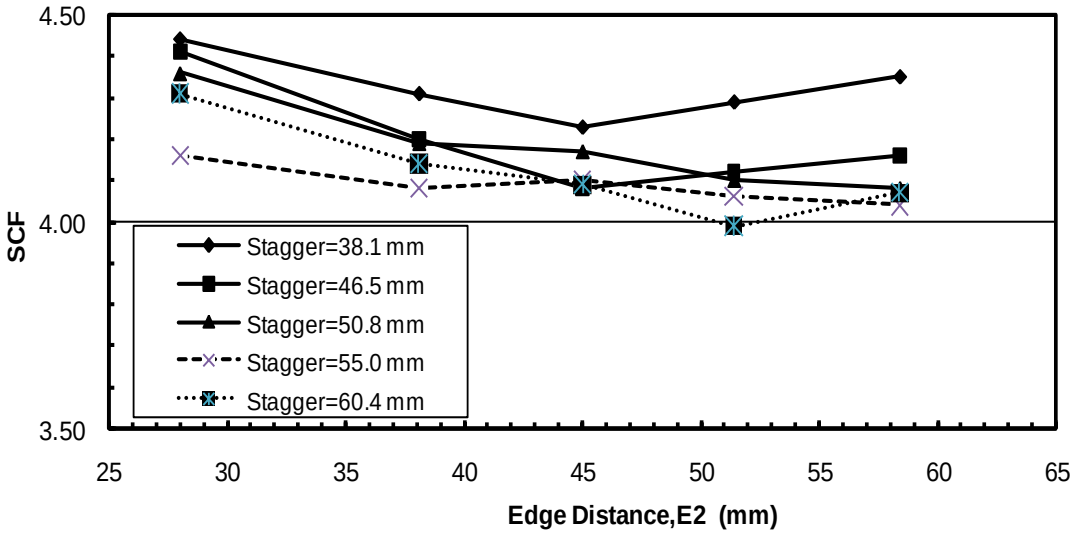

Figure 4-5: Effect of edge distance (for fixed stagger) on the stress concentration factor

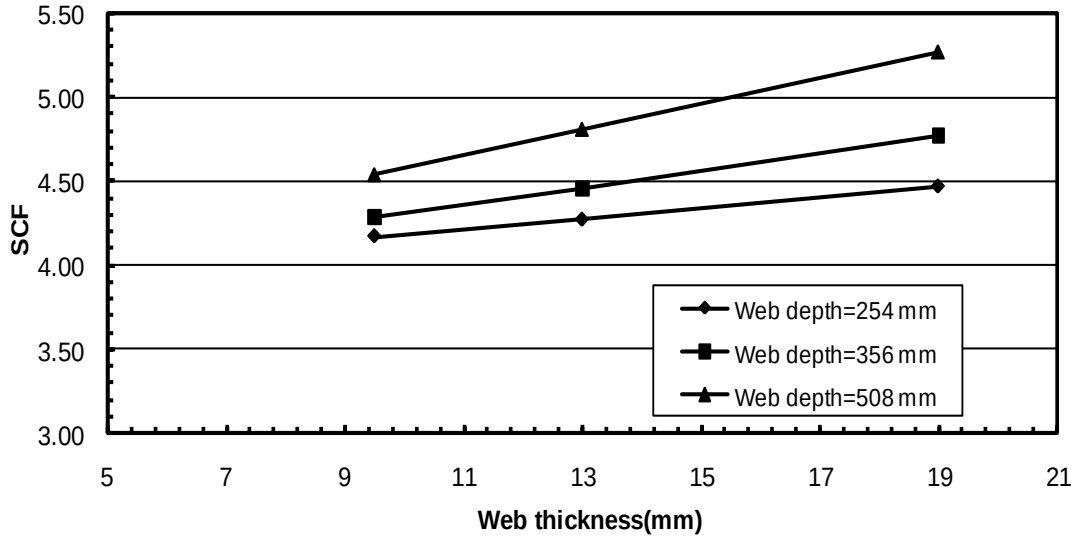

Figure 4-6: Effect of web thickness on the stress concentration factor

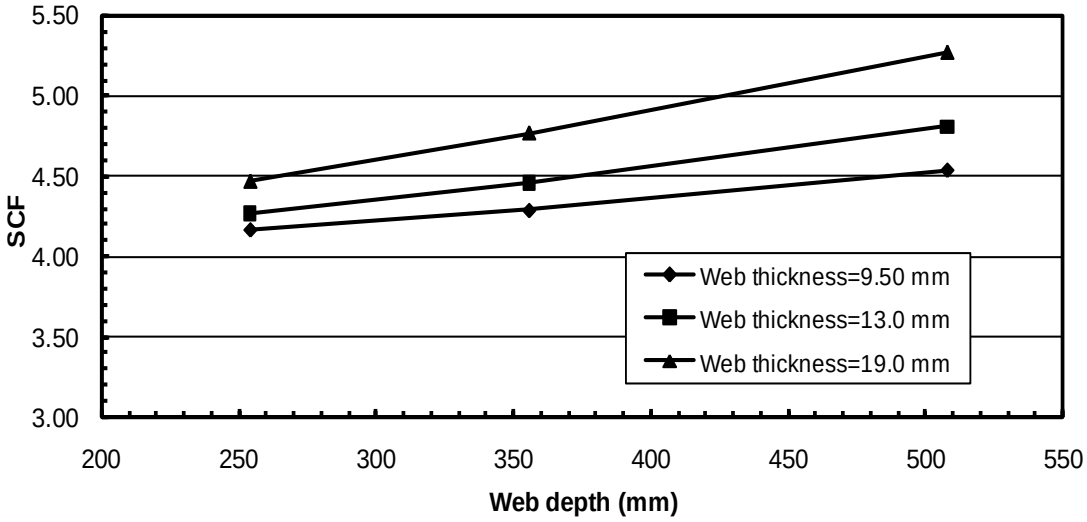

Figure 4-7: Effect of web depth on the stress concentration factor

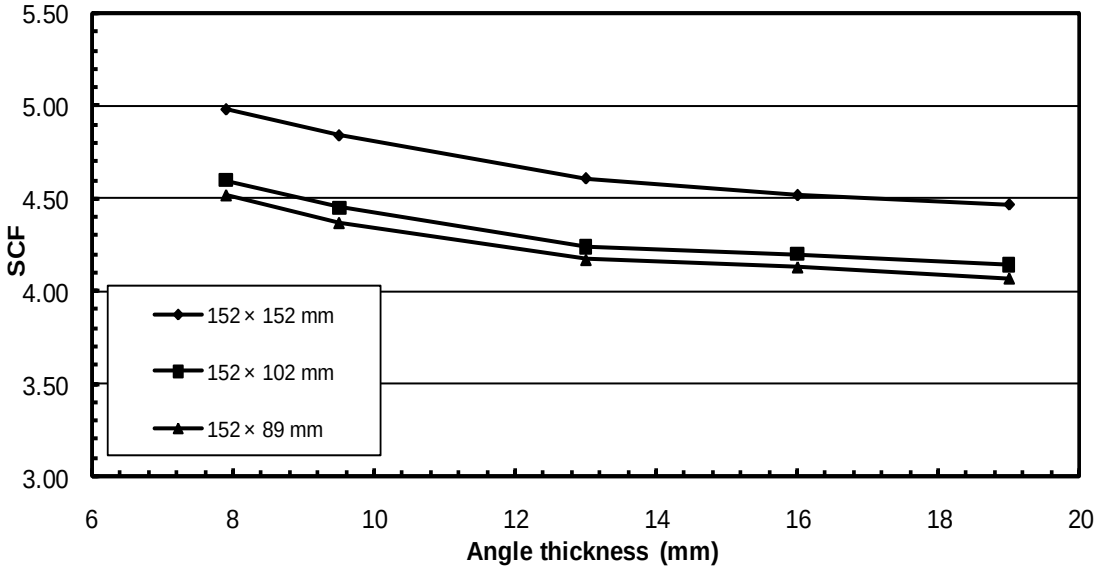

Figure 4-8: Effect of angle thickness on the stress concentration factor

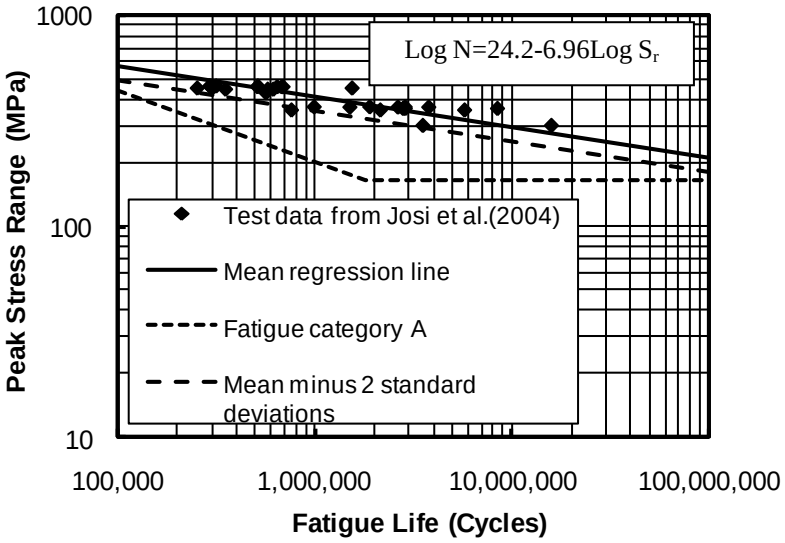

Figure 4-9: Test results and fatigue curve from Josi *et al*. (2004) compared to fatigue category A in terms of peak stress

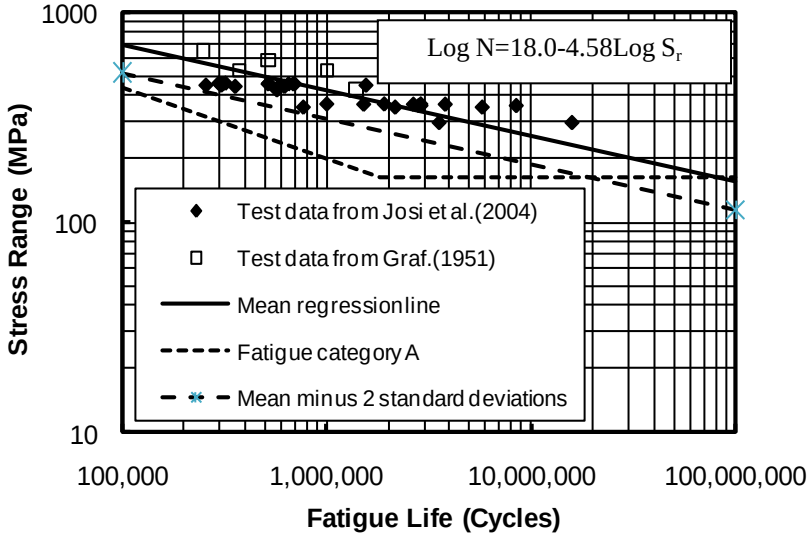

Figure 4-10: Mean fatigue curve for flat plates from two different sources

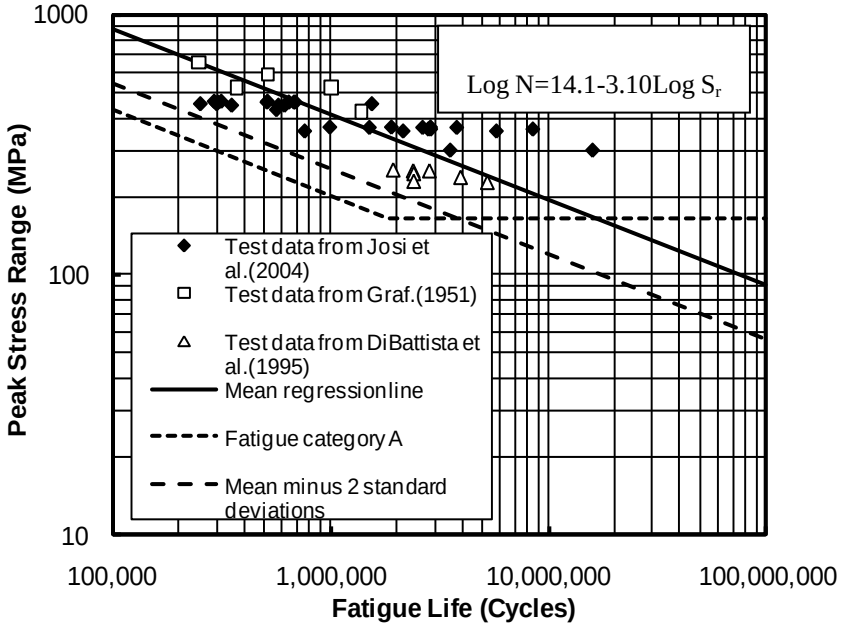

Figure 4-11: Comparison with fatigue curve for all test data with fatigue category A

CHAPTER 5

DEVELOPMENT OF SIMPLIFIED DESIGN EQUATION

5.1 INTRODUCTION

Accurate prediction of the stress concentration factor (SCF) in built-up members and flat plate lapped splice connections is essential for the accurate prediction of their fatigue life. Although the SCF can be obtained from a finite element analysis, such an approach is not desirable for design purposes. Hence, a simplified equation for the calculation of the SCF for most structural shapes is desirable.

A total of 71 built-up I section configurations were analyzed in a parametric study conducted with the finite element model developed in Chapter 3 and the results were presented in Chapter 4. Also Josi *et al*. (1999) has presented numerical and experimental work on the SCF for flat plates with staggered bolt holes. These results will be used to derive a simple relationship between connection size, hole pattern and the SCF. Although the equation can only be used for either built-up I members or flat plate details, it is believed to cover a large population of bridge connections in existence for which we need to assess their remaining fatigue life.

This chapter uses regression analysis to establish a trend between each parameter that were investigated in the previous chapter and the SCF for built-up I members. A multi-linear regression analysis was also performed using all the parameters investigated in order to obtain a design equation for SCF of built-up I members. An effort was made to simplify this design equation by looking at the significance of each parameter. For flat plates, using Josi *et al*. (2004) analysis results, a regression analysis was conducted to obtain a design equation for flat plates. The

linear correlation coefficient, R^2, was used to assess the correlation between each parameter and the SCF.

5.2 REGRESSION ANALYSIS FOR BUILT-UP I SECTIONS

In this section a linear regression analysis between the SCF and each of the parameters investigated in the previous chapter is presented. The parameters that were investigated in Chapter 4 include: hole stagger, gauge distance, edge distance, web size, angle size and area ratio. For each case, the equation and the R^2 value were obtained to demonstrate how well the least square regression model predicts the trend between the SCF and the parameter. In the following sections, A, B, C, D, E, and F are used to denote exponential, linear, logarithmic, quadratic, cubic, and a fourth order polynomial, respectively.

5.2.1 EFFECT OF HOLE STAGGER

In the previous chapter, it was observed that for built-up I tension members the SCF is inversely proportional to the stagger. To determine the best relationship between SCF and stagger, regression analyses were conducted for different regression models and five different gauge distances, namely, 38.1, 46.5, 50.8, 55.0, and 60.4 mm. Table 5-1 shows the R^2 values and the equations for different regression models for a gauge distance of 38.1 mm, and Figure 5-1 shows the corresponding plots of SCF versus stagger for a constant gauge of 38.1 mm, although a polynomial model fits best the data, it can seen that the simpler linear model provides a good fit with a R^2 value of 0.93. Figures and Tables A-1 to A-5 of Appendix A provide details of the effect of the stagger on the SCF for the other values of gauge distance.

5.2.2 EFFECT OF GAUGE DISTANCE

As demonstrated in chapter 4, the SCF reduces with increase in gauge distance, although this decrease was very small. It was also observed that as the gauge distance was varied, the edge distance E_1 also changed, which may have a direct influence on the SCF. A regression analysis was conducted to assess the effect of gauge distance on the SCF for a constant hole stagger. The R^2 values and equations for different regression models are shown in Table 5-2 for the case corresponding to a stagger of 38.1 mm. Tables A-6 to A-10 present similar information for other values of stagger varying from 38.1 mm to 60.4 mm. Figure 5-2 shows a plot of SCF versus gauge distance for a constant stagger of 38.1 mm. Equivalent plots for other staggers are presented in Figures A-6 to A-10 of Appendix A. For the stagger of 38.1 mm, Table 5-2 indicates that a simple linear least square regression model yields a R^2 value of 0.84, indicating a reasonably good fit.

5.2.3 EFFECT OF EDGE DISTANCE E_2

The edge distance close to the web (E_2) was varied to determine its effect on the SCF. For a constant angle leg size and gauge distance, as E_2 is varied the edge distance away from the web (E_1) also varies. For smaller values of edge distance E_2, the influence of the stress field in the leg joining the angle to the web becomes pertinent. Indeed, as the edge distance close to the web decreases, the stresses in the leg connected to the gusset plate increases. Although for small hole stagger (less than 50.8 mm), the stresses in the critical hole gradually reduces as the edge distance increases from 28.0 mm to 45.0 mm, it was observed that the stresses increase again as E_2 increases from 51.4 mm to 58.4 mm. For hole stagger greater than or equal to 50.8 mm, the SCF decreases as E_2 increases. A regression analysis was conducted to determine the relationship between the SCF and the edge distance as shown in Table 5-3, for a stagger of 38.1 mm. Figure 5-3 shows the effect of E_2 on the SCF for constant stagger of 38.1 mm. Figures and tables A-

11 to A-15 in Appendix A show the variation of SCF as a function of E_2 for all stagger values investigated. From tables and figures A-11 to A-15, it can be seen that the linear regression model does not predict the SCF reliably, showing R^2 values between 0.23 and 0.91 for different hole staggers. The linear model does not work well because the influence of E_2 on the SCF is dependent on other factors, such as the proximity of adjacent holes to the critical hole, the edge distance E_1 and the proximity of the rivet holes in the web to the critical hole. The polynomial regression models seem to give a good R^2 values, although we could argue that it is because of the number of data points used for the regression analysis is close to the order of the polynomial.

5.2.4 Effect of fastener hole diameter

It was observed in the previous chapter that, for a constant width of flange connected to the gusset plate, the SCF is higher at a diameter of 20.0 mm, but remained constant for hole diameters from 22.0 mm to 26.0 mm. This behaviour is not expected because it is expected that higher stresses (or approximately equal stresses if the change in diameter does not result in a significant net area change) will result as the net area reduces with an increase in hole diameter. Overall, the hole diameter seems to have a small effect on the SCF within the diameter commonly used in most existing bridges. The observation that the fastener diameter may not have a significant effect on the fatigue resistance of bearing type lap splices was also reported by Kulak (2005).

5.2.5 Effect of width of angle flange attached to gusset plate

Only two widths of angle flange connected to gusset plate were investigated, namely, 146 mm and 172 mm. The data presented in chapter 4 indicated an increase of 2.1 % in the SCF as the flange width increased from 146 to 172 mm. It should be noted, however, that as the angle width was increased, the edge distance

E_2 was increased while the gauge distance and the edge distance away from the web, E_1, remained constant.

5.2.6 EFFECT OF WEB THICKNESS AND WEB DEPTH

The effect of web thickness was investigated using web thickness of 9.5, 13.0 and 19.0 mm, for constant web depth of 254, 356, and 508 mm respectively. The SCF was found to increase as the web thickness increases for a constant web depth and within the range of web thickness and web depth above, a linear regression curve was found to result in a R^2 value of 1.00. The SCF vs. web thickness equation obtained for each web depth can be found in Table 5-4.

Based on the analysis of built-up members with three different web depths varying from 254 mm to 508 mm, as used in the investigation of the effect of web thickness, the SCF was also found to increase linearly with an increase in the web depth as shown in Table 5-5. The linear trend was observed for all three web thicknesses included in the analysis.

5.2.7 EFFECT OF ANGLE THICKNESS

The analysis results presented in Table 4-7 indicated that the SCF decreases as the angle thickness increases. Based on the results of analysis where the angle thickness was varied from 7.9 mm to 19.0 mm, regression analyses were conducted and the results are presented in Table 5-6 for a 152x152 mm angle. A total of five different models, designated A to E, were investigated, namely, an exponential model, a linear model, a logarithmic model and a second order and third order polynomials. This investigation was carried out for three angle sizes as indicated in Table 4-7 and tables and figures A-16 to A-18 from Appendix A. Figure 5-4 and Table 5-6 show that the plot of the straight line model provides a good fit of the data for a 152x152 mm angle.

5.2.8 EFFECT OF WEB TO FLANGE AREA RATIO

Since the SCF increases with an increase in web thickness and web depth, but decreases with an increase in angle size, a parameter that could capture this combined variation seems to be the area ratio. Hence different measures of area ratio are considered to see which one correlates best with the SCF. The area ratios considered in the following are:

a) web area to area of flanges attached to the gusset plates;
b) web area to the total area of the angles;
c) total area of built-up section to area of flanges attached to the gusset plates;
d) total area of built-up section to total area of the angles;
e) area of the web plus flanges attached to the web to the area of the flanges attached to gusset plates.

A regression analysis was carried out for each of the area ratios mentioned above, and plots of SCF versus area ratio are presented in Figures 5-5(a) to 5-5(e) for the five area ratios investigated. In each case the regression line and the correlation coefficient R^2 are shown. From an examination of the results presented in Figure 5-5, it is apparent that either the ratio of the total area to the area of the flanges attached to gusset plates or the ratio of the area of the web plus the flanges attached to the web to the area of the flanges attached to the gusset plates gives the best correlation, with an average R^2 value of 0.97 for both area ratios.

In order to account for the effect of shear lag that occurs in a structural member that is only partially connected (here we have a case where only the flange are connected), a regression analysis was carried out for the SCF divided by the "shear lag factor" $(1-x/L)$ versus the total area the flanges connected to the gusset plates. The shear lag factor is commonly used in design standards and was proposed by Munse and Chesson based on extensive testing on riveted joints. The maximum x/L used for the parametric study is 0.156. Figure 5-5(f) shows the

resulting plot, and the regression analysis yielded a R^2 value of 0.97. The maximum x/L used for the parametric study is 0.156.

5.3 PROPOSED DESIGN EQUATION FOR SCF

A total of 71 finite element analysis results were obtained from a parametric study and regression analyses were presented in the previous sections to assess how these parameters individually affect the SCF. Various regression models, linear and non-linear, were investigated to determine the relationship between these parameters and the SCF. The aim of this research is to derive a simplified equation to calculate the SCF as a function of all the parameters that affect the SCF for built-up members. Since a linear regression curve fits reasonably well most of the analysis data, and in order to keep the equation very simple to use for design purposes, a multi-linear regression analysis was conducted with all the 71 analysis results, resulting in a proposed design equation. An attempt was then made to further simplify the equation by removing the parameters that seem to have negligible effect on the SCF. Josi *et al.* (2004) also presented analysis results from flat plates for which a regression analysis was performed to fit a relationship between the various parameters and the SCF for double lapped joints.

5.3.1 PROPOSED DESIGN EQUATION FOR BUILT-UP I MEMBERS

A multi-linear regression analysis was conducted with the results obtained from the variation of the stagger, gauge distance, edge distance E_2 and area ratio. The analysis was conducted using Microsoft Excel, and the following equation is proposed for the SCF of a built-up I-shaped member in tension

$$SCF = 0.415 - \left(0.0058S + 0.0181G - 0.02E_1 - 0.013E_2 + 0.59\frac{A_T}{A_{fg}} \right) \frac{1}{1-\frac{x}{L}} \qquad (5\text{-}1)$$

Equation (5-1) results in an R^2 value of 0.96, an adjusted R^2 value of 0.95, and standard error of 0.05. Table 5-7(b) shows the analysis of variance (ANOVA) results for the built-up I section, and gives the significance of the overall equation

(that is, significance F value or P-value). From the regression P-values (which is the smallest level of significance that would lead to rejection of the null hypothesis with the given data as reported by Montgomery *et al.* (2003)) shown in Table 5-7(c) and the coefficient attached to each parameter in Equation 5-1., we can observe that the area ratio seem to have the highest influence on the SCF, since from the previous study the stagger and edge distance close to the web had an effect on the SCF. Therefore, the multi-linear regression analysis was repeated with these parameters only. Using any other combination of the hole layout did not yield any significant improvement in the accuracy of the equation. The analysis of variation (ANOVA) and the regression analysis results for the reduced model are shown in Table 5-8, and the following simplified equation is obtained for the SCF:

$$SCF = 3.014 - \left(0.00816S - 0.00595E_2 + 0.809\frac{A_T}{A_{fg}} \right) \frac{1}{1 - \frac{x}{L}} \qquad (5\text{-}2)$$

Tables 5-8 (a) to (c) show the ANOVA and regression results. An R^2 value of 0.95, adjusted R^2 value of 0.95 and a standard error of 0.058 are obtained from the regression analysis for Equation 5-2. Adjusted R^2 is preferred for use because while R^2 will always increase as a variable is added to the model, the adjusted R^2 will only increase when the new variable added to the model reduces the error mean square. Table 5-9 shows the SCF obtained using Equation (5-2) and the SCF obtained from the finite element analysis for the bottom and top chord details tested by DiBattista *et al.* (1998).It can be observed that the simplified equation gives a SCF in excellent agreement with that obtained from the finite element analysis conducted in the previous chapter, and the difference in the adjusted R^2 and standard error for both equations is approximately 1%. So we can conclude that the reduced Equation 5-2 for calculating the SCF gives good results.

5.3.2 PROPOSED DESIGN EQUATION FOR FLAT PLATES

Using the finite element analysis results presented by Josi *et al.*(1999) and presented in Table 5-10, where S, G, E, and A are the stagger, gauge, edge distance and the gross cross-sectional area, and S0, S1, S2, and S3 represent staggers of 0, 25.4, 50.8, and 76.2 mm, respectively. The G series specimens were obtained by varying the gauge and the P series specimens were the preliminary specimens. A multi-linear regression analysis was conducted, and the following equation was obtained for flat plates with seven transverse and two longitudinal lines of fasteners for the SCF:

$$SCF = 5.20 - 0.0009E^2 + 0.034G + 0.003S - 0.0018A \qquad (5\text{-}3)$$

From the ANOVA and regression analysis results presented in Table 5-11 (a) to (c), it can be seen that the R^2 value is 0.67, adjusted R^2 value is 0.59 and it has a standard error of 0.07. The ANOVA table shows the number of observations used in the analysis and shows the overall significance of the model.

5.4 FATIGUE CURVES USING THE PROPOSED DESIGN EQUATIONS

The purpose of deriving Equations to predict the SCF for built-up I members and flat plates is to determine the fatigue resistance of bolted or riveted tension members with staggered hole connections. Consequently, in addition to the SCF, one also needs to select the appropriate fatigue curve. A plot of the mean fatigue S-N curve obtained using the SCF obtained from Equation 5.3 is compared to S-N curve obtained using the finite element results for flat plates obtained by Josi *et al.* (1999) is presented in Figure 5-6, and as was be expected the 2 mean curves are identical. The mean minus two standard deviations S-N curve, which represents the proposed fatigue design curve, is also presented. The slope of the mean fatigue curve is 6.89 and the intercept is 24.0.

Figure 5-7 shows the fatigue curve obtained using the peak stress range obtained by using SCF obtained from the general Equation for built-up section and the

Equation for obtaining the SCF for flat plate, and this is compared to the mean fatigue curve plotted using the finite element results for both flat plate and built-up section. The fatigue lives used are as presented in the previous chapter. With this, the 95% confidence limit line for the fatigue curve obtained using the Equations is obtained. This gives a slope of 3.05, an intercept of 13.8, and a standard error of 0.318.It can be observed that the mean regression line for the finite element analysis and that of the mean regression line from the general Equation are significantly close. Similarly, the SCF obtained using the simplified Equation for built-up section is used with SCF obtained using the Equation for flat plate is used to obtain the fatigue curve. A slope and an intercept of 3.0 and 14.0 respectively is obtained. The simplified Equation seems to give a better slope which is close to that obtained from using the finite element result for both the flat plate and the built-up section. Figure 5-8 shows the fatigue curve and the 95% confidence limit, again from the figure it is obvious that there is not much difference between the SCF predicted using the Equations and that predicted by the finite element analysis.

Table 5-1: Effect of hole stagger on SCF (gauge = 38.1 mm)

Parameter varied	**Other parameters (mm)**	**Model**	**Equation**	**R^2**
Stagger	E_1= 57.1 E_2= 51.4 G= 38.1 L_t= 11.1 L_w= 146 W_t= 9.50 W_d= 356	A	$SCF = 4.44e^{-0.001S}$	0.93
		B	$SCF = -0.0061S + 4.43$	0.93
		C	$SCF = -0.343LnS + 5.46$	0.94
		D	$SCF = 0.0006S^2 - 0.0737S + 6.2977$	1.00
		E	$SCF = 0.0006S^2 - 0.0737S + 6.2977$	1.00
		F	$SCF = 0.0006S^2 - 0.0737S + 6.2977$	1.00

Table 5-2: Effect of gauge distance on the SCF (stagger = 38.1 mm)

Parameter varied	**Other parameters (mm)**	**Model**	**Equation**	**R^2**
Gauge distance	E_1= 57.1 E_2= 51.4 S= 38.1 L_t= 11.1 L_w= 146 W_t= 9.50 W_d= 356	A	$SCF = 4.644e^{-0.001G}$	0.90
		B	$SCF = -0.0064G + 4.63$	0.90
		C	$SCF = -0.35LnG + 5.68$	0.87
		D	$SCF = 0.0008G^2 - 0.0788G + 2.2707$	1.00
		E	$SCF = 0.0008G^2 - 0.0788G + 2.2707$	1.00
		F	$SCF = 0.0008G^2 - 0.0788G + 2.2707$	1.00

Table 5-3: Effect of edge distance on the SCF

Parameter varied	Other parameters (mm)	Model	Equation	R^2
Edge distance	E_1= 63.4 G= 55.2 S= 38.1 L_t= 11.1 L_w= 146 W_t= 9.50 W_d= 356	A	$SCF = 4.46e^{-7\times10^{-4}E_2}$	0.2
		B	$SCF = -0.003E_2 + 4.46$	0.2
		C	$SCF = -0.155InE_2 + 4.90$	0.3
		D	$SCF = 0.0006E_2^{\,2} - 0.0544E_2 + 5.5015$	0.9
		E	$SCF=5\times10^{-6}E_2^{\,3}-9\times10^{-6}E_2^{\,2}-0.0292E_2+5.166$	0.9
		F	$SCF=-5\times10^{-6}E_2^{\,3}+0.0008E_2^{\,3}-0.0535E_2^{\,2}+1.46E_2-9.96$	1.0

Table 5-4: Effect of web thickness

Parameter varied	Other parameters (mm)	Web depth (mm)	Equation	R^2
Web thickness	E_1= 40.0 E_2= 51.4 S= 38.1 L_t= 11.1 L_w= 146 W_t= 9.50	508	$SCF = 0.0768W_t + 3.8106$	1.00
		356	$SCF = 0.0506W_t + 3.806$	1.00
		254	$SCF = 0.0318W_t + 3.864$	1.00

Table 5-5: Effect of web depth

Parameter varied	Other parameters (mm)	Web thickness (mm)	Equation	R^2
Web depth	E_1= 40.0 E_2= 51.4 S= 38.1 L_t= 11.1 L_w= 146 W_t= 9.50	19.0	$SCF = 0.0032W_d + 3.66$	1.00
		13.0	$SCF = 0.0021W_d + 3.72$	1.00
		9.50	$SCF = 0.0015W_d + 3.7853$	0.99

Table 5-6: Effect of angle thickness (152x152 mm angle)

Parameter varied	Other parameters (mm)	Model	Equation	R^2
Angle thickness	E_1= 40.0 E_2= 51.4 S= 38.1 L_t= 11.1 L_w= 146 W_t= 89.0 W_d= 356	A	$SCF = 5.319e^{-0.01L_t}$	0.93
		B	$SCF = -0.046L_t + 5.29$	0.93
		C	$SCF = -0.595LnL_t + 6.18$	0.98
		D	$SCF = 0.0042L_t^2 - 0.158L_t + 5.763$	1.00
		E	$SCF = 0.0002L_t^3 - 0.011L_t^2 - 0.24L_t + 6.3$	1.00

Table 5-7: Results of regression analysis for general Equation for built-up I section

(a) Regression statistics

REGRESSION STATISTICS	
Multiple R	0.978
R^2	0.957
Adjusted R^2	0.953
Standard error	0.054
Number of observations	71

(b) ANOVA-1

	df	SS	MS	F	Significance F
Regression	5	4.18	0.835	287.95	6.21×10^{-43}
Residual	65	0.19	0.0029		
Total	70	4.36			

(c) ANOVA-2

	Coefficients	Standard error	t stat	P-value
Intercept	0.415	0.773	0.536	0.593
S	-0.00578	0.0012	-4.88	7.17×10^{-06}
G	-0.0181	0.0057	-3.16	0.002395
E_1	-0.0197	0.0056	-3.53	0.000778
E_2	-0.0135	0.0056	2.40	0.019106
A_T / A_{fg}	0.59	0.0697	8.46	4.52×10^{-12}

Table 5-8: Results of regression analysis for reduced Equation for built-up I section (Equation (5.2))

(a) Regression statistics

REGRESSION STATISTICS	
Multiple R	0.973
R square	0.947
Adjusted R	0.946
Standard error	0.058
Number of observations	71

(b) ANOVA-1

	df	SS	MS	F	Significance F
Regression	3	4.13	1.38	406.26	6.68×10^{-43}
Residual	67	0.227	0.0034		
Total	70	4.36			

(c) ANOVA-2

	Coefficients	Standard error	t stat	P-value
Intercept	3.014	0.102	29.52	3.92×10^{-40}
S	-0.00816	0.00092	-8.90	5.81×10^{-13}
E_2	-0.00595	0.00092	-6.46	1.41×10^{-08}
A_T / A_{fg}	0.809	0.0286	28.27	5.82×10^{-39}

Table 5-9: Predicted SCF and SCF from finite element for the built-up I section

Specimen type	Predicted SCF Eq. (5.1)	Predicted SCF Eq. (5.2)	Finite Element SCF
Bottom chord	4.22	4.20	4.24
Top Chord	4.27	4.25	4.29

Table 5-10: Finite Element analysis results for flat plates presented by Josi *et al* .(1999)

Specimen type	S (mm)	G (mm)	E (mm)	A (mm^2)	SCF
S0	0	60.4	25.3	2118	3.95
P	0	60.4	25.3	2118	3.80
S1	25.3	44.5	25.3	1815	4.08
S2	50.9	44.5	25.3	1815	4.17
S3	76.2	44.5	25.3	1815	4.17
	102	44.5	25.3	1815	4.18
	12.8	51.9	25.3	1958	4.00
	38.1	51.9	25.3	1958	4.08
	50.9	51.9	25.3	1958	4.19
	76.2	51.9	25.3	1958	4.19
	12.7	60.4	25.3	2118	4.01
G	38.1	60.4	25.3	2118	4.09
	50.9	60.4	25.3	2118	4.20
	76.2	60.4	25.3	2118	4.24
	38.1	44.5	38.1	2299	3.94
	38.1	44.5	44.5	2543	4.04
	38.1	44.5	50.9	2783	4.17
	50.9	44.5	38.1	2299	4.00
	50.9	44.5	44.5	2543	4.04
	50.9	44.5	50.9	2783	4.12
	76.2	44.5	38.1	2299	3.99
	76.2	44.5	44.5	2543	4.03
	76.2	44.5	50.9	2783	4.11

Table 5-11: Results of regression analysis for Equation for flat plate

(a) Regression statistics

REGRESSION STATISTICS	
Multiple R	0.817
R square	0.668
Adjusted R	0.594
Standard error	0.067
Observation	23

(b) ANOVA-1

	df	SS	MS	F	Significance F
Regression	4	0.165	0.0413	9.04	0.000346
Residual	18	0.082	0.00457		
Total	22	0.247			

(c): ANOVA-2

	Coefficients	Standard error	t stat	P-value
Intercept	5.20	0.421	12.3	3.19×10^{-10}
E^2	0.000911	0.00026	3.51	0.00252
G	0.00342	0.00930	3.67	0.001738
S	0.00271	0.000608	4.45	0.000308
A	-0.00183	0.000512	3.57	0.002174

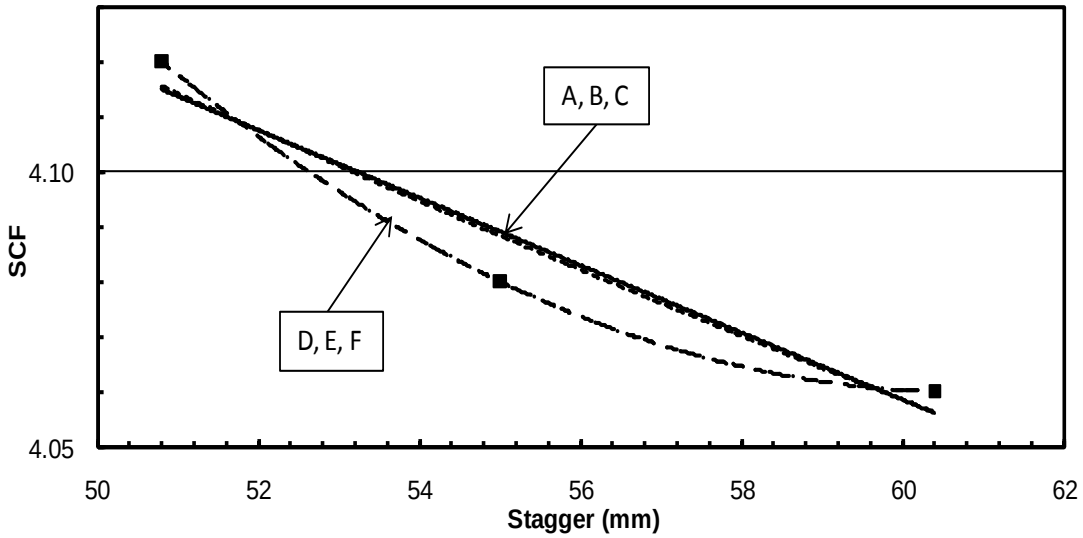

Figure 5-1: Effect of stagger on the SCF (gauge = 38.1 mm)

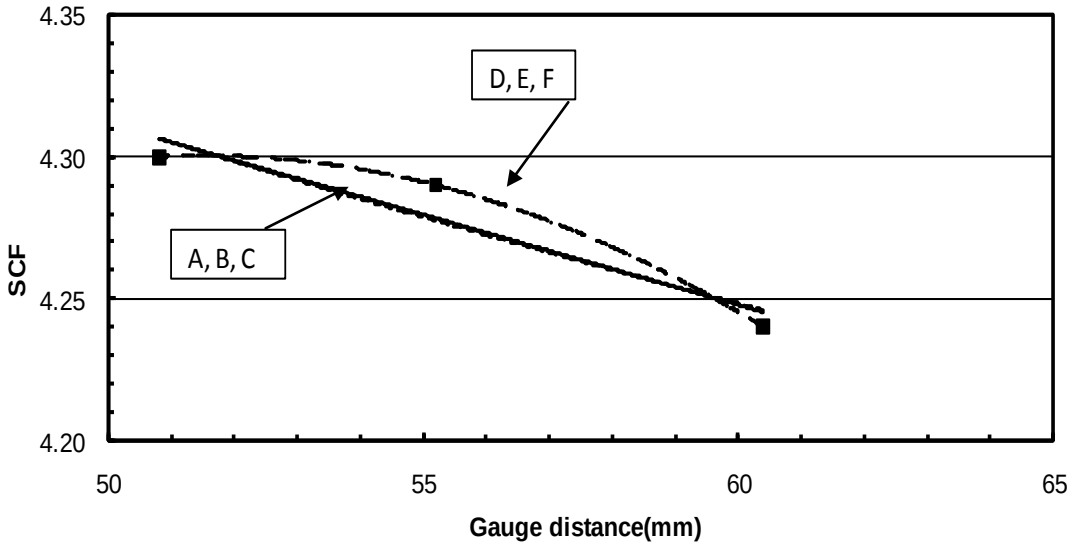

Figure 5-2: Effect of gauge distance on the SCF (stagger = 38.1 mm)

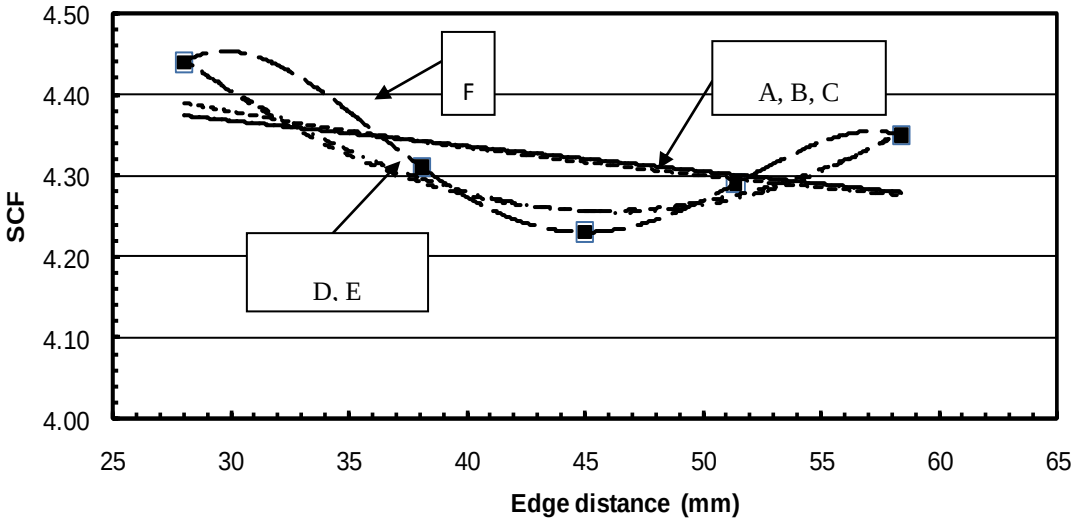

Figure 5-3: Effect of edge distance, E_2 on the SCF

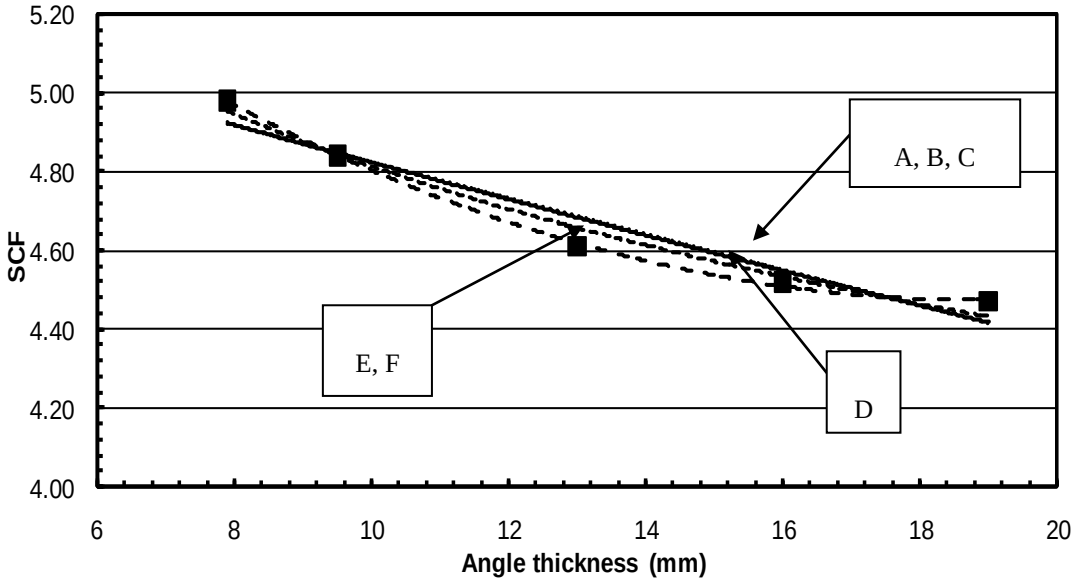

Figure 5-4: Effect of angle thickness on the SCF

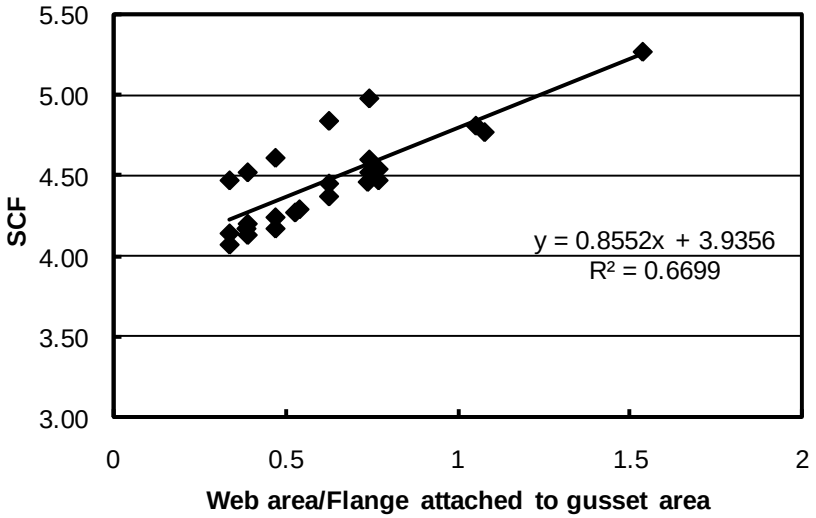

(a) Web area to area of flanges attached to gusset plates

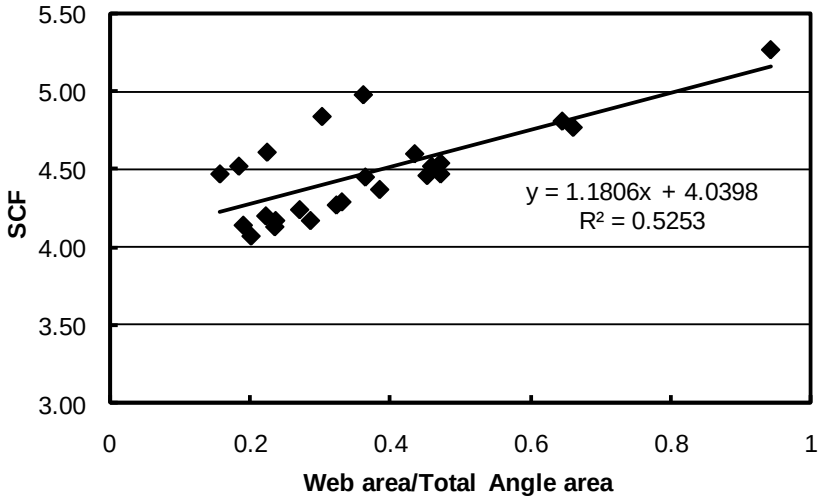

(b) Web area to the total area of the angle

Figure 5-5: Effect of shear lag and area ratios on the SCF

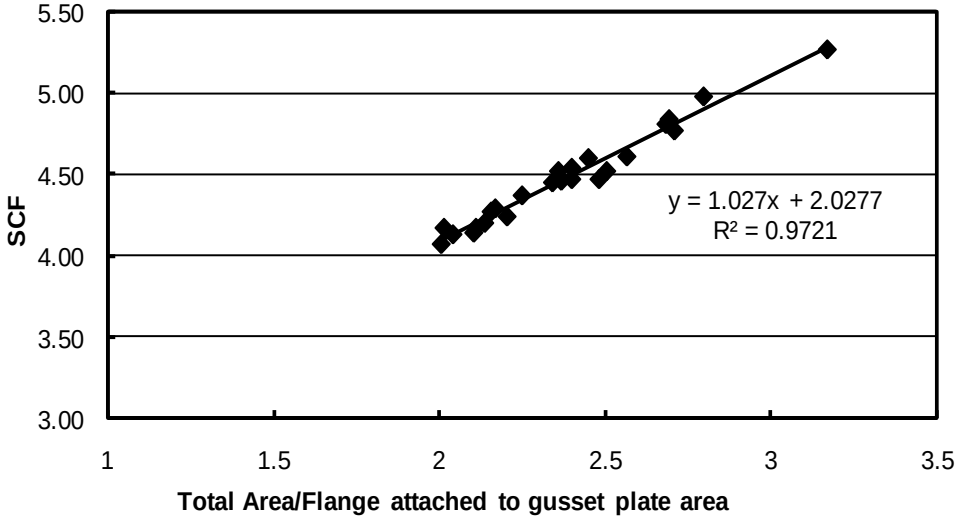

(c) Total area of built-up section to area of flange attached to gusset plate

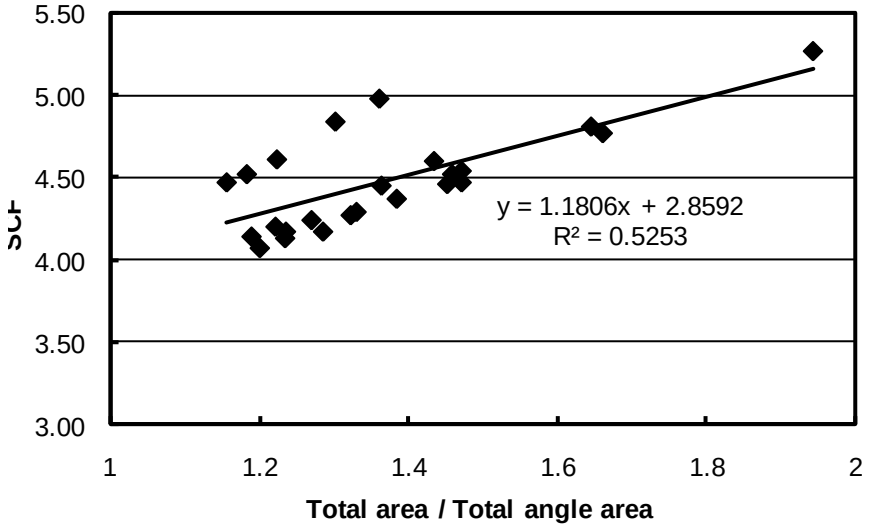

(d) SCF against area ratio

Figure 5-5: Effect of shear lag and area ratios on the SCF (cont`d)

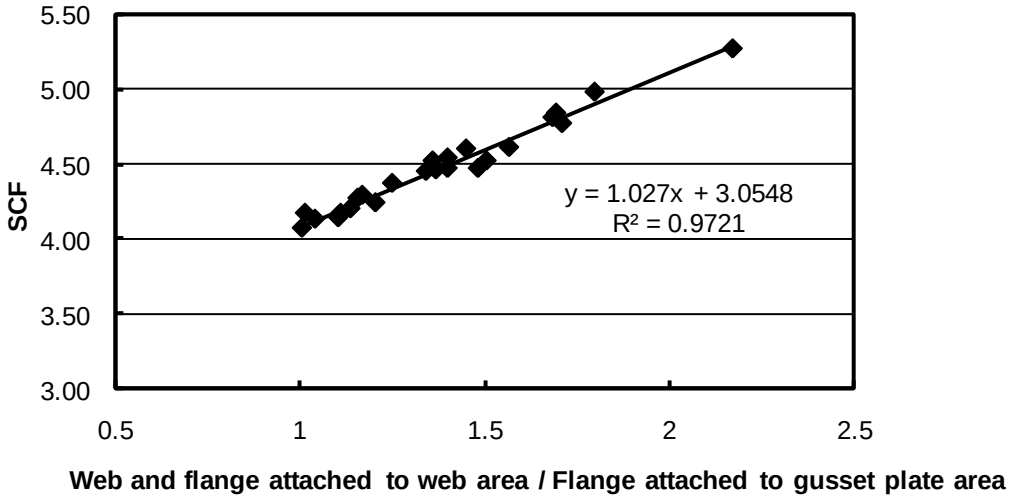

(e) SCF against area ratio

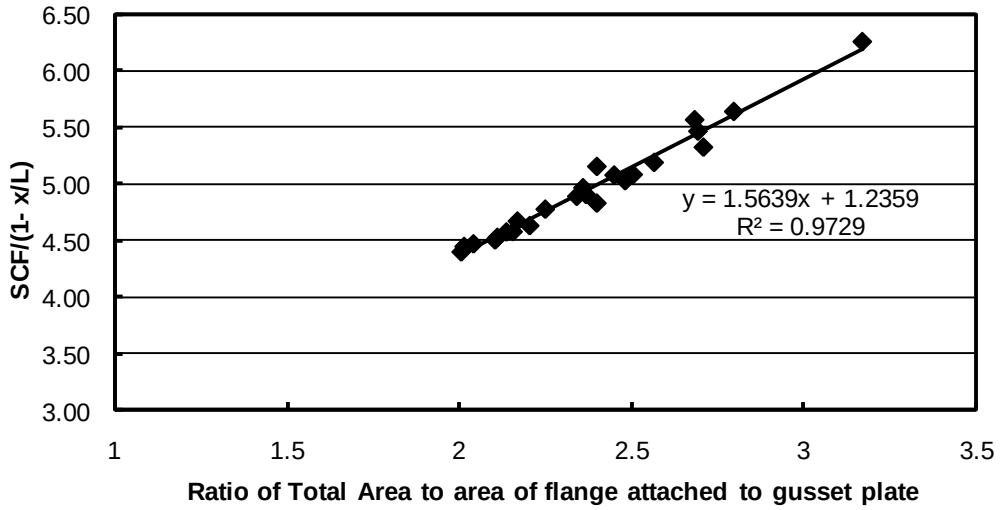

(f) Effect of area with a correction for shear lag effect

Figure 5-5: Effect of shear lag and area ratios on the SCF (Cont'd)

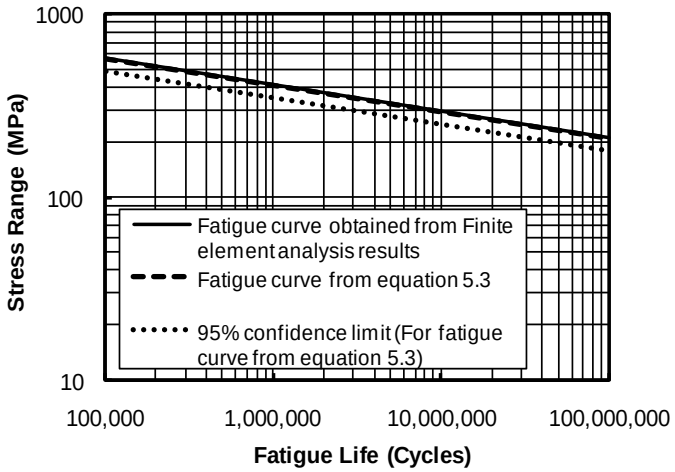

Figure 5-6: Fatigue curve from the use of the SCF Equation for flat plates

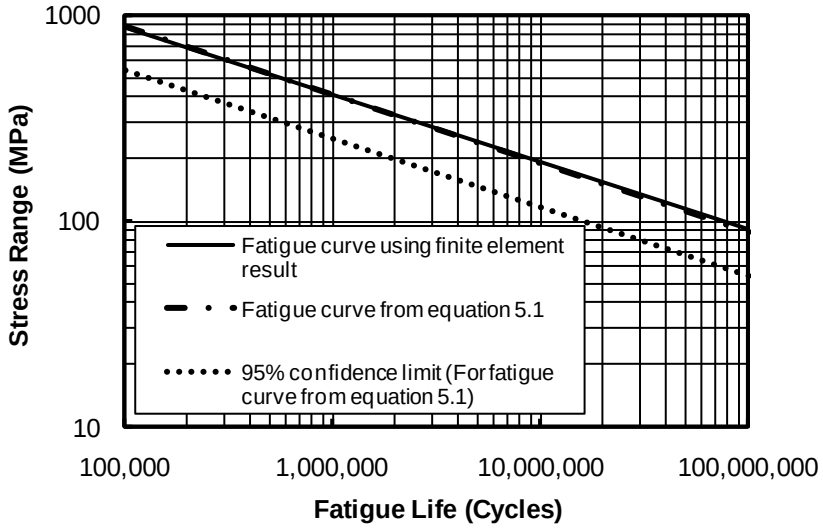

Figure 5-7: Fatigue curve from the use of general SCF Equation for built-up I members

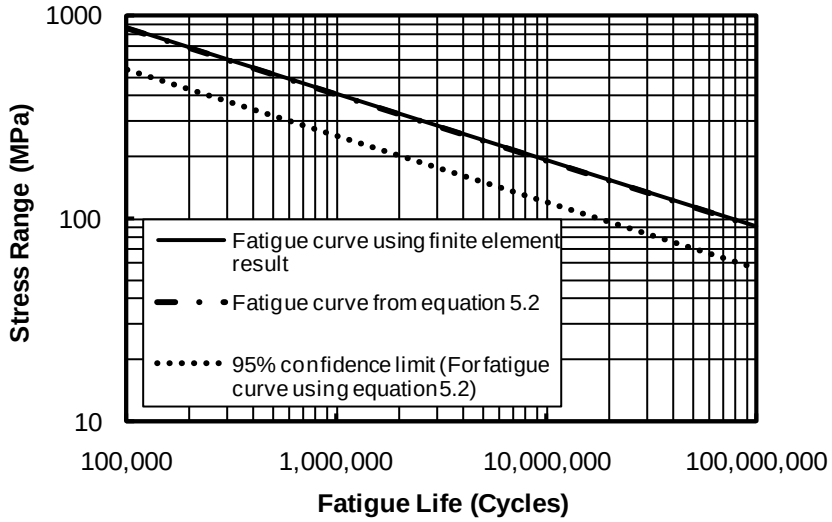

Figure 5-8: Fatigue curve from the use of simplified SCF Equation for built-up I members

CHAPTER 6

SUMMARY, CONCLUSIONS AND RECOMMENDATIONS

6.1 SUMMARY

The fatigue resistance of riveted and bearing type connections is affected by the presence of stress concentration around the fastener holes. The governing stress on the critical cross-section is influenced by a combination of the presence of the hole, bearing of the fastener against the plate, and interaction between adjacent fastener holes. Since fatigue cracks have been observed to propagate on a plane perpendicular to the axis of the member even when the minimum net tension area is located on an inclined plane, a definition of the net section stress that accounts for possible interaction between the holes adjacent to the critical section is needed. Therefore, it becomes important to understand the influence of the connection size and hole pattern (such as stagger, gauge distance, edge distance) on the stress concentration factor (SCF) at the critical section from which the peak stress and fatigue resistance of a bearing type bolted or riveted connection.

Extensive finite element analyses were carried out to determine the influence of connection size, hole stagger, gauge and edge distance on the SCF of built-up I sections in bearing type connections. A total of 71 finite element results were used to obtain an Equation to compute the SCF for built-up I sections. Also, using the analysis results on flat plate double lap splice presented by Josi *et al.* (1999), an Equation for the SCF in double lap splice connections was derived. Using the SCF equations derived from finite element analysis results and fatigue test data obtained in the literature, a design curve for the assessment of the fatigue resistance of riveted connections with staggered bolt holes was proposed.

6.2 CONCLUSIONS

Based on the results of a numerical analysis and an examination of experimental data from other researchers, the following conclusions can be drawn:

1. An increase in the stiffness of the fastener and gusset plate assembly increases the SCF only by a very small amount.
2. For a constant edge distance close to the web, E_2, and gauge distance G, an increase in fastener stagger decreases the SCF in built-up I sections.
3. For a given stagger, an increase in gauge distance leads to a negligible change in SCF.
4. For a given hole stagger and gauge distance, the SCF decreases with an increase in E_2.
5. In a built-up I section the SCF increases as a linear function of the web thickness, web depth, and the ratio of the total gross sectional area of the connection to the area the area of the angle leg in contact with the gusset plate.
6. The SCF increases as the ratio of the total area of the built-up member to the area of the flange leg connected to the gusset plate increases. This ratio is well known to affect shear lag in built-up I sections and correcting the SCF for this shear lag effect provides a good correlation between the area ratio and the SCF.
7. The fatigue resistance of riveted built-up members can be estimated using the fatigue category A curve with a stress range calculated based on the gross section stress range multiplied by the SCF obtained from Equation 5.2 or 5.3. A slope of 7 for the S-N curve is recommended for in evaluating the fatigue resistance of these connections

6.3 RECOMMENDATIONS

The SCF for built-up I section bearing type details should be calculated using the following Equation:

$$SCF = 3.014 - \left(0.00816S - 0.00595E_2 + 0.809\frac{A_T}{A_{fg}} \right) \frac{1}{1-\frac{x}{L}} \qquad (5\text{-}2)$$

and the SCF for flat plates in bearing type connections should be calculated using the following Equation:

$$SCF = 5.20 + 0.0009E^2 + 0.034G + 0.003S - 0.0018A_T \quad (5\text{-}3)$$

A method that calculates the stress range by multiplying the SCF by the gross section applied stress should be used to describe the fatigue behaviour of bearing type connections. A slope of 7 is recommended for the S-N curve for design purposes.

Further research work is needed to establish the SCF for structural shapes other than built-up I sections and flat plates, such as built-up box sections. More testing is needed to establish the endurance limit to be used for the fatigue design curve, since we have limited fatigue testing done on bearing type details.

List of References

1. Canadian Standards Association (CAN/CSA S16-01). (2006). Canadian Highway Bridge Design Code Ontario, Canada.
2. Chen, H., Grondin, G. Y., and Driver, R. G. (2005). "Fatigue Resistance of High Performance Steel." Structural Engineering Rep. No. 258, Dept. of Civil and Environmental Engineering, University of Alberta, Edmonton, Alberta.
3. DiBattista, J. D., and Kulak. G. L. (1995). "Fatigue of riveted tension members." Structural Engineering Rep. No. 211, Dept. of Civil and Environmental Engineering, University of Alberta, Edmonton, Alberta.
4. Fisher, J. W., Albrecht, P. A., Yen, B. T., Klingerman, D. J., and McNamee, B. M. (1974). "Fatigue Strength of Steel Beams with Welded Stiffeners and Attachments." NCHRP Report 147, pp. 85.
5. Fisher, J. W., Frank, K. H., Hirt, M. A., and McNamee, B. M. (1970). "Effect of Weldments on the Fatigue Strength of Steel Beams." NCHRP Report 102, pp. 114.
6. Fisher, J.W., G.L. Kulak and Smith, I.F.C. (1998). A Fatigue Primer for Structural Engineers, National Steel Bridge Alliance, American Institute of Steel Construction, Chicago, Illinois.
7. Graf, O. (1951). Versuche and geschranben Verdbindungen, Bericht 16, Deutscher Ausschuss für Stahlbau, Stahlbau GmbH, Cologne.
8. Howland, R. C. (1930). "On the Stresses in the Neighborhood of a Circular Hole in a Strip under Tension," *Phil. Trans. Roy. Soc.* (London) A, Vol. 229, p. 67.
9. Josi, G., Grondin, G. Y., and Kulak, G. L. (1999). "Fatigue of bearing type shear splices." Structural Engineering Rep. No. 227, Dept. of Civil and Environmental Engineering, University of Alberta, Edmonton, Alberta.
10. Josi, G., Grondin, G. Y., and Kulak, G. L. (2004). "Fatigue of joints with staggered holes." *Journal of Bridge Engineering*, ASCE. Vol. 9, No 6, pp. 614-622.

11. Kim, N., Sankar, B. V. (2009). *Introduction to Finite Element Analysis and Design*, John Wiley and Sons, New York.
12. Kulak, G. L., (2005). *High Strength Bolting for Canadian Engineers*, Canadian Institute of Steel Construction, Ontario, Canada.
13. Kulak, G. L., Fisher, J. W., and Struik, J. H. A. (1987). *Guide to design criteria for bolted and riveted joints*, 2nd Ed., Wiley, New York.
14. Montgomery, D. C., Runger, G. C. (2003). *Applied Statistics and Probability for Engineers*, 3rd Ed., John Wiley and Sons, New York.
15. Moore, A. M., Rassati, G. A., Swanson, J. A. (2008). "Evaluation of Current Resistance Factors for High-Strength Bolts" Final report submitted to the Research Council on Structural Connections.
16. Munse, W. H., Chesson, E. Jr. (1963). "Riveted and Bolted Joints: Net Section Design." *Journal of the Structural Division*, ASCE. Vol.89 (STI), pp.107-126.
17. Pilkey, W. D. (1997). *Peterson's Stress Concentration Factors*, 2nd Ed., John Wiley & Sons, New York.
18. Schulz, K. J., (1941). "Over den Spannungstoestand in doorborde Platen," (On the State of Stress in Perforated Plates), Doctoral Thesis, Techn. Hochschule, Delft. (in Dutch).

Appendix A

Regression Analysis of Finite Element Results

Regression Analysis of Finite Element Results

Regression analysis of the finite element results was performed to investigate the effect of the hole stagger, gauge distance, edge distance, web size, angle size and area ratio on the SCF. Microsoft excel was used to obtain different models used to describe the variation between the SCF, as the dependent variable versus the parameters listed above.

This appendix is used to supplement Chapter 5. Table A-1 to A-5 and Figure A-1 to A-5 show the effect of stagger on the SCF for constant gauge distances. Table A-6 to A-10 and Figure A-6 to A10 show the effect of gauge distance on the SCF, and Table A-11 to A-15 and Figure A11 to A-15 presents the effect of edge distance on the SCF. The effect of angle thickness on the SCF was investigated for equal and unequal angle sizes and Table A-16 to A-18 and Figure A-16 to A-18 present these plots. All the tables has in column 1 the parameter that is varied, column 2 has the value of all other parameters in the built-up member, column 3 shows the model type, where A, B, C, D, E, and F are used to denote exponential, linear, logarithmic, quadratic, cubic, and a fourth order polynomial, respectively, the same notations are also used in the figures.

A linear model seems to explain the trend between the SCF and the hole stagger, gauge distance, web thickness, web depth, but does not give good prediction for the effect of the edge distance E_2 on the SCF, at low stagger of 38.1 and 46.5 mm, and when E_2 becomes large, such as beyond 51.4 mm.

Table A-1: Effect of hole stagger on SCF (gauge = 38.1 mm)

Parameter varied	Other parameters (mm)	Model	Equation	R^2
Stagger	E_1= 57.1 E_2= 51.4 G= 38.1 L_t= 11.1 L_w= 146 W_t= 9.50 W_d= 356	A	$SCF = 4.44e^{-0.001S}$	0.93
		B	$SCF = -0.0061S + 4.43$	0.93
		C	$SCF = -0.343LnS + 5.46$	0.94
		D	$SCF = 0.0006S^2 - 0.0737S + 6.2977$	1.00
		E	$SCF = 0.0006S^2 - 0.0737S + 6.2977$	1.00
		F	$SCF = 0.0006S^2 - 0.0737S + 6.2977$	1.00

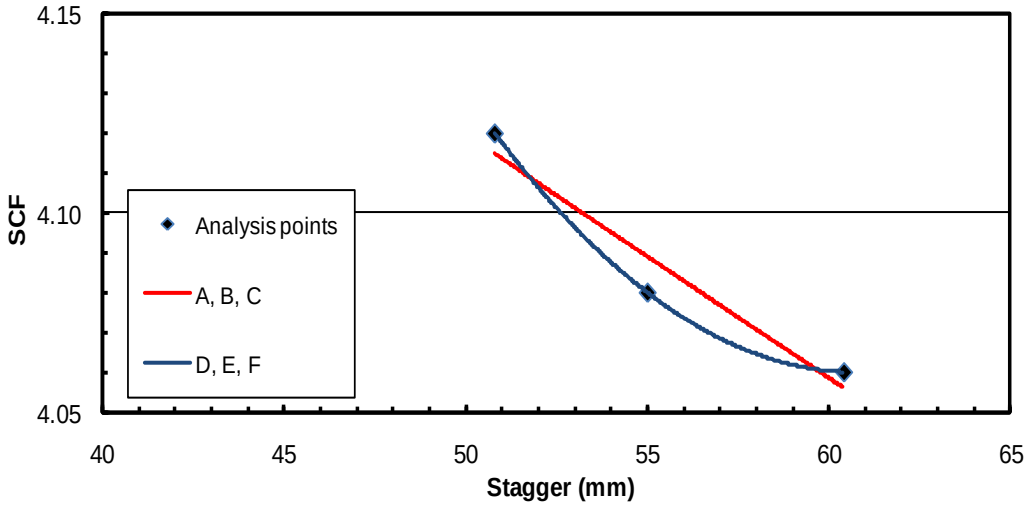

Figure A-1: Effect of hole stagger on SCF (gauge = 38.1 mm)

Table A-2: Effect of hole stagger on SCF (gauge = 46.5 mm)

Parameter varied	Other parameters (mm)	Model	Equation	R^2
Stagger	E_1= 48.7 E_2= 51.4 G= 46.5 L_t= 11.1 L_w= 146 W_t= 9.50 W_d= 356	A	$SCF = 4.43e^{-0.001S}$	0.93
		B	$SCF = -0.006S + 4.41$	0.93
		C	$SCF = -0.322LnS + 5.37$	0.94
		D	$SCF = 0.0003S^2 - 0.0404S + 5.33$	0.98
		E	$SCF = 8\times10^{-5}S^3 - 0.012S^2 - 0.63S - 6.5$	1.00
		F	$SCF = 8\times10^{-5}S^3 - 0.012S^2 - 0.63S - 6.5$	1.00

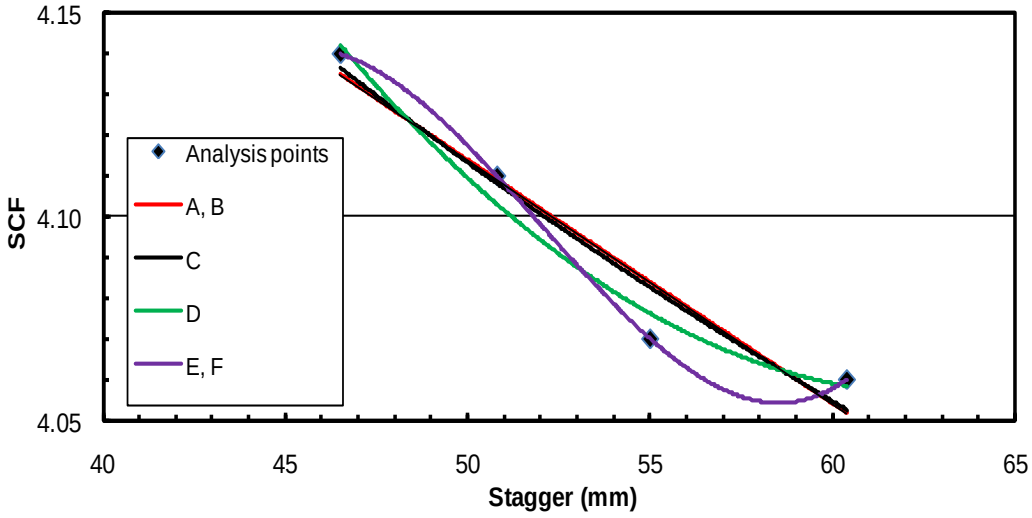

Figure A-2: Effect of hole stagger on SCF (gauge = 46.5 mm)

Table A-3: Effect of hole stagger on SCF (gauge = 50.8 mm)

Parameter varied	Other parameters (mm)	Model	Equation	R^2
Stagger	E_1= 43.9 E_2= 51.4 G= 50.8 L_t= 11.1 L_w= 146 W_t= 9.50 W_d= 356	A	$SCF = 4.81e^{-0.003S}$	0.95
		B	$SCF = -0.0128S + 4.76$	0.95
		C	$SCF = -0.625LnS + 6.56$	0.97
		D	$SCF = 0.0003S^2 - 0.0432S + 5.4912$	0.98
		E	$SCF=-5\times10^{-5}S^3+0.008S^2-0.4S+11.7$	1.00
		F	$SCF=9\times10^{-7}S^4-0.01S^3+0.02S^2-0.9S+17.2$	1.00

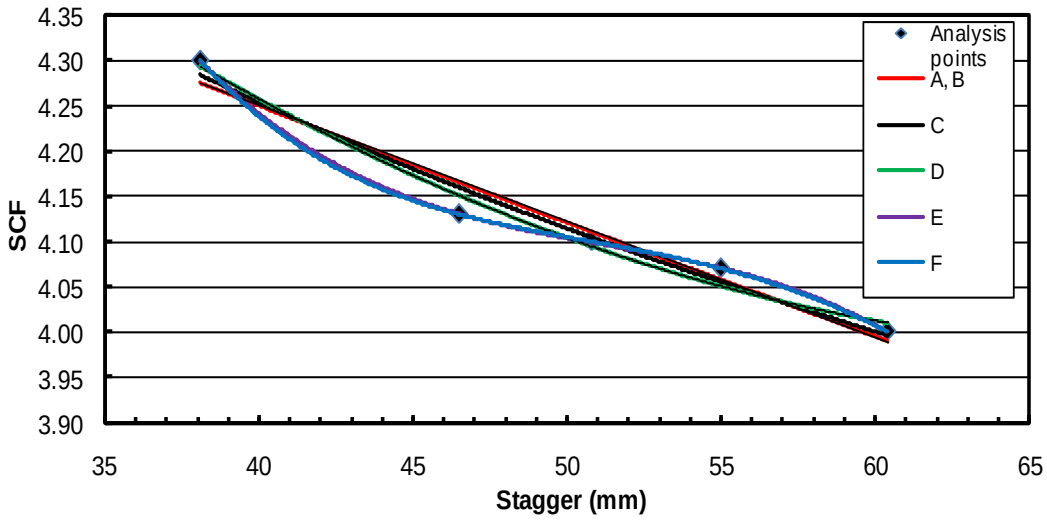

Figure A-3: Effect of hole stagger on SCF (gauge = 50.8 mm)

Table A-4: Effect of hole stagger on SCF (gauge = 55.0 mm)

Parameter varied	Other parameters (mm)	Model	Equation	R^2
Stagger	E_1= 40.2 E_2= 51.4 G= 55.0 L_t= 11.1 L_w= 146 W_t= 9.50 W_d= 356	A	$SCF = 4.80e^{-0.003S}$	0.96
		B	$SCF = -0.0128S + 4.75$	0.95
		C	$SCF = -0.623LnS + 6.54$	0.97
		D	$SCF = 0.0003S^2 - 0.0395S + 5.39$	0.98
		E	$SCF=-6\times10^{-5}S^3+0.009S^2-0.45S+11.9$	1.00
		F	$SCF=5\times10^{-6}S^4-0.001S^3+0.09S^2-3.1S+43.9$	1.00

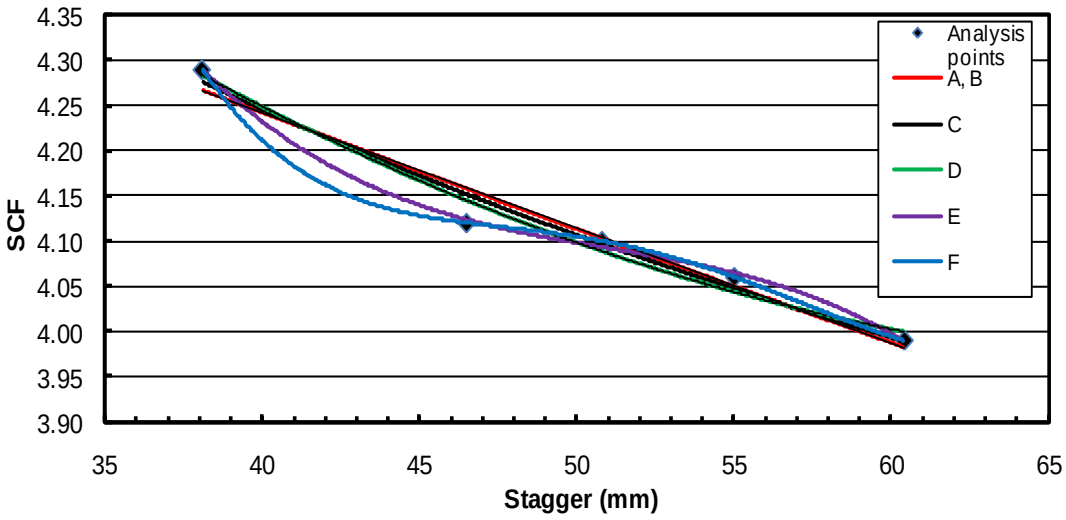

Figure A-4: Effect of hole stagger on SCF (gauge = 55.0 mm)

Table A-5: Effect of hole stagger on SCF (gauge = 60.4 mm)

Parameter varied	Other parameters (mm)	Model	Equation	R^2
Stagger	E_1= 34.9 E_2= 51.4 G= 60.4 L_t= 11.1 L_w= 146 W_t= 9.50 W_d= 356	A	$SCF = 4.697e^{-0.003S}$	0.99
		B	$SCF = -0.0113S + 4.66$	0.99
		C	$SCF = -0.545LnS + 6.22$	0.99
		D	$SCF = 0.0001S^2 - 0.022S + 4.92$	0.99
		E	$SCF = -3\times10^{-5}S^3 + 0.0046S^2 - 0.24S + 8.37$	1.00
		F	$SCF = -2\times10^{-6}S^4 + 0.0005S^3 - 0.03S^2 + 0.92S - 5.7$	1.00

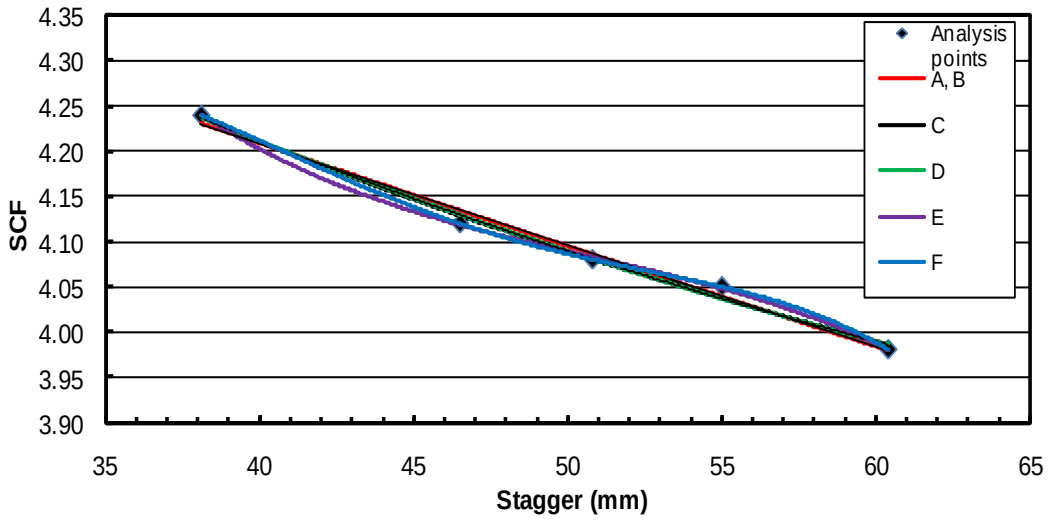

Figure A-5: Effect of hole stagger on SCF (gauge = 60.4 mm)

Table A-6: Effect of gauge distance on SCF (stagger = 38.1 mm)

Parameter varied	Other parameters (mm)	Model	Equation	R^2
Gauge distance	E_2= 51.4 S= 38.1 L_t= 11.1 L_w= 146 W_t= 9.50 W_d= 356	A	$SCF = 4.64e^{-0.001G}$	0.90
		B	$SCF = -0.0064G + 4.63$	0.90
		C	$SCF = -0.35LnG + 5.68$	1.00
		D	$SCF = -0.0008G^2 + 0.0788G + 2.27$	1.00
		E	$SCF = -0.0008G^2 + 0.0788G + 2.27$	1.00
		F	$SCF = -0.0008G^2 + 0.0788G + 2.27$	1.00

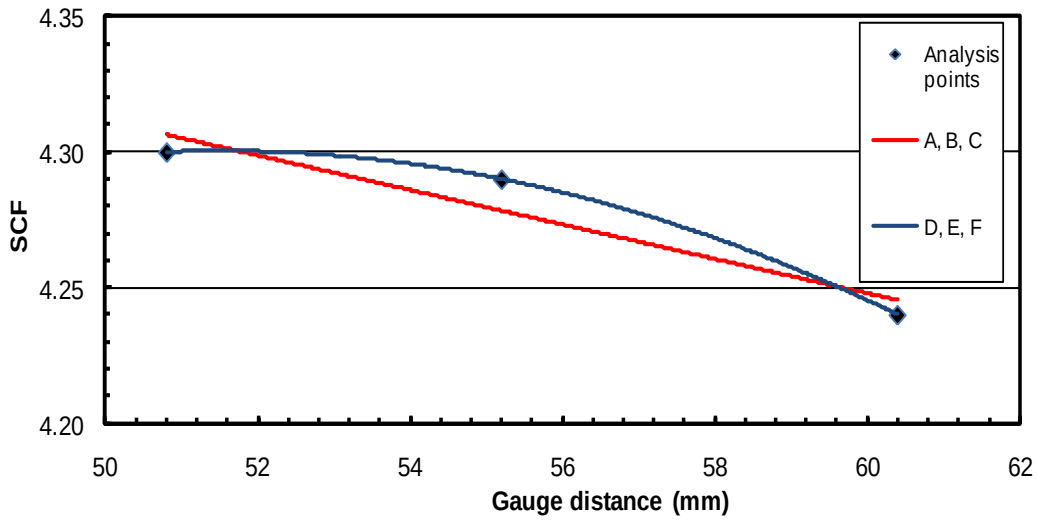

Figure A-6: Effect of gauge distance on SCF (stagger = 38.1 mm)

Table A-7: Effect of gauge distance on SCF (stagger = 46.5 mm)

Parameter varied	Other parameters (mm)	Model	Equation	R^2
Gauge distance	E_2= 51.4 S= 46.5 L_t= 11.1 L_w= 146 W_t= 9.50 W_d= 356	A	$SCF = 4.21e^{-4\times10^{-4}G}$	0.86
		B	$SCF = -0.0015G + 4.21$	0.86
		C	$SCF = -0.08LnG + 4.45$	0.88
		D	$SCF = 0.0001G^2 - 0.016G + 4.59$	0.98
		E	$SCF=2\times10^{-5}G^3-0.0025G^2+0.125G+2.10$	1.00
		F	$SCF=2\times10^{-5}G^3-0.0025G^2+0.125G+2.10$	1.00

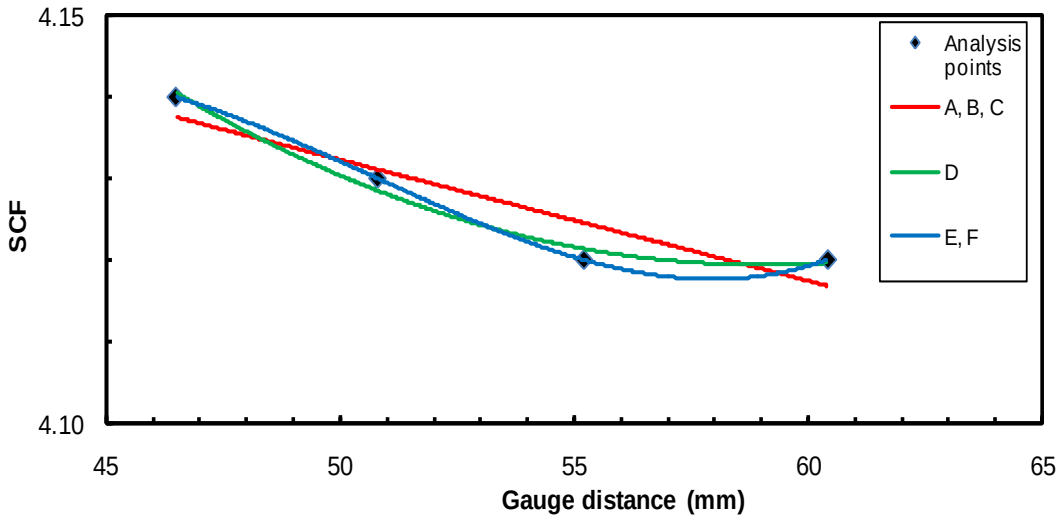

Figure A-7: Effect of gauge distance on SCF (stagger = 46.5 mm)

Table A-8: Effect of gauge distance on SCF (stagger = 50.8 mm)

Parameter varied	Other parameters (mm)	Model	Equation	R^2
Gauge distance	E_2= 51.4 S= 50.8 L_t= 11.1 L_w= 146 W_t= 9.50 W_d= 356	A	$SCF = 4.19e^{-4\times10^{-4}G}$	0.91
		B	$SCF = -0.0017G + 4.19$	0.92
		C	$SCF = -0.08LnG + 4.41$	0.89
		D	$SCF = -4\times10^{-5}G^2 + 0.0026G + 4.08$	0.95
		E	$SCF=-7\times10^{-6}G^3+0.001G^2-0.048G+4.89$	0.97
		F	$SCF=-3\times10^{-6}G^4+0.0006G^3-0.045G^2+1.45G-13.2$	1.00

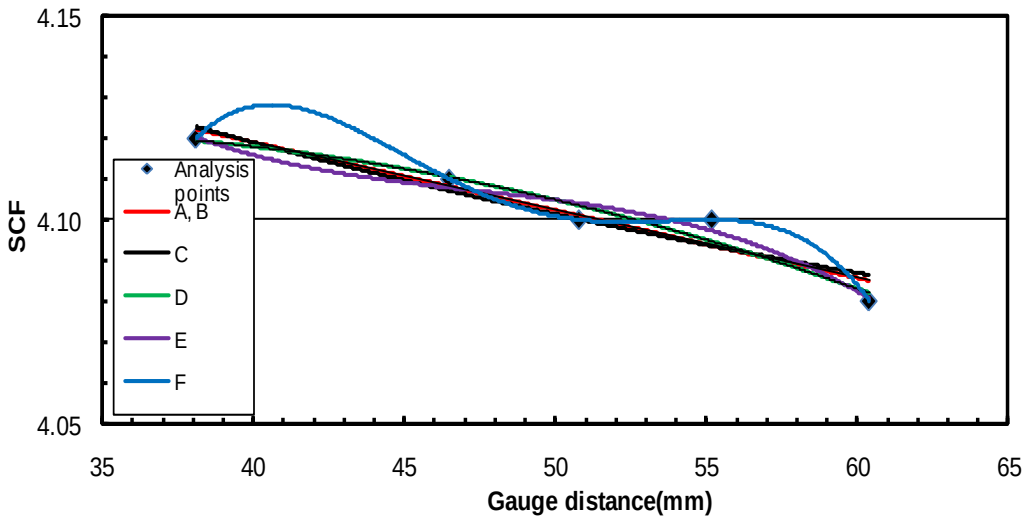

Figure A-8: Effect of gauge distance on SCF (stagger = 50.8 mm)

Table A-9: Effect of gauge distance on SCF (stagger = 55.0 mm)

Parameter varied	Other parameters (mm)	Model	Equation	R^2
Gauge distance	E_2= 51.4 S= 55.0 L_t= 11.1 L_w= 146 W_t= 9.50 W_d= 356	A	$SCF = 4.13e^{-3\times10^{-4}G}$	0.93
		B	$SCF = -0.0013G + 4.13$	0.93
		C	$SCF = -0.061LnG + 4.31$	0.90
		D	$SCF = -4\times10^{-5}G^2 + 0.0022G + 4.05$	0.97
		E	$SCF=-4\times10^{-6}G^3+0.0005G^2-0.0242G+4.47$	0.98
		F	$SCF=2\times10^{-6}G^4-0.0004G^3+0.0285G^2-0.94G+15.5$	1.00

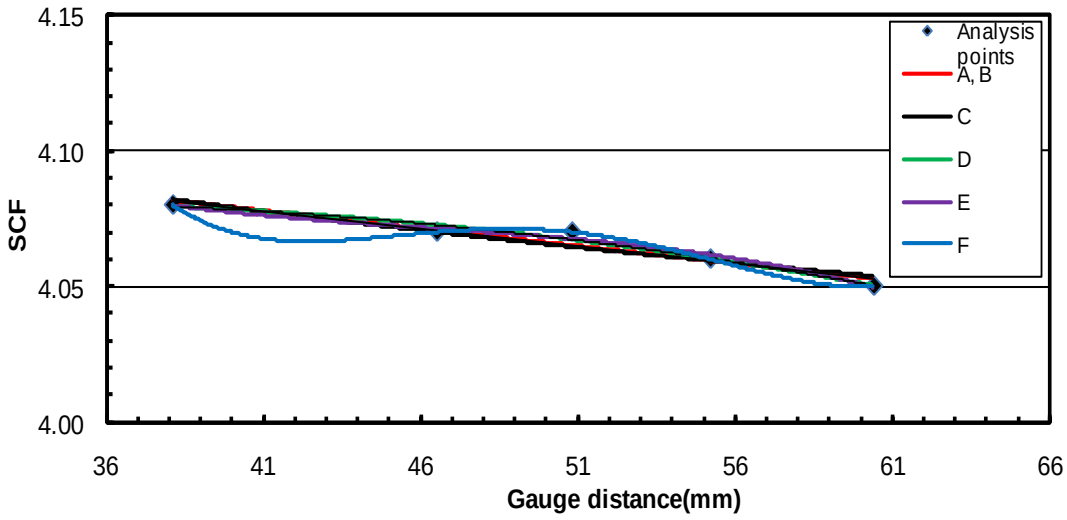

Figure A-9: Effect of gauge distance on SCF (stagger = 55.0 mm)

Table A-10: Effect of gauge distance on SCF (stagger = 60.4 mm)

Parameter varied	Other parameters (mm)	Model	Equation	R^2
Gauge distance	E_2= 51.4 S= 60.4 L_t= 11.1 L_w= 146 W_t= 9.50 W_d= 356	A	$SCF = 4.23e^{-0.001G}$	0.82
		B	$SCF = -0.0042G + 4.23$	0.82
		C	$SCF = -0.198LnG + 4.79$	0.81
		D	$SCF = -4\times10^{-5}G^2 - 0.0004G + 4.14$	0.82
		E	$SCF=5\times10^{-5}G^3-0.007G^2+0.34G-1.24$	0.94
		F	$SCF=-1\times10^{-5}G^4+0.0022G^3-0.164G^2+5.47G-63.48$	1.00

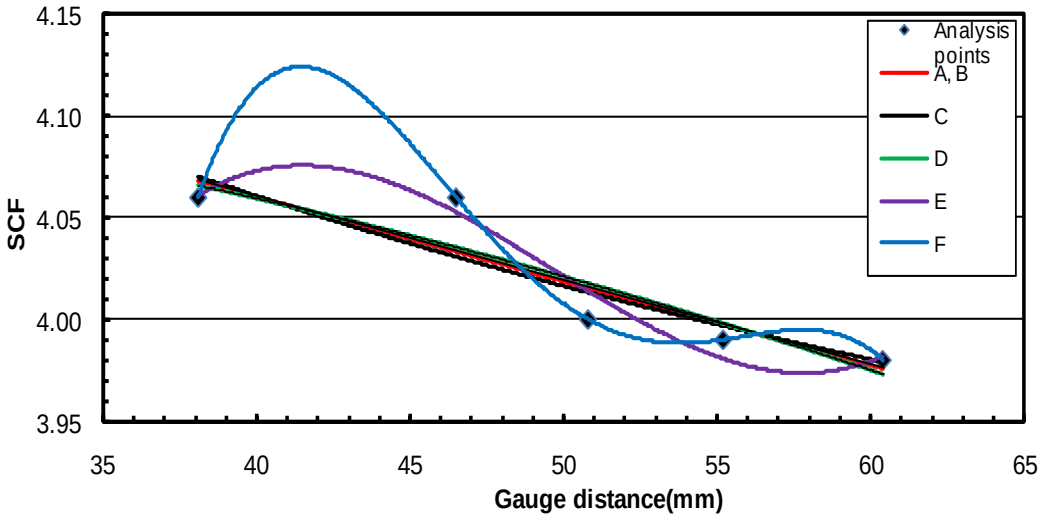

Figure A-10: Effect of gauge distance on SCF (stagger = 60.4 mm)

Table A-11: Effect of edge distance on SCF (stagger = 38.1 mm)

Parameter varied	Other parameters (mm)	Model	Equation	R^2
edge distance	G= 55.2 S= 38.1 L_t= 11.1 L_w= 146 W_t= 9.50 W_d= 356	A	$SCF = 4.46e^{-7\times10^{-4}E_2}$	0.22
		B	$SCF = -0.003E_2 + 4.46$	0.23
		C	$SCF = -0.155LnE_2 + 4.90$	0.32
		D	$SCF = 0.0006E_2^{\,2} - 0.054E_2 + 5.50$	0.95
		E	$SCF=5\times10^{-6}E_2^{\,3}-9\times10^{-6}E_2^{\,2}-0.029E_2+5.17$	0.95
		F	$SCF=-5\times10^{-6}E_2^{\,4}+0.0008E_2^{\,3}-0.0535E_2^{\,2}+1.46E_2-9.96$	1.00

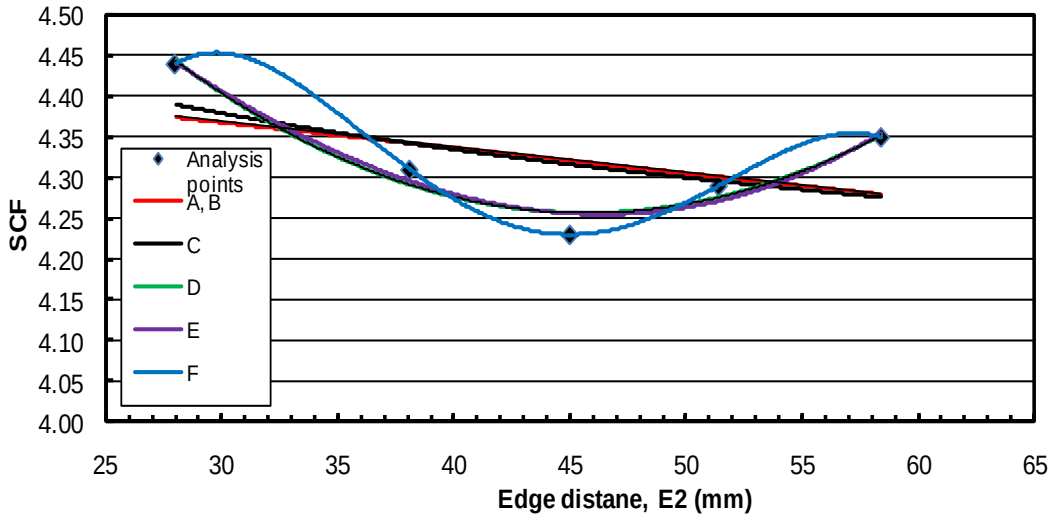

Figure A-11: Effect of edge distance on SCF (stagger = 38.1 mm)

Table A-12: Effect of edge distance on SCF (stagger = 46.5 mm)

Parameter varied	Other parameters (mm)	Model	Equation	R^2
edge distance	G= 55.2 S= 46.5 L_t= 11.1 L_w= 146 W_t= 9.50 W_d= 356	A	$SCF = 4.57e^{-0.002E_2}$	0.58
		B	$SCF = -0.0084E_2 + 4.56$	0.23
		C	$SCF = -0.375LnE_2 + 5.60$	0.69
		D	$SCF = 0.0007E_2^2 - 0.071E_2 + 5.83$	0.98
		E	$SCF=3\times10^{-6}E_2^3+0.0003E_2^2-0.055E_2+5.62$	0.98
		F	$SCF=-5\times10^{-6}E_2^4+0.0009E_2^3-0.0577E_2^2+1.56E_2-10.77$	1.00

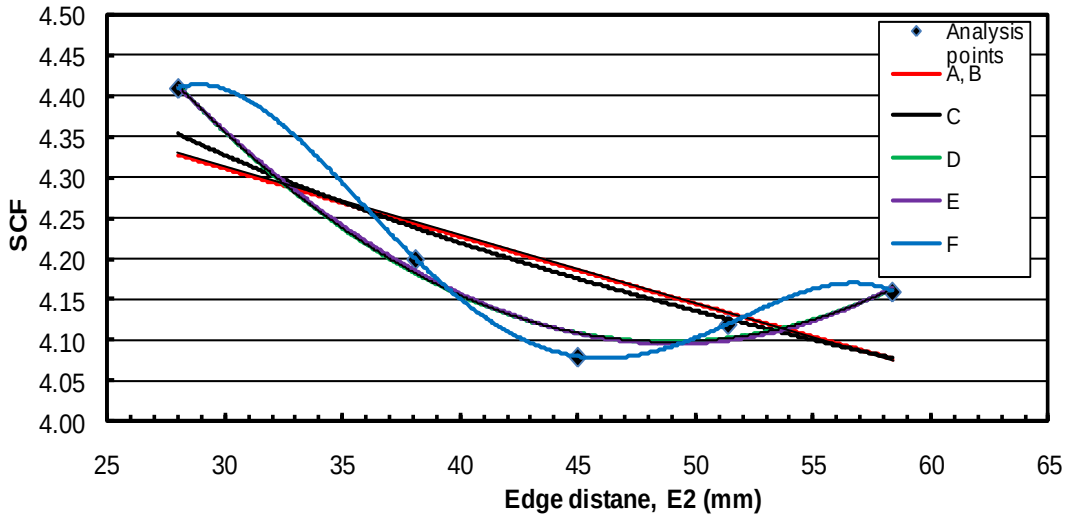

Figure A-12: Effect of edge distance on SCF (stagger = 46.5 mm)

Table A-13: Effect of edge distance on SCF (stagger = 50.8 mm)

Parameter varied	Other parameters (mm)	Model	Equation	R^2
edge distance	G= 55.2 S= 50.8 L_t= 11.1 L_w= 146 W_t= 9.50 W_d= 356	A	$SCF = 4.59e^{-0.002E_2}$	0.92
		B	$SCF = -0.009E_2 + 4.57$	0.91
		C	$SCF = -0.379LnE_2 + 5.61$	0.96
		D	$SCF = 0.0002E_2^2 - 0.0303E_2 + 5.008$	0.98
		E	$SCF=-1\times10^{-5}E_2^3+0.0017E_2^2-0.092E_2+5.83$	0.98
		F	$SCF=4\times10^{-6}E_2^4-0.0007E_2^3+0.046E_2^2-1.33E_2+18.4$	1.00

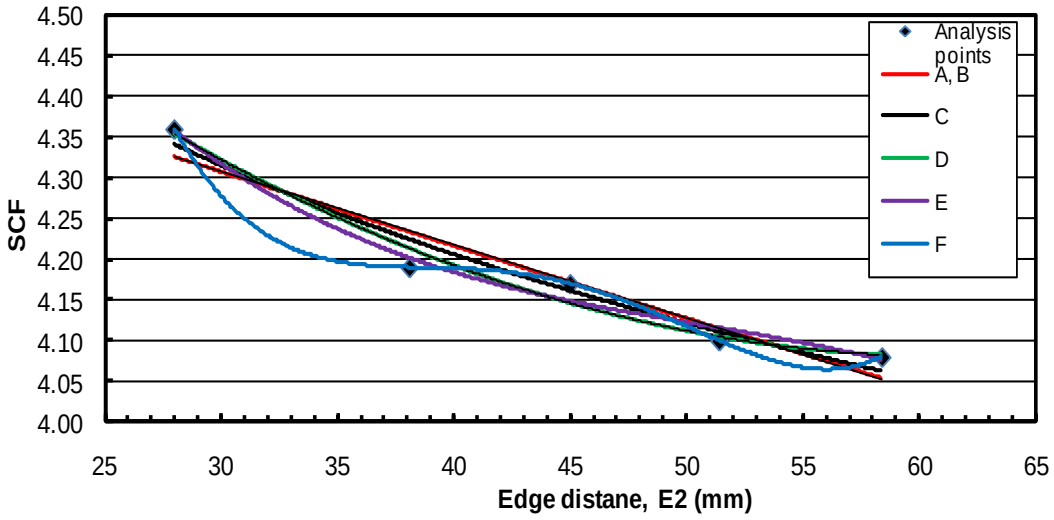

Figure A-13: Effect of edge distance on SCF (stagger = 50.8 mm)

Table A-14: Effect of edge distance on SCF (stagger = 55.0 mm)

Parameter varied	Other parameters (mm)	Model	Equation	R^2
edge distance	G= 55.2 S= 55.0 L_t= 11.1 L_w= 146 W_t= 9.50 W_d= 356	A	$SCF = 4.25e^{-9\times10^{-4}E_2}$	0.84
		B	$SCF = -0.0036E_2 + 4.25$	0.84
		C	$SCF = -0.15LnE_2 + 4.65$	0.87
		D	$SCF = 6\times10^{-5}E_2^{\,2} - 0.0089E_2 + 4.35$	0.87
		E	$SCF=-1\times10^{-5}E_2^{\,3}+0.0019E_2^{\,2}-0.086E_2+5.38$	0.93
		F	$SCF=3\times10^{-6}E_2^{\,4}-0.0006E_2^{\,3}+0.04E_2^{\,2}-1.14E_2+16.14$	1.00

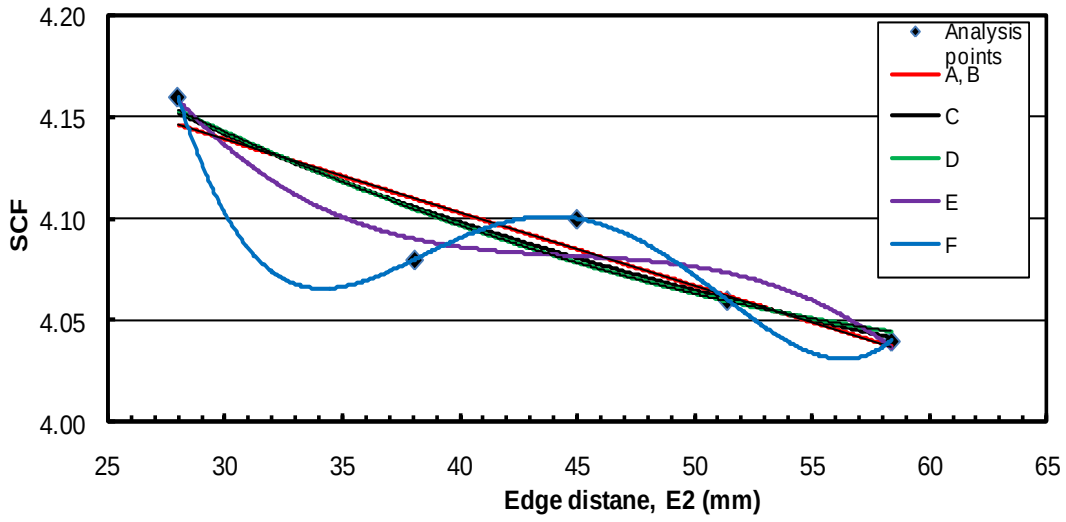

Figure A-14: Effect of edge distance on SCF (stagger = 55.0 mm)

Table A-15: Effect of edge distance on SCF (stagger = 60.4 mm)

Parameter varied	Other parameters (mm)	Model	Equation	R^2
edge distance	G= 55.2 S= 60.4 L_t= 11.1 L_w= 146 W_t= 9.50 W_d= 356	A	$SCF = 4.52e^{-0.002E_2}$	0.75
		B	$SCF = -0.009E_2 + 4.51$	0.75
		C	$SCF = -0.38LnE_2 + 5.55$	0.83
		D	$SCF = 0.0005E_2^{\,2} - 0.049E_2 + 5.32$	0.94
		E	$SCF=2\times10^{-5}E_2^{\,3}-0.0026E_2^{\,2}+0.0795E_2 + 3.61$	0.96
		F	$SCF=2\times10^{-5}E_2^{\,3}-0.0026E_2^{\,2}+0.0795E_2 +3.61$	1.00

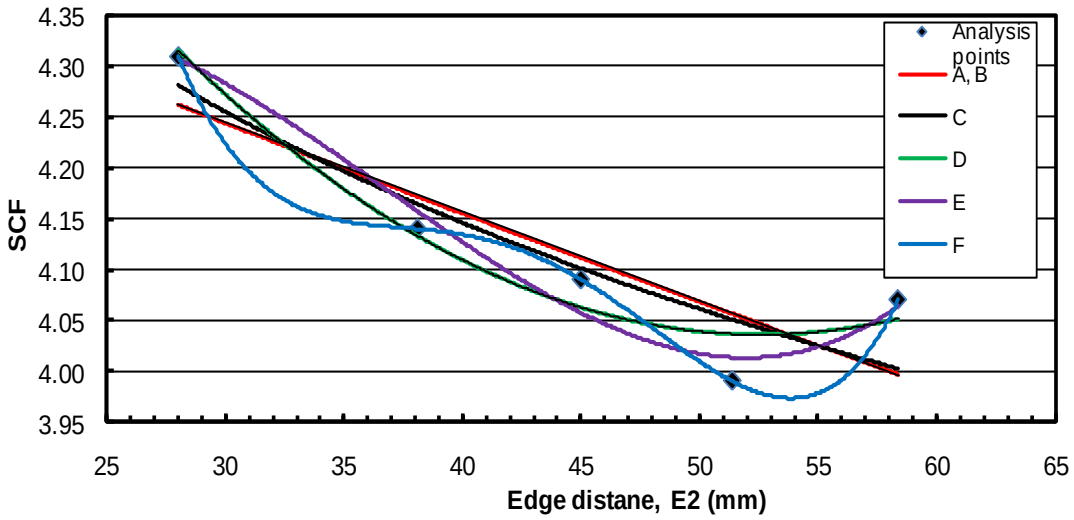

Figure A-15: Effect of edge distance on SCF (stagger = 60.4 mm)

Table A-16: Effect of angle thickness on SCF (angle size =152×152 mm)

Parameter varied	Other parameters (mm)	Model	Equation	R^2
angle thickness	G= 55.2 S= 38.1 L_t= 11.1 L_w= 146 W_t= 9.50 W_d= 356	A	$SCF = 5.32e^{-0.01L_t}$	0.93
		B	$SCF = -0.046L_t + 5.29$	0.93
		C	$SCF = -0.595LnL_t + 6.18$	0.98
		D	$SCF = 0.0042L_t^2 - 0.158L_t + 5.96$	1.00
		E	$SCF=-0.0002L_t^3+0.0107L_t^2-0.24L_t+6.31$	1.00

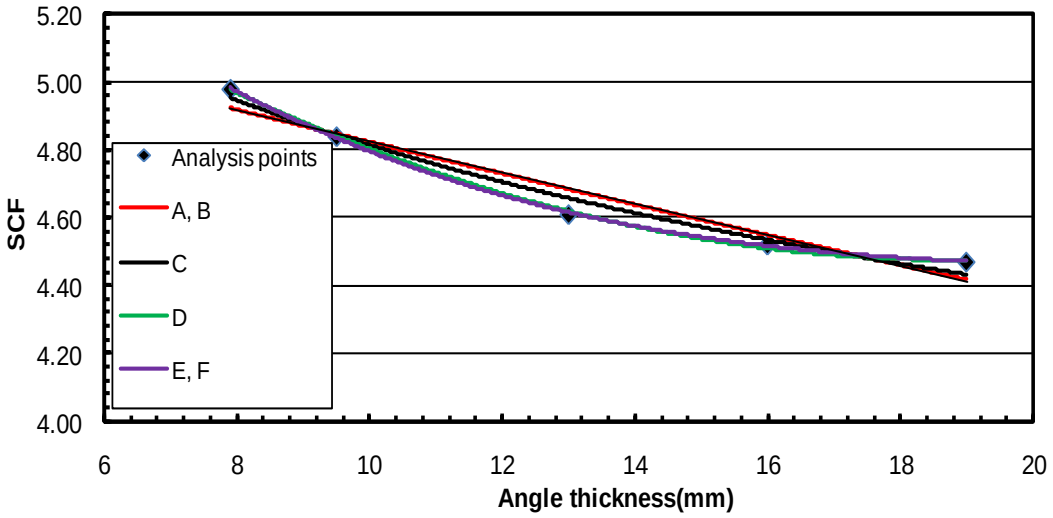

Figure A-16: Effect of angle thickness on SCF (angle size =152×152 mm)

Table A-17: Effect of angle thickness on SCF (angle size =152×102 mm)

Parameter varied	Other parameters (mm)	Model	Equation	R^2
angle thickness	G= 55.2 S= 38.1 L_t= 11.1 L_w= 146 W_t= 9.50 W_d= 356	A	$SCF = 4.87e^{-0.01L_t}$	0.90
		B	$SCF = -0.04L_t + 4.85$	0.90
		C	$SCF = -0.52LnL_t + 5.64$	0.95
		D	$SCF = 0.0042L_t^2 - 0.152L_t + 5.53$	0.99
		E	$SCF=-0.0005L_t^3+0.0254L_t^2-0.43L_t+6.64$	1.00

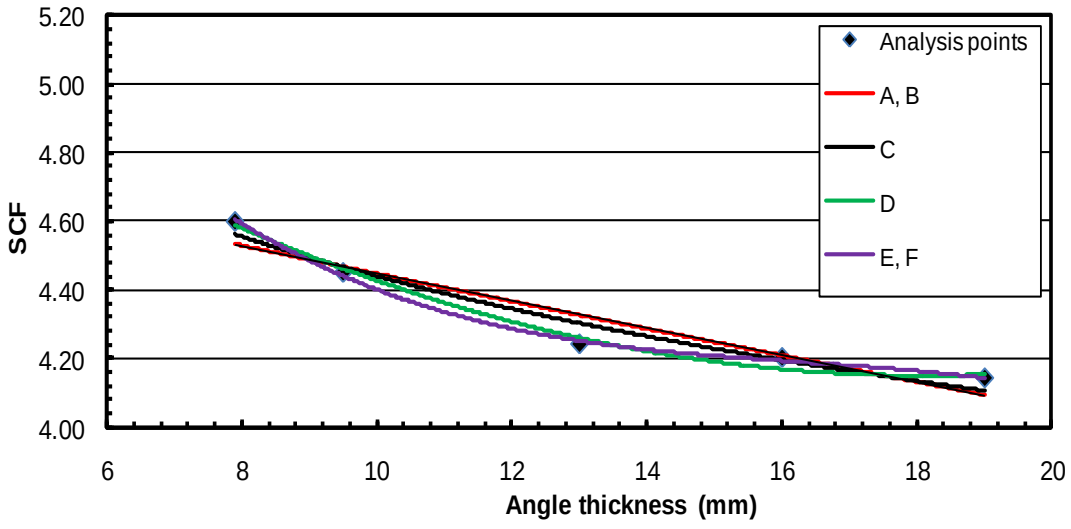

Figure A-17: Effect of angle thickness on SCF (angle size =152×102 mm)

Table A-18: Effect of angle thickness on SCF (angle size =152×89 mm)

Parameter varied	Other parameters (mm)	Model	Equation	R^2
angle thickness	G= 55.2 S= 38.1 L_t= 11.1 L_w= 146 W_t= 9.50 W_d= 356	A	$SCF = 4.78e^{-0.01L_t}$	0.90
		B	$SCF = -0.039L_t + 4.76$	0.90
		C	$SCF = -0.506LnL_t + 5.53$	0.95
		D	$SCF = 0.0041L_t^2 - 0.147L_t + 5.42$	0.99
		E	$SCF=-0.0005L_t^3+0.026L_t^2-0.43L_t+6.57$	1.00

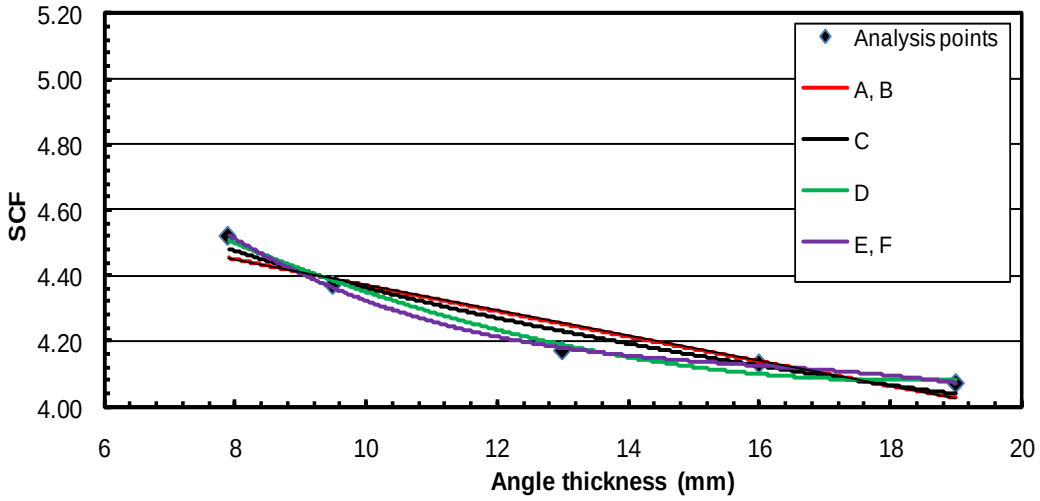

Figure A-18: Effect of angle thickness on SCF (angle size =152×89 mm)